

1 **Evaluating Longitudinal Control Strategies for Autonomous Vehicles**

2 Louis Sungwoo Cho¹ and Alireza Talebpour²

3 ¹Graduate Research Assistant, Department of Civil Engineering, University of Illinois at
4 Urbana-Champaign, 205 N Mathews Ave, Urbana, IL, 61801. Email: louissc2@illinois.edu

5 ²Assistant Professor, Department of Civil Engineering, University of Illinois at Urbana-Champaign,
6 205 N Mathews Ave, Urbana, IL, 61801. Email: ataleb@illinois.edu

7 **ABSTRACT**

8 Maintaining appropriate inter-vehicle distances is critical for enhancing the safety, stability,
9 and efficiency of traffic flow for autonomous vehicles. Varying longitudinal control strategies can
10 significantly influence vehicle dynamics, traffic stability, and roadway capacity. This comparative
11 study evaluates Constant Spacing Policy (CSP), Constant Time Headway (CTH), Traffic Flow
12 Stability (TFS), Constant Safety Factor (CSF), and the Intelligent Driver Model (IDM). The genetic
13 algorithm was calibrated to determine the most optimal parameters for the aforementioned control
14 spacing models. Highway vehicular trajectory datasets from I-294L1, I-90/94, and self-driving data
15 from Phoenix, Arizona, were utilized for simulation and evaluation. Calibration results indicate that
16 the CSP and CSF models exhibited the most robust performance, achieving the lowest root mean
17 square error (RMSE) and highest R^2 values across the datasets. The CSP model achieved strong
18 stability under low-density traffic conditions by maintaining consistent vehicle spacing with minimal
19 perturbations. The CSF model was the most effective policy for high-density traffic scenarios,
20 capturing critical situations like abrupt acceleration and deceleration. Although the CTH model
21 tracked reasonably under stable conditions, it was more sensitive to speed fluctuations, resulting
22 in errors during dynamic or congested traffic scenarios. The TFS model consistently produced
23 higher errors across different traffic densities, suggesting limited adaptability to rapidly changing

24 environments. The IDM model demonstrated strong versatility and realistic driving behavior across
25 a wide range of scenarios but required precise calibration to optimize its performance in high-density
26 and unpredictable traffic conditions. This study provides a comprehensive comparative analysis
27 of renowned control spacing strategies for autonomous vehicles, highlighting stability, safety, and
28 adaptability in self-driving operations under varying traffic conditions.

29 **INTRODUCTION**

30 Controlling inter-vehicular spacing between vehicles is essential to maintain safety for au-
31 tonomous vehicles. Various research done by transportation engineers integrate concepts from
32 macroscopic and microscopic traffic properties to safely guide self-driving vehicles along the road
33 while mitigating the risk of major roadway accidents. However, real-world driving maneuvers
34 are overlooked by existing control policies in complex traffic conditions, limiting the ability to
35 adapt to scenarios such as sudden lane changes, varying vehicle interactions, or abrupt braking
36 events. Addressing these challenges requires robust calibration methods that can accurately replicate
37 observed vehicular behavior, ensuring both reliability and safety.

38 One significant challenge is the procedure of accurately calibrating the spacing policies to
39 replicate the vehicle trajectories. Existing models overlook the intricate interactions between
40 kinematic variables such as acceleration, spacing, and relative speed leading to discrepancies
41 between predicted maneuvers and the actual maneuver. The aforementioned challenges of the
42 control spacing models undermine the reliability in complex traffic scenarios.

43 This study addresses these challenges by leveraging vehicular trajectory data from Interstate
44 highways to calibrate the most optimal parameters for each control spacing policy by using the
45 genetic algorithm. This approach provides a robust framework for optimizing model parameters, and
46 replicating the observed behavior. The results from this sophisticated calibration process contribute
47 to the development of more reliable and adaptable control spacing policies, paving the way for safer
48 and more efficient autonomous systems.

49 The primary objective of this study is to evaluate the performance of various control spacing
50 models used for safely and efficiently maintaining spacings between autonomous vehicles. The goal

51 is to assess the ability of the control spacing models capturing critical driving dynamics such as
52 vehicle speed, spacing, acceleration, and relative speed which could be used for autonomous vehicles.
53 The genetic algorithm calibrates the most optimal parameter values needed for each control spacing
54 policy. By fine-tuning the parameters for control spacing policies, the results were calibrated to
55 closely align the simulated trajectories with the observed vehicle trajectories, ensuring improved
56 accuracy and consistency with real-world vehicular trajectory data.

57 To evaluate the performance of each model, the calibrated parameters were validated by
58 comparing the predicted trajectories generated by the model against the actual observations for a
59 comprehensive assessment of the model's accuracy and reliability. Additionally, the study examined
60 how each control spacing model performed under varying traffic conditions, from free-flowing
61 scenarios to congested scenarios. This thorough analysis highlights the strengths and limitations of
62 each control spacing model under various traffic conditions.

63 BACKGROUND STUDY

64 Various research studies on control spacing models for car-following behavior in autonomous
65 vehicles have been conducted in recent years ([D. SWAROOP and IOANNOU 1994](#)). These models
66 can be broadly categorized into those that rely on Vehicle-to-Vehicle (V2V) communication, those
67 that function independently of communication systems, and hybrid approaches that integrate multiple
68 strategies ([Wu et al. 2020](#)). Communication-based models leverage real-time data exchange by
69 getting information through sensors to enhance vehicle coordination and string stability, while non-
70 communication-based approaches rely on predefined control spacing laws to safely maneuver diverse
71 traffic scenarios. Hybrid models aim to balance the advantages of both, improving adaptability
72 under varying traffic conditions.

73 The selection and fine-tuning of control parameters are critical in optimizing vehicle safety,
74 improving traffic flow efficiency, and maintaining stability across various driving conditions. It
75 is important to meticulously adjust the parameters that govern control spacing policies to enable
76 Adaptive Cruise Control (ACC) systems to adapt to diverse traffic environments. These refined
77 adjustments help mitigate stop-and-go oscillations, enhance traffic safety, and improve overall

78 traffic flow. Furthermore, precise tuning ensures a smoother transition between acceleration and
79 deceleration, reducing abrupt braking events and minimizing perturbations in vehicle platoons. This
80 process is critical in maintaining string stability, preventing abrupt changes in the vehicle's behavior
81 in small speed fluctuations that could propagate through traffic and lead to unnecessary congestion.

82 The most commonly studied spacing policies for vehicles are Constant Spacing Policy (CSP),
83 Constant Time Headway (CTH), and Traffic Flow Stability (TFS). The Intelligent Driver Model
84 (IDM), developed by Treiber, Hennecke, and Helbing ([Treiber et al. 2000](#)), is a widely used car-
85 following model for microscopic traffic flow simulations. The model provides a robust framework
86 for modeling vehicle interactions under various driving conditions, making it useful in research
87 related to traffic flow dynamics. In addition to these commonly used control spacing policies,
88 Constant Safety Factor (CSF) policy is essential for adjusting inter-vehicle spacing based on safety
89 margins such as adjusting safety factor to take into account of variations in speed, time headway,
90 and braking. These safety measures are critical to allow ACC systems to operate safely and mitigate
91 collisions. Thus, the Constant Factor Safety (CSF) policy was also used to compare the calibration
92 among the aforementioned commonly used control spacing policies.

93 Additionally, other approaches such as Variable Time Headway (VTH), Cooperative Adaptive
94 Cruise Control (CACC) with String Stability, Model Predictive Control (MPC), Lateral and
95 Longitudinal Control, and Closed-Loop Dynamics have been explored to optimize vehicle interactions
96 and traffic efficiency. The control spacing models for car-following behavior can further be classified
97 based on their reliance on communication systems: those that operate with Vehicle-to-Vehicle (V2V)
98 communication, those without communication, and hybrid approaches that integrate both strategies.

99 Models with Communication

100 Models that incorporate communication-based control strategies have various approaches to
101 simulate the car-following behavior of vehicles. Model Predictive Control (MPC) can help mitigate
102 traffic flow disturbances caused by lane-changing maneuvers while maintaining CTH ([An and](#)
103 [Talebpour 2019](#)). The proposed approach optimizes both the lateral trajectory of a lane-changing
104 Connected Automated Vehicles (CAV) and the longitudinal control of a Connected and Automated

105 Vehicles (CAV) in the target lane for simulation. The study proposed a MPC framework for the
106 target-lane vehicle to effectively respond to lane changes, while a predefined set of lateral trajectories
107 was evaluated for the vehicle changing lanes. The optimal trajectory was selected based on its ability
108 to minimize the required deceleration of the impacted vehicle, reducing acceleration disturbances
109 and shockwave propagation. Analytical and simulation results show that the integrated control
110 strategy enhances traffic stability and abate perturbations in the vehicle platooning system.

111 Gap regulation and gap-closing controllers to enhance string stability in traffic flow ([Milanés et al. 2014](#))
112 was analyzed in another study. These two main controllers take advantage of the
113 Vehicle-to-Vehicle (V2V) communication to enhance coordination between autonomous vehicles.
114 The Cooperative Adaptive Cruise Control (CACC) system that augments traditional Adaptive
115 Cruise Control (ACC) was used to model the vehicles by integrating wireless Vehicle-to-Vehicle
116 communication. One controller was in charge of managing in scenarios where a vehicle joins the
117 platoon. The other controller regulated the car-following behavior. The Infiniti M56s cars were used
118 for experimental validation to demonstrate the capability of the proposed CACC system being able
119 to significantly improve traffic stability and coordination.

120 Tuning control model parameters is a commonly used approach to enhance overall system
121 stability for car-following behavior. One study optimizes the ACC system parameters by leveraging
122 the Controller Area Network (CAN) communication framework to improve car-following behavior
123 and to preclude fatal traffic collisions ([Moon et al. 2009](#)). The proposed ACC system integrates
124 collision avoidance system by classifying driving scenarios into safe, warning, and dangerous modes
125 using a non-dimensional warning index and time to collision metrics. Various control strategies are
126 utilized based on the classifications. The parameters for the optimization process were fine-tuned
127 through a confusion-matrix method using manual-driving data in scenarios with no traffic accidents.
128 The study compares the vehicle-following characteristics of the system to real-world manual driving
129 to emphasize that integrating both ACC and collision avoidance systems can successfully replicate
130 human-driving behavior in both high-speed cruising and low-speed stop-and-go traffic scenarios.
131 Additionally, experimental validation in real-vehicle tests corroborates that the system effectively

132 prevents vehicles from following too close to each other enhancing both safety and driver comfort
133 across various driving conditions.

134 A study on Semi-Autonomous Adaptive Cruise Control (SAACC) systems explores the integration
135 of a radio-frequency communication framework to enhance highway safety and traffic flow capacity
136 ([Rajamani and Zhu 2002](#)). Unlike traditional Adaptive Cruise Control (ACC) or fully automated
137 highway systems (AHS) that rely on tightly coordinated vehicle platoons, SAACC operates without
138 having to form vehicle platoons or be too dependent on dynamic frequency allocation. The system
139 consistently maintains a user-defined cruising speed until a target vehicle is detected in the same lane.
140 Under this condition, the system adjusts the ego vehicle's following distance based on real-time
141 communication signals. The proposed SAACC approach enables vehicles to maintain smaller
142 time gaps safely while ensuring string stability and minimizing actuator input efforts compared to
143 standard autonomous ACC systems. Simulation results demonstrate that SAACC are more accurate
144 and smoother in tracking vehicles, mitigates control efforts, and increases robustness to variations in
145 vehicle dynamics, making it a viable solution for mixed-traffic environments.

146 One study examines truck platooning with Cooperative Adaptive Cruise Control (CACC),
147 emphasizing the benefits and challenges of using the Constant Time Headway (CTH) model in uphill
148 driving conditions ([Chen et al. 2018](#)). The study highlights critical issues where truck platoons
149 controlled by the CACC model become asymptotically unstable on steep grades due to the limited
150 acceleration capabilities of heavy vehicles. This instability prevents trucks from tracking the vehicle
151 platoon after an uphill terrain, leading to spacing errors. In order to resolve this issue, the study
152 proposes new control strategies to complement existing controllers and enhance stability. These
153 strategies mitigate the adverse effects of low crawl speeds and ensure that truck platoons remain
154 string stable irrespective of uphill grades. The results underscore the need for refined control policies
155 in uneven road conditions where elevation changes impact the overall dynamics of the vehicle and
156 traffic flow.

157 One study explores the Variable Time Headway (VTH) concept. This method dynamically
158 adjusts the inter-vehicle headway. The headway is increased during acceleration and decreased

159 during deceleration (Yanakiev and Kanellakopoulos 1995). This adaptive spacing policy enhances
160 string stability, ensuring that perturbations are not amplified during vehicle platooning. Unlike
161 constant spacing policies, which require inter-vehicle communication to maintain string stability,
162 VTH allows autonomous vehicles to achieve stability without explicit coordination by adjusting
163 the time headway based on velocity errors. This modification significantly abates transient spacing
164 errors, improves responsiveness to traffic fluctuations, and minimizes the risk of traffic shockwaves
165 propagating in the vehicle platoon and mitigates stop-and-go congestion. Additionally, VTH allows
166 for smaller inter-vehicle distances in autonomous platoon operation.

167 Constant spacing with communication is a widely used control model for enhancing vehicle
168 coordination in platooning. Several studies have investigated this approach, including the integration
169 of Adaptive Cruise Control (ACC), spacing policies, and Cooperative Adaptive Cruise Control
170 (CACC) to improve string stability (Naus et al. 2010). One study proposes a decentralized CACC
171 controller that relies on a wireless communication link with the nearest preceding vehicle, allowing
172 vehicles to maintain small inter-vehicle spacings. To take into consideration of vehicles with possibly
173 different characteristics, a frequency-domain condition for the string stability system was derived.
174 The study demonstrates that a velocity-dependent inter-vehicle spacing policy, supported by wireless
175 communication, enables stable platooning, whereas a constant spacing system that is independent of
176 velocity may lead to instability.

177 One study explores the use of linear kinetic properties in Adaptive Cruise Control (ACC)
178 and Cooperative Adaptive Cruise Control (CACC) systems to optimize inter-vehicle spacing in
179 platoons (Luu et al. 2020). The proposed spacing control algorithm leverages on-board sensors and
180 communicates only with the preceding vehicle to regulate following distances. The study evaluates
181 string stability by leveraging a frequency-domain analysis and Nyquist diagrams. The control
182 algorithm ensures that each vehicle maintains a stable spacing while mitigating perturbations that
183 could propagate through the platoon. Numerical simulations demonstrate the model's potential for
184 improving platoon coordination and roadway capacity.

185 Traffic flow stability analysis was conducted in this research by leveraging deterministic

acceleration models and Vehicle-to-Vehicle (V2V) communication (Talebpour and Mahmassani 2016). The study proposed a simulation framework that differentiates between connectivity and automation, modeling various vehicle types with distinct communication capabilities. A stability analysis of mixed traffic streams demonstrates that CAVs significantly enhance string stability, with automation proving more effective than connectivity alone in preventing shockwave formation and propagation, underscoring the potential of V2V communication and automation in optimizing highway traffic flow and mitigating congestion.

Model Predictive Control (MPC) is also a notable controller to address complex traffic scenarios. These studies have experimented how MPC can be used in multi-stage lane-changing movements of vehicles in dynamic traffic conditions (Cesari et al. 2017), predictive optimization of lane-changing decisions through the integration of game theory and MPC (Wang et al. 2015), and Distributed MPC for heterogeneous vehicle platoons, which tracks leader speed and maintains desired gaps under unidirectional topologies (Zheng et al. 2017). MPC enhances Adaptive Cruise Control (ACC) and Cooperative Adaptive Cruise Control (CACC) strategies, allowing vehicles while maintaining traffic stability to adjust their speed and spacing dynamically. Some studies have also integrated learning-based approaches with MPC to improve adaptability in uncertain environments, where vehicles must anticipate and react to unpredictable traffic fluctuations. These findings underscore the importance of optimizing vehicle control and coordination in scenarios where lane-changing behavior happens frequently.

This study proposes a data-driven, stochastic optimization-based Model Predictive Control (MPC) framework that enhances stability, robustness, and safety in longitudinal cooperative driving by incorporating Vehicle-to-Vehicle (V2V) communication (Zhao and Zhang 2020). To address uncertainties in traffic dynamics, the framework integrates an online learning-based driving dynamics prediction model that anticipates the uncertain states of preceding vehicles. The predictions were incorporated into a constrained finite horizon optimal control problem to optimize the acceleration and deceleration commands for CAVs. The study calibrates the Distributionally Robust Stochastic Optimization (DRSO) model with Distributionally Robust Chance Constraints (DRCC) to ensure

213 reliable control under uncertain conditions. Additionally, Semi-definite Programming (SDP)
214 relaxation technique was applied to perform real-time computation. Experimental validation using
215 Next Generation Simulation (NGSIM) data demonstrates that the proposed approach maintains
216 string stability and robust cooperative driving performance under various traffic conditions by
217 properly tuning key parameters such as prediction horizon length and time headway parameters.

218 Hybrid models incorporating communication have been analyzed. One study integrates Adaptive
219 Cruise Control (ACC) and Model Predictive Control (MPC) to enable smooth platoon merging
220 through vehicle platooning control ([An and Talebpour 2022](#)). Another study examines the impact
221 of Vehicle-to-Vehicle (V2V) communication on traffic flow stability, analyzing how information
222 availability influences critical density and percolation within vehicular networks ([Talebpour et al.](#)
223 [2018](#)).

224 Cooperative Adaptive Cruise Control (CACC) has also been studied for its effects on traffic-flow
225 stability and throughput. By leveraging V2V communication, CACC systems provide reference
226 values that enhance traffic characteristics, such as string stability, particularly in mixed traffic
227 conditions ([van Arem et al. 2006](#)). Another study integrates lateral and longitudinal controllers
228 and develops a finite state system to improve autonomous vehicle platooning. The longitudinal
229 control system consists of upper and lower-level controllers, while the lateral controller ensures safe
230 lane-changing behavior ([Rajamani et al. 2000](#)).

231 **Models without Communication**

232 Constant Time Headway (CTH) can be used by models without having to rely on communication
233 between vehicles. One study analyzes the vehicle dynamics using a continuous-time deterministic
234 car-following model by leveraging Pipe's Model to simulate steady-state car-following behavior
235 ([Sipahi et al. 2009](#)). The study explores the effects of multiple driver reaction and actuation delays on
236 stability, providing a comprehensive characterization of stability regions within the delay parameter
237 space. By running the frequency-sweeping algorithms, the research simplifies the stability analysis
238 and analyzes how drivers' behavior, decision-making delays, and response times affect the overall
239 traffic flow stability.

240 A research on how string stability can be achieved without relying Vehicle-to-Vehicle (V2V)
241 communication was conducted by leveraging a kinematic linear model with multi-anticipation ([Donà et al. 2022](#)). The study highlights that most commercially available ACC systems are unstable. While
242 increasing time headway intervals can stabilize traffic, it reduces roadway capacity. To address this
243 major issue, the study proposed an alternative solution that utilizes recent advancements in RADAR
244 sensing technology. By monitoring the behaviors of two vehicles downstream, the proposed multi-
245 anticipative ACC system ensures string stability across a wide range of traffic conditions without
246 requiring inter-vehicle communication. Analytical and simulation-based evaluations demonstrate
247 that this approach not only enhances traffic stability overall, but also increases road capacity, even in
248 the presence of external perturbations. Furthermore, Pareto optimization was performed to derive the
249 optimal tuning conditions for the time headway policies. The results suggest that multi-anticipative
250 ACC provides a viable solution for mitigating congestion and improving traffic flow without having
251 to build connectivity-based infrastructure.
252

253 Additionally, the performance of commercially available Adaptive Cruise Control (ACC) systems
254 has been analyzed, revealing significant limitations in achieving string stability ([Ciuffo et al. 2021](#)). A
255 large-scale experiment involving ACC-equipped vehicles was conducted to study their car-following
256 behavior under real-world driving conditions. The study evaluates how target time gaps were
257 maintained based on observed distributions across different vehicle brands. Results indicate that
258 current ACC implementations struggle to maintain consistent inter-vehicle spacing, leading to string
259 instability and disruptions in traffic flow. This instability arises due to variations in control logic
260 among different manufacturers and the inability of ACC systems to adapt dynamically to changes in
261 vehicle ordering and settings. The findings underscore the critical role of Constant Time Headway
262 (CTH) policies in mitigating these issues, highlighting the need for more robust control strategies to
263 ensure stable car-following behavior and prevent unintended traffic disturbances as ACC adoption
264 increases.

265 A study examining Constant Time Headway (CTH) policies proposed a novel framework for
266 designing and evaluating spacing policies ([Santhanakrishnan and Rajamani 2003](#)). The research

assesses spacing policies in terms of string stability, traffic flow stability, and roadway capacity. While the standard CTH policy guarantees string stability, findings indicate that this policy does not perform well in reduced traffic capacity and can cause instability in traffic flow. To address these limitations, the study introduces an ideal spacing policy, formulated as a nonlinear function of speed, which improves both string and traffic flow stability while enhancing overall capacity.

Several studies have used constant spacing approaches. One study explores intelligent cruise control strategies within an Automated Vehicle Control System (AVCS) framework. A commonly used controllers for autonomous vehicles called PID controllers were used to adjust the inter-vehicle spacings effectively (Ioannou et al. 1993). Multiple control system tests were performed by using a validated nonlinear longitudinal vehicle model before implementation in real-world vehicles. The proposed control approach ensures smooth and reliable vehicle following by utilizing onboard sensors that measure relative distance and speed without relying on Vehicle-to-Vehicle (V2V) communication. The overall stability is maintained through a meticulously designed throttle and brake control systems in conjunction with the Constant Time Headway (CTH) policy. Simulation and experimental results emphasize that the integrated system provides stable and responsive vehicle spacing, even in scenarios where the lead vehicle exhibits erratic speed variations.

Another study utilizes partial differential equations (PDEs) to model traffic flow stability in intelligent cruise control systems operating under constant spacing policies (Darbha and Rajagopal 1999). The study distinguishes between two fundamental stability concepts in traffic flow analysis: string stability, which ensures predictable inter-vehicle spacing in a platoon, and traffic flow stability, which accounts for velocity and density variations due to vehicles entering or leaving the flow. The study also highlights that traffic flow stability depends not only on vehicle-following control laws but also on the spacing policy leveraged by the control system. By analyzing the coupled equations governing automatic vehicle following and traffic density, the study investigates the critical role of constant spacing policies in determining highway capacity and traffic stability.

Additionally, a comparative study evaluates various spacing policies, focusing on the impact on safety, traffic flow efficiency, and user acceptance (Wang and Rajamani 2004b). The study

examines the stability of highway traffic under Adaptive Cruise Control (ACC) systems. This study shows that traffic flow stability under a CTH policy is highly dependent on boundary conditions at highway inlets and exits. Furthermore, the research proposes an unconditionally stable spacing policy, which guarantees stability under all boundary conditions. Simulation results highlight the practical consequences of instability, showing that alternative spacing policies outperform the CTH policy in maintaining smooth and efficient traffic flow. One key finding from this study is that the ACC systems should not rely only on the CTH policy.

Other studies have utilized Model Predictive Control (MPC). One study investigates distributed MPC for managing headway and cruise control in vehicle platooning ([Maxim et al. 2017](#)). Another study focuses on adjusting ACC parameters to alleviate traffic congestion and improve flow efficiency ([Kesting et al. 2008](#)). Additionally, predictive optimization and non-linearity compensation were applied to enhance the longitudinal dynamics of vehicular systems ([Li et al. 2011](#)).

Furthermore, additional studies include a physics-based lumped mass model that incorporates braking and aerodynamic forces for control optimization ([Nilsson et al. 2016](#)), and a bidirectional control approach utilizing decentralized dynamics for improved stability ([Barooah et al. 2009](#)). Another study presents a microscopic traffic flow model that integrates both lateral and longitudinal dynamics to address two-dimensional traffic flow challenges. This model effectively handles collision avoidance, lane-changing, and lateral friction ([Delpiano et al. 2020](#)).

Alternative Models

Several studies analyze the performance of Adaptive Cruise Control (ACC) and Cooperative Adaptive Cruise Control (CACC) systems. One of the studies analyzes how the Constant Time Headway (CTH) approach can be integrated with ACC and CACC models under uncertainty conditions ([Zhou et al. 2017](#)). One research study leverages a rolling horizon stochastic optimal control strategy, taking into consideration for uncertainties in system dynamics and sensor measurements. Modeling uncertainties were perceived as normally distributed disturbances in both the state and measurement equations. A multi-objective function was defined by incorporating bounded acceleration limits and collision protection constraints. The resulting optimization problem was formulated as a

321 linearly constrained Linear Quadratic Gaussian (LQG) problem, which is solved using the separation
322 principle.

323 One study analyzed how traffic flow stability can be induced by the Constant Time Headway
324 (CTH) policy using three different modeling paradigms: a microscopic model, a spatially discrete
325 model, and a spatially continuous model ([Li and Shrivastava 2002](#)). The analysis shows that traffic
326 stability properties can vary across these paradigms unless the control policy and traffic dynamics
327 are consistently formulated. To ensure consistency, a biasing strategy was introduced, determining
328 whether the feedback control being applied to the system is downstream, upstream, or collocated
329 with respect to the vehicle. According to the study results, it was determined that for ACC-equipped
330 vehicles utilizing forward-looking sensors, a downstream biasing strategy results in exponentially
331 stable traffic flow on circular highways. Furthermore, traffic stability can be maintained on open
332 highways if entry and exit conditions follow the downstream biasing strategy.

333 A research on integrating Adaptive Cruise Control (ACC) and Cooperative Adaptive Cruise
334 Control (CACC) traffic dynamics into a Gas-Kinetic (GKT) macroscopic traffic flow model was
335 conducted ([Delis et al. 2015](#)). In this approach, an acceleration/deceleration term to simulate the
336 dynamics of ACC and CACC vehicles on traffic flow was proposed. In addition to this, a novel
337 relaxation-based approach that tracks the time/space-gap principle was also introduced. This method
338 assigns relaxation time to multiple CACC leading vehicles and only the direct leader was assigned
339 to ACC leading vehicles. The partial differential equations for the nonlinear system were used for
340 numerical approximation using a high-resolution finite volume scheme with a Weighted Essentially
341 Non-oscillatory (WENO) discretization method. The calibrated results corroborates that CACC
342 enhances traffic flow stability, particularly in response to perturbations on a ring road and merging
343 flows at an on-ramp. Compared to ACC, the CACC model enhances dynamic equilibrium capacity
344 and mitigates congestion more effectively, particularly in bottleneck locations.

345 Human drivers tend to drive relying on the speed and position of the preceding and following
346 vehicles to adjust the state and control inputs of the vehicle. Longitudinal vehicle models can be
347 used to simulate real-world traffic maneuvers by incorporating engine, throttle, and brake dynamics

348 to replicate human-driving behaviors ([Zhang et al. 1999](#)). This study proposed an Autonomous
349 Intelligent Cruise Control (AICC) system, where the relative speed and inter-vehicle spacing
350 determines the actions the following vehicle can take to maintain a desired spacing between the
351 vehicles, ensuring platoon stability bi-directionally. This system has been effective in controlling
352 time headway between vehicles and maintaining constant inter-vehicle spacings.

353 One study ([Kilic et al. 2015](#)) leverages a hierarchical control approach to Adaptive Cruise Control
354 (ACC) as part of an Advanced Driver Assistance System (ADAS). The System-of-Systems (SOS)
355 framework to unify multiple ADAS functionalities were proposed. The ACC system was structured
356 into High-Level Control (HLC), Low-Level Control (LLC), and sensor units to enhance adaptability
357 and efficiency. Using a finite state machine, the HLC dynamically adjusts the vehicle's speed, either
358 by maintaining a minimum safe following distance or by tracking a desired velocity. The Model
359 Predictive Controller (MPC) tracks the movement of the target vehicle and generate optimal control
360 actions for the distance control state. The throttle and brake actions are maneuvered by the LLC. By
361 leveraging the hierarchical structure, the proposed ACC system enhances vehicle response, enhances
362 safety, and facilitates integration with other ADAS technologies such as collision avoidance and
363 blind spot detection.

364 DATA DESCRIPTION

365 The high-fidelity Third Generation Simulation (TGSIM) dataset ([Federal Highway Administration](#)
366 ([FHWA](#)) [2024](#)) was utilized for analyzing vehicle trajectories ([Talebpour et al. 2024](#)), ([Ammourah](#)
367 [et al. 2024](#)). The holistic dataset focuses on complex urban, multi-modal road networks capable of
368 traffic simulations of control algorithms ([Ammourah et al. 2024](#)) to be conducted. For this research,
369 datasets from the I-90/94, and level 1 autonomy vehicles in I-294 were utilized with bi-directional
370 lanes represented by positive and negative signs for each lane number.

371 Each control model in this study was calibrated using the dataset's high-resolution, 10 Hz data,
372 offering an intricate perspective on vehicular movements ([Ammourah et al. 2024](#)). The datasets
373 include important trajectory attributes such as time in seconds, longitudinal and lateral coordinates
374 in meters respectively, velocity in meters per second, and acceleration in meters per second squared,

375 enabling a comprehensive analysis of movement patterns and vehicle dynamics for control. In
376 addition to this, the datasets are utilized to track each vehicle's motion in highways.

377 In addition to the TGSIM datasets, the Phoenix dataset was also used for running simulations.
378 The Phoenix dataset has trajectory data including key attributes such as lateral and longitudinal
379 coordinates in meters, speed in meters per second, acceleration in meters per second squared
380 collected by the LiDAR sensors in the Waymo self-driving cars. By comparing simulations in the
381 Phoenix dataset with the TGSIM datasets, the simulated environments were analyzed to evaluate
382 the interactions between the ego vehicle and the surrounding vehicles in varying traffic conditions
383 ([Zhang et al. 2025](#)).

384 MATHEMATICAL FORMULATION

385 This study analyzes Constant Spacing Policy (CSP), Constant Time Headway (CTH), Traffic
386 Flow Stability (TFS), Constant Safety Factor (CSF), and the Intelligent Driver Model (IDM) The
387 aforementioned control spacing policies are widely used to safely maintain the distance between
388 vehicles which can be potentially used for safe autonomous driving.

389 The CSP model maintains fixed longitudinal gaps between the ego and the leader vehicles,
390 commonly used in vehicle platooning. The CTH model dynamically adjusts the following distance
391 based on the time interval between vehicles. The TFS policy aims to stabilize traffic flow and
392 mitigate stop-and-go traffic waves. The CSF policy prioritizes maintaining safety and to mitigate
393 collision avoidance by dynamically adjusting inter-vehicle spacings. Lastly, the IDM dynamically
394 adjusts inter-vehicle gaps based on the velocity difference to the leading vehicle, incorporating both
395 acceleration and deceleration dynamics to model realistic driving behavior.

396 This study conducts a thorough analysis of optimizing the calibration performance of control
397 spacing models, providing a comprehensive assessment of vehicle interactions on roadways. By
398 examining dynamic behavior, the study evaluates how various control strategies influence traffic
399 flow efficiency, safety, and stability.

400 **Constant Spacing Policy**

401 The Constant Spacing Policy (CSP) maintains a constant spacing between the vehicles from the
402 preceding vehicle with a low computation load ([Wu et al. 2020](#)). The spacing error variable δ_i for
403 the Constant Spacing Policy can be defined as:

404
$$\delta_i = x_i - x_{i-1} + L \quad (1)$$

405 where x_i is the position of the ego vehicle and x_{i-1} is the position of the leading vehicle, and L being
406 the desired spacing. The control law used in this policy is defined as ([Swaroop and Hedrick 1999](#)) :

407
$$\ddot{x}_i = -k_v \dot{\delta}_i - k_p \delta_i \quad (2)$$

408 where k_v, k_p are constants and $\dot{\delta}_i$ is the relative speed between the ego and the leader vehicles.

409 **Constant Time Headway Policy**

410 To ensure that the desired spacing increases proportionally with the speed, the Constant Time
411 Headway (CTH) dynamically adjusts inter-vehicle spacing in proportion to vehicle speed based
412 on the time headway between the ego and the leader vehicles ([Wu et al. 2020](#)). The spacing error
413 variable δ_i for the Constant Time Headway policy can be defined as:

414
$$\delta_i = x_i - x_{i-1} + h v_i + d_{min} \quad (3)$$

415 where d_{min} is the safety distance between the ego and the leader vehicles, h is the time headway
416 between two vehicles, and v_i is the speed of the i-th vehicle,. The control law used in this policy is
417 defined as ([Ioannou and Chien 1993](#)):

418
$$\ddot{x}_i = -\frac{1}{h}(\dot{\epsilon}_i + \lambda \delta_i) \quad (4)$$

419 where $\dot{\epsilon}$ is the rate of change for the spacing error, and λ is an arbitrary constant.

420 **Traffic Flow Stability Spacing Policy**

421 However, the main challenge of the CTH spacing policy is that the stabilizing the traffic flow is
 422 not guaranteed. To resolve this issue, the Traffic Flow Stability (TFS) spacing policy was devised.
 423 The TFS spacing policy was designed based on the Greenshield's relation, providing better traffic
 424 flow stabilization while ensuring safety ([Wu et al. 2020](#)). The spacing error variable δ_i used for the
 425 Traffic Flow Stability spacing policy can be defined as:

$$426 \quad \delta_i = x_i - x_{i-1} + \frac{1}{\rho_m(1 - \frac{v_h}{v_f})} \quad (5)$$

427 where ρ_m is the traffic density, v_f is the speed parameter, v_i is the speed of the i-th vehicle. The
 428 control law used in this policy is defined as ([Wang and Rajamani 2004a](#)) :

$$429 \quad \ddot{x}_i = -\rho_m(v_f - v_i)(1 - \frac{v_i}{v_f})(\dot{\epsilon}_i + \lambda\delta_i) \quad (6)$$

430 where $\dot{\epsilon}$ is the rate of change of spacing error, λ is the control gain and δ_i is the spacing error of the
 431 i-th vehicle.

432 **Constant Safety Factor Policy**

433 Safety is an inevitable factor that must be taken account for autonomous driving. To mitigate the
 434 possibility of road collisions and to improve driving safety, the Constant Safety Factor (CSF) spacing
 435 policy was proposed. Specifically, the emergency braking process was meticulously analyzed for
 436 the CSF policy ([Wu et al. 2020](#)). The spacing error variable δ_i used for the Constant Safety Factor
 437 policy can be defined as:

$$438 \quad \delta_i = x_i - x_{i-1} + d_{min} + t_d v + K D_{stop} \quad (7)$$

439 where t_d is the time delay, K is the safety factor and the stopping distance D_{Stop} defined as:

$$440 \quad D_{stop} = -\frac{v_i^2}{2j_i} \quad (8)$$

441 where j_i is the max deceleration value of the i -th value set as -7.32 m/s^2 . The control law used in
 442 this policy is defined as (Zhao and El Kamel 2010) :

443

$$\ddot{x}_i = -\frac{\dot{\epsilon}_i + \lambda \delta_i}{t_d - \frac{\gamma}{j_i} \dot{x}_i} \quad (9)$$

444 where λ is a positive control gain, t_d is the time delay in the longitudinal control system, γ is the
 445 safety coefficient, and j_i is the average deceleration value of the i -th vehicle during the maximum
 446 brake action.

447 **Intelligent Driver Model**

448 The Intelligent Driver Model (IDM) is a notable model to emulate human driving behavior using
 449 microscopic traffic properties. The spacing s between the ego vehicle and the leader vehicle can be
 450 defined as (Treiber et al. 2000):

451

$$s = x_i - x_{i-1} \quad (10)$$

452 where x_i and x_{i-1} are the position of the ego vehicle and the leader vehicle respectively. The relative
 453 velocity Δv is defined as:

454

$$\Delta v = v_i - v_{i-1} \quad (11)$$

455 where v_i is the speed of the ego vehicle and v_{i-1} is the speed of the leader vehicle. The acceleration
 456 formula can be defined as:

457

$$\dot{v} = a \left(1 - \left(\frac{v}{v_0} \right)^4 - \left(\frac{s^*(v, \Delta v)}{s} \right)^2 \right) \quad (12)$$

458 where v is the velocity of the ego vehicle, v_0 is the desired velocity, T is the safe time headway, a is
 459 the maximum acceleration, s is the spacing between vehicles. The desired spacing $s^*(v, \Delta v)$ can be
 460 calculated by using the following formula below:

461

$$s^*(v, \Delta v) = s_0 + T v - \frac{v \Delta v}{2\sqrt{ab}} \quad (13)$$

462 where s_0 is the minimum safe distance between vehicles, and b is the comfortable deceleration.

463 The analysis of the aforementioned spacing policies evaluate the ability to emulate real-world
 464 traffic dynamics effectively. This includes assessing the holistic impact on traffic flow stability, safety,
 465 efficiency, and adaptability to diverse traffic conditions. By analyzing the various spacing policies,
 466 the study provides a comprehensive analysis of each model's performance with the requirements
 467 of modern control systems, offering guidance for optimizing control strategies in both normal and
 468 complex driving scenarios to enhance the overall safety and efficiency of simulating trajectories for
 469 autonomous vehicles.

470 **PARAMETER OPTIMIZATION**

471 The genetic algorithm was leveraged in this study to determine the optimal parameters for each
 472 control spacing policy to model the car-following simulation. The algorithm iteratively evaluates
 473 possible solutions based on a fitness function that minimizes speed deviation between the simulated
 474 follower and the target follower. Through selection, crossover, and mutation, the population evolves
 475 over multiple generations to converge toward an optimal set of control parameters for each control
 476 spacing policy during calibration.

477 **Fitness Function**

478 The fitness function evaluates the effectiveness of the car-following model parameters by
 479 comparing simulated speed profiles with target speeds and minimizing the difference between the
 480 two variables. Multiple error metrics were integrated to quantify the deviation between the simulated
 481 follower generated by the control parameters and the target follower. Lower deviation indicates
 482 better adherence to the desired trajectory, leading to a higher fitness score. This approach ensures
 483 that the optimized parameters conduce to optimal results.

484

$$\Delta v = v_{sim} - v_{target} \quad (14)$$

485 where v_{sim}, v_{target} are the speed of the simulated follower and the target follower respectively. In
 486 addition to this, the error metrics which are Mean Squared Error (MSE), Root Mean Squared Error
 487 (RMSE), Mean Absolute Error (MAE), Mean Absolute Percentage Error (MAPE), Normalized Root
 488 Mean Squared Error (NRMSE), Sum of Squared Errors (SSE), R^2 value, Speed Deviation Penalty,
 489 Total Difference, and the fitness function $f(x)$ are calculated as by using the following formulas.

$$490 \text{MSE} = \frac{1}{N} \sum_{i=1}^N (\Delta v_i)^2 \quad (15)$$

$$491 \text{RMSE} = \sqrt{\text{MSE}} \quad (16)$$

$$492 \text{MAE} = \frac{1}{N} \sum_{i=1}^N |\Delta v_i| \quad (17)$$

$$493 \text{MAPE} = \frac{100}{N} \sum_{i=1}^N \left| \frac{\Delta v_i}{v_{target}} \right| \quad (18)$$

$$494 \text{NRMSE} = \frac{\text{RMSE}}{\max(v_{target}) - \min(v_{target})} \quad (19)$$

$$495 \text{SSE} = \sum_{i=1}^N (\Delta v_i)^2 \quad (20)$$

$$496 R^2 = 1 - \frac{\text{SSE}}{\sum_{i=1}^N (v_{target_i} - \bar{v}_{target})^2} \quad (21)$$

$$497 \sigma = \sum_{i=0}^N (v_{sim_i} - v_{target_i})^2 \quad (22)$$

$$498 \text{Total Difference} = \sum_{i=1}^N |\Delta v_i| \quad (23)$$

499

$$f(x) = \frac{1}{\sigma + 10^{-6}} \quad (24)$$

500

Genetic Algorithm

501 The genetic algorithm used in this study initializes a certain number of individuals with random
 502 values within the specified parameter ranges given an appropriate population size. For each iteration,
 503 the genetic algorithm runs for a set number of generations, computing fitness values and ranking
 504 individuals accordingly. The top $\frac{N}{2}$ individuals are selected, and the crossover operation is performed
 505 by swapping segments between two parents. The mutation step introduces a random adjustment
 506 of either -0.1 or 0.1 to the offspring to introduce noise. The new population was formed with
 507 these offspring, iteratively refining the parameters during the optimization process. This calibration
 508 effectively optimizes the parameters needed for the car-following model for each spacing policy
 509 ([Thede 2004](#)).

510

Car-following Behavior

511 The car-following behavior calculates the desired position depending on the control spacing
 512 policy being used initially, then the gap distance between the ego and the leader vehicle is calculated
 513 by using the following formula:

514

$$\Delta_i = x_i - x_{i-1} \quad (25)$$

515 where x_i is the ego vehicle and x_{i-1} is the leader vehicle. The safety distance is then calculated
 516 based on the control spacing model being used. The parameters are then fed into the function
 517 which calculates the acceleration a of the vehicle for the specific control policy being leveraged.
 518 The respective position and the speed are updated using the calibrated values. The speed of the
 519 simulated vehicle is updated by the following equation:

520

$$v_{i+1} = v_i + at \quad (26)$$

Algorithm 1 Genetic Algorithm for Car-Following Model Optimization

```
1: Input: Population size  $N$ , number of generations  $G$ 
2: Initialize: Generate  $N$  individuals with random values in the parameter ranges:
3: for each generation  $g = 1$  to  $G$  do
4:   Evaluate fitness: Compute fitness for each individual
5:   Sort population: Rank individuals based on fitness
6:   Select parents: Choose top  $N/2$  individuals
7:   Crossover: Generate offspring by swapping parts of two parents
8:   for each offspring do
9:     Select crossover point randomly
10:    Create child solutions:

$$\text{child}_1 = (\text{parent}_1[:, \text{crossover\_point}], \text{parent}_2[\text{crossover\_point}:])$$


$$\text{child}_2 = (\text{parent}_2[:, \text{crossover\_point}], \text{parent}_1[\text{crossover\_point}:])$$

11:  end for
12:  Mutation:
13:  for each child  $i$  do
14:    if random probability < mutation rate then
15:       $\text{child}_i = \text{child}_i + \delta, \quad \delta \sim U(-0.1, 0.1)$ 
16:    end if
17:  end for
18:  Replace population: Form the new population with parents and offspring
19: end for
20: Return: Best individual and associated error metrics
```

521 where v_i is the previous speed of the vehicle at time t seconds and the acceleration a is calibrated
522 using the respective control spacing policy. The position of the vehicle is then updated by the
523 following equation:

524

$$x_{i+1} = x_i + v_i t + \frac{1}{2} a t^2 \quad (27)$$

525 where x_{i+1} is the updated position of the simulated vehicle, and x_i is the previous position of the
526 simulated vehicle during the simulation process. The car-following model is called through the
527 optimization process, where the genetic algorithm calibrates the most optimal parameters for the
528 five of the control spacing policies.

529 The calibration process iteratively refines the parameters by minimizing the error between
530 simulated trajectories and the ground truth trajectory by calling the fitness function, allowing the

531 control spacing models to adapt to various traffic conditions and maintain stability to mitigate sudden
532 fluctuations in position and speed.

533 **RESULTS AND DISCUSSION**

534 For each control spacing policy, the genetic algorithm was used to calibrate the car-following
535 model. The sophisticated calibration process tunes the optimal parameters for each of the control
536 spacing policies by taking into account of the dynamic responses of surrounding vehicles under
537 various driving conditions. The I-294L1, I-90/94 and the Phoenix self-driving vehicle datasets were
538 used for calibrating the optimal parameters and simulating the trajectories generated by each control
539 spacing policy. The overall process is critical to enhance safety and maximize efficiency of traffic
540 flow for autonomous vehicles.

541 **Parameter Bound Selection and Limits**

542 To maintain consistency throughout the genetic algorithm calibration process, key parameters
543 such as population size, number of generations, and mutation rate were standardized across all
544 control spacing models analyzed in this study, as shown in Table 1. By fixing these parameters
545 needed for the genetic algorithm, this ensures that there are no inconsistencies in the optimization
546 process.

547 In addition to predetermining the parameters for the genetic algorithm, the parameter bounds
548 for each control spacing model were meticulously selected. The bounds were adjusted to preclude
549 unrealistic acceleration values from being used for the calibration process which could result in the
550 simulated vehicle making impulsive behavior or instability.

551 Standardizing the parametric limits ensures that comparisons between different control spacing
552 models remain valid and to prevent fluke during the calibration process. Additionally, maintaining
553 fixed parameter boundaries prevent anomalies during the calibration process, reducing the likelihood
554 of convergence to unrealistic or non-generalizable solutions. This approach enhances the reliability
555 of the simulated results.

556 **CSP Parameter Ranges**

557 For the Constant Spacing Policy (CSP), the position tracking constant (k_p), speed correction
558 coefficient (k_v), and desired spacing in meters ($S_{desired}$) parameters were optimized. The parameters
559 were assigned with appropriate ranges to facilitate the search for an optimal solution, as presented in
560 Table 2. The position tracking constant (k_p) adjusts the position relative to the target spacing. The
561 lower bound prevents slow reactions to ensure that the vehicle does not respond slowly to changes
562 in the leader vehicle's movement. The upper bound prevents excessive oscillations which could
563 lead to unstable behavior. The speed correction coefficient (k_v) adjusts the influence of the speed
564 differences between the ego and the leader vehicle. The minimum value ensures that the speed
565 correction is gradual while the upper value prevents the aggressive speed changes of the ego vehicle
566 which could lead to abrupt acceleration and deceleration cycles. The desired spacing ($S_{desired}$)
567 ensures the safe distance between the ego and the leader vehicle. The range allows the ego vehicle
568 not to follow too closely with the leader vehicle or unnecessarily slow down if the gap between the
569 ego and the leader vehicle is sufficient enough.

570 **CTH Parameter Ranges**

571 For the Constant Time Headway policy (CTH), the time headway in seconds (t_h), the minimum
572 safety distance in meters (d_{min}), and damping factor (λ) parameters were optimized. The parameters
573 were given an appropriate range respectively to ease finding an optimal solution shown in Table
574 3. The time headway (t_h) represents the time interval between the ego and the leader vehicles
575 to ensure safe following distance. The lower bound prevents the ego vehicle from dangerously
576 following closely to the leader vehicle. The upper bound ensures that the ego vehicle does not
577 unnecessarily slow down which could lead to big gaps causing inefficient traffic flow. The minimum
578 safety distance (d_{min}) is the safety buffer between the ego and the leader vehicles. The lower bound
579 is the minimum safe distance to ensure collisions and the upper bound prevents the ego vehicle from
580 unnecessarily slowing down. The damping factor (λ) stabilizes the vehicle's response to speed
581 fluctuations and time interval adjustments. The lower bound ensures that the damping factor is not
582 too weak while the upper bound prevents the adjustments being too aggressive, allowing smooth

583 transitions in vehicle dynamics.

584 **TFS Parameter Ranges**

585 For the Traffic Flow Stability policy (TFS), the traffic density in vehicles per meter (ρ_m),
586 damping factor (λ), and free flow speed in meters per second (v_f) parameters were optimized. The
587 parameters were given an appropriate range respectively to find an optimal solution shown in Table
588 4. The traffic density (ρ_m) ranges have been adjusted to ensure that the vehicle does not fall into
589 unrealistic free-flow speed conditions. The range was chosen to replicate the typical traffic density
590 along the freeways. The range for the damping factor (λ) balances the transient oscillations of the
591 model and to stabilize traffic flow. The lower bound of the free flow speed (v_f) reflects the moderate
592 traffic conditions and the upper bound represents the traffic conditions under optimal conditions.

593 **CSF Parameter Ranges**

594 For the Constant Safety Factor (CSF) policy, the safe distance in meters (d_{min}), damping factor
595 (λ), and braking dynamics coefficient (γ) were optimized to ensure safe and efficient car-following
596 behavior. The maximum deceleration for the i -th vehicle was set to -7.32 m/s^2 , while the time
597 delay was fixed at 0.05 seconds to account for realistic driver response times. Each parameter
598 was assigned an appropriate range to facilitate the search for an optimal solution, as presented
599 in Table 5. By calibrating these parameters using a genetic algorithm, the CSF policy enhances
600 stability and responsiveness, particularly in scenarios involving sudden braking or dense traffic
601 conditions. The range for the minimum safe distance (d_{min}) is slightly less than for other control
602 spacing policies because the safety factor (K) and braking dynamics coefficient (γ) were taken into
603 account for the CSF model. The damping factor smooths out the speed variations in response to the
604 changes in leader vehicle's movement. This range was chosen to enhance stability in both dense
605 traffic conditions and to prevent excessive stop-and-go oscillations. The lower bound of the safety
606 factor (K) ensures the vehicle reacts appropriately to speed changes while the upper bound prevents
607 aggressive responses to speed changes. The braking coefficient (γ) adjusts how aggressively the
608 braking is applied on the vehicle. The lower bound allows gradual braking adjustments while the
609 upper bound ensures braking in unprecedented situations.

610 **IDM Parameter Ranges**

611 Finally, for the Intelligent Driver Model (IDM), key parameters such as the minimum safe
612 distance (s_0) in meters, free-flow speed (v_0) in meters per second, time headway (T) in seconds,
613 maximum acceleration (a_{\max}) in m/s^2 , and comfortable deceleration (b) in m/s^2 were optimized
614 to ensure safe and efficient car-following behavior. Each parameter was assigned a carefully chosen
615 range to balance realism and computational efficiency, facilitating the search for an optimal solution,
616 as presented in Table 6.

617 The chosen parameter ranges reflect realistic driving conditions and vehicle dynamics. The
618 maximum acceleration range of 0.1 to 3.0 m/s^2 accounts for the diversity in vehicle performance,
619 from low-powered cars to high-performance vehicles. The desired velocity (v_0) is set between
620 10.0 and 30.0 m/s to cover typical urban and highway speed limits. The minimum spacing (s_0) is
621 constrained between 3.0 and 6.0 meters, ensuring that vehicles maintain a reasonable gap even at
622 low speeds. A time headway (T) range of 0.5 to 3.0 seconds accommodates variations in driver
623 behavior, from aggressive to conservative following. Finally, the comfortable deceleration (b) is
624 limited between 0.5 and 3.0 m/s^2 to capture a balance between smooth and emergency braking
625 scenarios. By calibrating the chosen ranges for the parameters using a genetic algorithm, the IDM
626 framework enhances stability and responsiveness, particularly in challenging traffic conditions such
627 as sudden braking events or high-density congestion.

628 After determining the appropriate parameter ranges for optimization, the genetic algorithm
629 calibrated the car-following model for each control spacing policy. High-fidelity Interstate highway
630 datasets were utilized to model the simulated trajectories, ensuring realistic traffic conditions.
631 Through iterative evolution, the genetic algorithm performed multiple mutations and crossovers,
632 refining the intrinsic parameter values to achieve optimal performance. The final set of optimized
633 parameters was selected based on their ability to enhance vehicle stability, responsiveness, and
634 overall traffic efficiency.

635 **Simulated Trajectories**

636 The position-versus-time and speed-versus-time graphs were plotted to visualize the behavior
637 of the simulated follower vehicle in relation to both the leader vehicle and the target vehicle under
638 the various control spacing policies implemented. The following plots illustrate how the follower
639 vehicle adjusts its position and velocity over time in response to changes in the leader's motion,
640 allowing for a comparative analysis of the effectiveness of each spacing policy. Each graph assesses
641 the ability of each policy to maintain safe following distances, minimizing speed fluctuations, and
642 ensuring smooth acceleration and deceleration transitions.

643 **CSP I-294 Simulated Results**

644 For the Constant Spacing Policy (CSP), the simulated results for the I-294 dataset are illustrated
645 in Figures 1 through 6. Overall, the CSP policy effectively aligns the simulated trajectories with the
646 target trajectories, demonstrating strong consistency in position tracking. However, minor speed
647 deviations were observed during the simulation, where the model occasionally followed the leader
648 vehicle's speed pattern or slightly deviated from the target vehicle's speed profile. These variations
649 suggest that small adjustments in the CSP model's responsiveness may be necessary to better adapt
650 to dynamic traffic conditions.

651 The optimized parameter ranges for the CSP policy in the I-294L1 dataset are shown in Figure
652 7. The desired spacing ($S_{desired}$) had the largest range, strongly indicating variability among the
653 optimized values and suggesting that vehicle spacing preferences fluctuate across different driving
654 conditions. Conversely, the control gains (k_v) and (k_p) were tightly clustered at lower values,
655 ensuring consistent stability in vehicle acceleration and deceleration behavior.

656 Figure 8 shows that the distributions of (k_v) and (k_p) are skewed to the right, indicating that
657 most optimized values are concentrated near the lower end of the range but with occasional higher
658 values. The ($S_{desired}$) is skewed to the left, showing that while some vehicles can maneuver traffic
659 with relatively smaller gaps, in some situations, the vehicles may need larger spacing. The wide
660 spread in ($S_{desired}$) suggests that variations in traffic density and driving behavior strongly influence
661 optimal spacing. These observations indicate that CSP maintains consistent vehicle control while

662 allowing adaptive spacing flexibility, making it suitable for highway driving scenarios with varying
663 traffic densities.

664 **CSP I-90/94 Simulated Results**

665 The simulated results for the I-90/94 dataset are presented in Figure 9 using the Constant Spacing
666 Policy (CSP) model. As shown in Figure 9(a), the simulated follower vehicle tracks the target
667 follower with minimal deviation, demonstrating strong CSP model performance on the I-90/94
668 highway dataset. Although a slight position deviation is observed for vehicle 195 in Figure 9(b), the
669 simulated follower closely tracks the target speed profile overall, indicating reliable model behavior
670 under varying traffic conditions.

671 The optimized parameter ranges for the I-90/94 dataset using the CSP policy, illustrated in
672 Figure 10, presents a significant variation across parameters. The desired spacing ($S_{desired}$) shows
673 the largest range, suggesting variability in vehicle gap preferences, which could be influenced by
674 traffic density and individual driving behaviors. In contrast, the control gains (k_v) and (k_p) remain
675 tightly clustered, indicating consistent vehicle response and stability in acceleration and deceleration
676 adjustments.

677 Figure 11 further reveals that the parameters follow discrete distributions, highlighting the
678 presence of distinct optimized values rather than a continuous spread. The narrow range of (k_v)
679 and (k_p) ensures the uniformity in control behavior, ensuring reliable adjustments in response to
680 speed changes. Meanwhile, the broader distribution of ($S_{desired}$) suggests that while most vehicles
681 maintain a consistent following distance, some scenarios demand significantly larger gaps to ensure
682 safe and stable car-following behavior. These findings indicate that CSP effectively maintains
683 consistent vehicle dynamics while allowing adaptability in spacing preferences, ensuring reliability
684 for highway driving conditions.

685 **CSP Phoenix Simulated Results**

686 The simulated results for the Phoenix dataset are presented in Figure 12 using the Constant
687 Spacing Policy (CSP) model. As shown in Figure 12(a) and Figure 12(c), the simulated follower
688 closely aligns with the calibrated position and speed of the target follower for vehicle 13 in Run

689 6 and vehicle 2 in Run 9NS. Minor deviations were observed for vehicle 2 in Run 9ES, shown
690 in Figure 12(b), where the speed tracking slightly diverged from the target profile. These results
691 demonstrate that the CSP model performs reliably under varying traffic scenarios in the Phoenix
692 dataset.

693 The optimized parameter ranges for the CSP policy in the Phoenix dataset, as shown in Figure
694 13, highlight contrasts in parameter ranges. The desired spacing ($S_{desired}$) exhibits wider range
695 compared to the tightly clustered values of the control gains (k_v) and (k_p). This suggests that
696 vehicles demonstrate more variability in maintaining inter-vehicle distances, potentially due to
697 differences in traffic flow conditions and driver behaviors unique to the Phoenix dataset.

698 Figure 14 shows that the optimized parameters follow discrete distributions, with values
699 concentrated at specific points rather than being continuously spread. The clustering of (k_v)
700 and (k_p) indicates that acceleration and speed control adjustments remain relatively stable across
701 different scenarios, ensuring uniform response characteristics. Conversely, the broader distribution
702 of ($S_{desired}$) implies that spacing preferences are more dynamic, possibly adapting to varying traffic
703 densities and driving patterns. These findings suggest that while CSP effectively maneuvers the
704 vehicle control dynamics, allowing flexibility in spacing between vehicles under the Phoenix dataset.

705 CTH I-294L1 Simulated Results

706 For the Constant Time Headway (CTH) policy, the simulated results for the I-294L1 dataset
707 are presented in Figures 15 through 20. By dynamically adjusting the time intervals, the CTH
708 model was able to closely track the target trajectories across a variety of traffic conditions. Despite
709 some speed variations between the simulated follower and the target follower, the position tracking
710 remained consistently accurate, demonstrating the effectiveness of the CTH strategy in maintaining
711 safe and efficient vehicle following.

712 The optimized parameter ranges for the CTH model in the I-294L1 dataset, as shown in Figure
713 21, strongly indicate variation among key parameters used for optimization. The parameters (t_h) and
714 d_{min} exhibit broad ranges, suggesting significant tuning variability in time headway and minimum
715 distance settings. In contrast, (λ) is tightly clustered around low values, indicating a high degree of

716 stability and minimal fluctuation during optimization.

717 Figure 22 illustrates the skewed distributions of (t_h) and (d_{min}) , where certain values appear
718 more frequently than others, implying potential biases toward specific parameter configurations.
719 The distribution of (λ) is notably sparse. This suggests that while (t_h) and d_{min} require more
720 flexible adjustments to accommodate diverse traffic conditions, (λ) remains relatively fixed to ensure
721 consistency in the CTH model's control strategy, indicating that the CTH model effectively adapts
722 to different traffic dynamics.

723 **CTH I-90/94 Simulated Results**

724 The simulated results for the I-90/94 dataset are presented in Figure 23 using the Constant Time
725 Headway (CTH) policy. As shown in Figure 23(a) and Figure 23(b), the controller is able to track
726 the position of the target vehicles with minimal deviations in the speed patterns. These results
727 demonstrate that the CTH model maintains effective longitudinal control even under varying traffic
728 conditions present in the I-90/94 dataset.

729 The optimized parameter ranges for the CTH model in the I-90/94 dataset illustrates variations
730 across different parameters. Figure 24 shows that (t_h) and (d_{min}) have relatively wider ranges,
731 indicating greater flexibility in their tuning to adapt to different traffic conditions. In contrast, (λ)
732 remains tightly clustered around low values, suggesting that this parameter is more constrained to
733 ensure stability in the model's response.

734 Furthermore, Figure 25 shows that all optimized parameters follow discrete distributions,
735 implying that the parameter tuning converges to specific values rather than a continuous range. This
736 suggests that certain parameter settings are more favorable for achieving stable and reliable control
737 behavior under varying highway conditions. The narrow clustering of (λ) shows that consistent
738 system dynamics were maintained, while the broader range of (t_h) and (d_{min}) indicates that time
739 headway and minimum distance must be more adaptable to handling fluctuations in traffic flow.

740 **CTH Phoenix Simulated Results**

741 The simulated results for the Constant Time Headway (CTH) model on the Phoenix dataset
742 are presented in Figure 26. As shown in Figure 26(a) and Figure 26(d), the simulated follower

743 closely aligns with the calibrated position and speed of the target follower for vehicle 13 in Run 6
744 and vehicle 2 in Run 9NS. However, noticeable speed deviations are observed for vehicle 31 in Run
745 8EW and vehicle 2 in Run 9ES, illustrated in Figure 26(b) and Figure 26(c), respectively. These
746 deviations suggest that factors such as acceleration responsiveness or varying traffic conditions may
747 have influenced the model’s performance in maintaining consistent speed tracking.

748 The optimized parameter ranges for the CTH model in the Phoenix dataset illustrate variations
749 across parameters. As shown in Figure 27, (d_{min}) shows a relatively wider range compared to (t_h) ,
750 indicating flexible tuning parameters. In contrast, the (λ) values remain tightly clustered, suggesting
751 minimal variations in controlling fluctuating behavior and ensuring system stability.

752 Figure 28 clearly shows a bimodal distribution for both (t_h) and (d_{min}) , implying that certain
753 values are consistently favored during calibration. This strongly indicates the presence of distinct
754 driving conditions or vehicle behaviors leading to the model selecting preferred parameter values
755 over others. The narrow spread of (λ) maintains smooth acceleration adjustments and prevents
756 excessive fluctuations in speed. These findings highlight the importance of adaptive tuning for (t_h)
757 and (d_{min}) , while (λ) remains a relatively stable control parameter across different scenarios.

758 **TFS I-294L1 Simulated Results**

759 For the Traffic Flow Stability (TFS) policy, the simulated results for the I-294L1 dataset are
760 presented in Figures 29 through 35. The TFS model focuses on stabilizing traffic flow by minimizing
761 sudden changes in position and speed. As shown in the figures, the simulated follower vehicles
762 generally align well with the target trajectories, demonstrating effective performance in maintaining
763 both position and speed tracking. Some minor deviations are observed, which may be attributed to
764 dynamic traffic fluctuations and the stability control parameters. Overall, the TFS model exhibits
765 strong consistency in promoting stable and safe longitudinal vehicle behavior across different runs
766 and vehicles.

767 The optimized parameter ranges for the TFS model in the I-294L1 dataset shows variability
768 across different parameters, as shown in Figure 36. The (v_f) had the largest range, indicating
769 significant variations in free-flow speed due to changing traffic conditions and driving behaviors. In

770 contrast, (ρ_m) and (λ) remain tightly clustered, suggesting that these parameters have maintained
771 consistency during the calibration process.

772 Figure 37 illustrates the skewness of the parameter distributions. Specifically, (ρ_m) and (λ) are
773 left-skewed, implying that lower values were more frequently selected during optimization, while
774 (v_f) is skewed to the right, indicating that higher values were more frequently selected, reflecting
775 varying traffic flow speeds and free-flow conditions in the dataset.

776 **TFS I-90/94 Simulated Results**

777 The simulated results for the Traffic Flow Stability (TFS) model on the I-90/94 dataset are
778 presented in Figure 38. As shown in Figure 38(a) and Figure 38(b), the TFS controller successfully
779 tracks the target vehicle positions with minimal deviations in the speed patterns. These results
780 demonstrate the robustness of the TFS model in maintaining stable longitudinal behavior under the
781 traffic conditions present on the I-90/94 highway.

782 The optimized parameter ranges for the TFS model in the I-90/94 dataset, as shown in Figure
783 39, indicate small variations across parameters. While (v_f) has the highest range, the numeric
784 values remain tightly clustered, suggesting a consistent free-flow speed across different calibration
785 instances. Similarly, (ρ_m) and (λ) maintain low ranges with minimal variation, indicating that traffic
786 flow sensitivity and stability adjustments are relatively uniform across different traffic scenarios.

787 Figure 40 illustrates that the optimized parameters follow discrete distributions, with values
788 concentrated at specific numeric points rather than being continuously spread out. This pattern
789 suggests that the model favors specific parameter values during optimization, potentially due to
790 traffic dynamics constraints in the dataset. The consistent clustering of (ρ_m) and (λ) stabilizes flow
791 fluctuations, while the narrow distribution of (v_f) suggests the vehicle maintaining appropriate
792 free-flow speed.

793 **TFS Phoenix Simulated Results**

794 The simulated results for the Traffic Flow Stability (TFS) model on the Phoenix dataset are
795 presented in Figure 41. As shown in Figure 41(a) and Figure 41(c), the simulated follower closely
796 aligns with the calibrated position and speed of the target follower for vehicle 13 in Run 6 and

797 vehicle 2 in Run 9NS. Minor deviations are observed for vehicle 2 in Run 9ES, as shown in
798 Figure 41(b), where the simulated speed slightly diverges from the target profile. Overall, the TFS
799 model demonstrates reliable performance in maintaining stable longitudinal control across various
800 traffic conditions in the Phoenix dataset.

801 The optimized parameter ranges for the TFS model in the Phoenix dataset, as shown in Figure 42,
802 indicate minimal variability across parameters. The free-flow speed (v_f) remains highly consistent,
803 with values tightly clustered around a high range, suggesting a uniform traffic flow behavior in the
804 dataset. Similarly, (ρ_m) and (λ) has minimal variation, indicating that traffic density sensitivity and
805 stability adjustments remain relatively consistent across different calibration runs.

806 Figure 43 shows that the optimized parameters follow discrete distributions, with values
807 concentrated at specific numeric points rather than being continuously spread. This pattern suggests
808 that the TFS model consistently selects specific parameter values during calibration. The narrow
809 clustering of (ρ_m) and (λ) suggests that their roles in regulating flow stability remain uniform,
810 maintaining consistent traffic dynamics.

811 **CSF I-294L1 Simulated Results**

812 For the Constant Safety Factor (CSF) policy, the simulated results for the I-294L1 dataset are
813 presented in Figures 44 through 50. The CSF model adjusts the trajectories by incorporating safety
814 parameters, including the safety factor (K), braking coefficient (γ), and minimum safety distance
815 (d_{min}), to better align the simulated follower with the target vehicle. As observed across the figures,
816 the CSF model demonstrates strong consistency in position tracking, closely following the target
817 trajectories. Although some variations in speed profiles are observed, the overall behavior remains
818 stable, highlighting the effectiveness of the CSF model in promoting safe and stable longitudinal
819 control.

820 The optimized parameter ranges for the CSF model in the I-294L1 dataset, as illustrated in Figure
821 51, shows significant variability across parameters. The parameter (d_{min}) has the highest degree
822 of variability, with a broad range, indicating that the minimum desired spacing fluctuates based
823 on different traffic conditions. Conversely, (K), (λ), and (γ) has relatively narrower distributions.

824 However, multiple outliers have been shown, suggesting that in certain calibration cases, the
825 optimization process deviated from the primary values chosen.

826 Figure 52 shows that the distribution of (λ) is skewed to the right, with lower values appearing
827 more frequently, indicating that most optimized solutions favor smaller stability coefficients.
828 Similarly, the majority of (γ) values are concentrated near zero, implying that braking adjustments
829 were not applied aggressively in the optimization process. Additionally, the multi-modal distributions
830 observed for (d_{min}) and (K) suggest that multiple distinct parameter groupings exist, due to safety
831 adjustments in response to varied traffic conditions.

832 The outliers in (K) , (λ) , and (γ) suggests occasional extreme parameter values, which may be
833 the result of unusual traffic flow dynamics or specific cases where it was necessary for the CSF
834 model to apply more aggressive control actions to maintain stability and safety. It is indicative that
835 the outlier numeric values had to be used in response of the vehicle trying to adjust the unusual
836 traffic condition to ensure safety in driving.

837 **CSF I-90/94 Simulated Results**

838 The simulated results for the Constant Safety Factor (CSF) model on the I-90/94 dataset are
839 presented in Figure 53. As shown in Figure 53(a) and Figure 53(b), the CSF controller successfully
840 tracks the target vehicle positions with minimal deviations in the speed profiles. These results
841 highlight the robustness of the CSF model in maintaining safe longitudinal behavior under the
842 varying traffic conditions observed on the I-90/94 highway.

843 The optimized parameter ranges for the CSF model in the I-90/94 dataset, as depicted in Figure
844 54, show limited variation across most parameters. The parameter (d_{min}) shows the widest range,
845 evidently showing the CSF policy's emphasis on maintaining safe following distances under varying
846 traffic conditions. Conversely, the parameters (K) , (λ) , and (γ) remain tightly clustered, suggesting
847 that the control gains and braking adjustments are more consistent across different scenarios.

848 Figure 55 shows that the optimized parameters follow discrete distributions, with values
849 concentrated at specific numerical points rather than being continuously spread out. The tight
850 clustering of (K) and (λ) indicates that the model consistently stabilizes around particular parameter

values, minimizing fluctuations in vehicle behavior. Similarly, (γ) is clustered near the value zero, suggesting that braking was not applied too aggressively. Thus, smoother deceleration patterns were shown rather than abrupt braking maneuvers.

There were no outlier values during calibration which suggests that the optimization process consistently converged to a well-defined solution space, ensuring the model's reliability in maintaining stable vehicle behavior. However, the broader spread in (d_{min}) indicates greater adaptability in determining safe spacing based on external traffic conditions.

CSF Phoenix Simulated Results

The simulated results for the Constant Safety Factor (CSF) model on the Phoenix dataset are presented in Figure 56. As shown in Figure 56(a) and Figure 56(c), the simulated follower closely aligns with the calibrated position and speed of the target follower for vehicle 13 in Run 6 and vehicle 2 in Run 9NS. Minor deviations are observed for vehicle 2 in Run 9ES, as illustrated in Figure 56(b), where the speed profile slightly diverges from the target trajectory. Overall, the CSF model demonstrates strong consistency in maintaining safe and stable vehicle following behavior across different traffic conditions in the Phoenix dataset.

The optimized parameter ranges for the CSF policy in the Phoenix dataset are presented in Figure 57, showing variations across different parameters. The parameter (K) exhibits the widest range, suggesting greater adaptability in control response under varying traffic conditions. The parameter (d_{min}) also shows a relatively wide range, indicating that safe following distances are more flexible just like the parameter (K) .

In contrast, the parameters (λ) and (γ) remain tightly clustered, suggesting consistent values across different calibration scenarios. An outlier value is observed in (d_{min}) , indicating a result where the optimized parameter deviates from the general range calibrated. Figure 58 illustrates that the parameters follow discrete distributions, with values concentrated at specific points rather than being continuously spread out. This suggests that the optimization process consistently favors certain parameter values.

877 **IDM I-294L1 Simulated Results**

878 For the Intelligent Driver Model (IDM), the simulated results for the I-294L1 dataset are
879 presented in Figures 59 through 64. The IDM model calibrates vehicle trajectories by optimizing key
880 parameters, including the maximum acceleration (a), desired speed (v_0), minimum safe distance
881 (s_0), time headway (T), and comfortable deceleration (b). As shown in the figures, the simulated
882 follower trajectories closely align with the target position profiles, demonstrating strong position
883 tracking performance. Although minor variations in speed are observed across some runs, the
884 overall longitudinal behavior remains stable, indicating the robustness of the IDM calibration under
885 varying traffic conditions.

886 The optimized parameter ranges for the IDM model in the I-294L1 dataset are presented in
887 Figure 65, illustrating variability among different parameters. The desired speed (v_0) exhibits the
888 widest range, indicating that vehicles frequently operate at a relatively higher free-flow speed while
889 maintaining safe following distances while driving in the highway.

890 Conversely, the parameters maximum acceleration (a_{max}), time headway (T), and comfortable
891 deceleration (b) remain tightly clustered at the calibrated ranges, implying that the system requires
892 minimal abrupt adjustments to ensure stability in traffic flow. The safe distance between vehicles
893 (s_0) also shows moderate variability, indicating some adaptation in stopping distances based on
894 different driving behaviors.

895 Furthermore, as illustrated in Figure 66, the optimized parameters follow multi-modal distribu-
896 tions, reflecting the diversity in driving behavior across different traffic conditions. This suggests
897 that the calibration process effectively captures varying driving tendencies, from conservative to
898 more aggressive driving styles, ensuring robust adaptation of the IDM model in real-world highway
899 environments.

900 **IDM I-90/94 Simulated Results**

901 The simulated results for the Intelligent Driver Model (IDM) on the I-90/94 dataset are presented
902 in Figure 67. As shown in Figure 67(a) and Figure 67(b), the IDM controller successfully tracks the
903 target vehicle positions with minimal deviations in the speed profiles. These results demonstrate the

904 effectiveness of the IDM calibration in maintaining stable longitudinal behavior across the varying
905 traffic conditions observed on the I-90/94 highway.

906 The optimized parameter ranges for IDM in the I-90/94 dataset are illustrated in Figure 68,
907 showing variations across different parameters. The desired speed (v_0) has the widest range,
908 suggesting that vehicles frequently travel at free-flow speed while maintaining a safe following
909 distance. This indicates flexibility in speed adaptations.

910 In contrast, parameters such as the maximum acceleration (a_{max}), time headway (T), and
911 comfortable deceleration (b) remain within a tighter range, implying consistent acceleration and
912 braking behaviors with minimal sudden adjustments required for maintaining traffic stability. The
913 safe distance between vehicles (s_0) also shows some variation, indicating variations in stopping
914 distance.

915 Furthermore, as shown in Figure 69, the optimized parameters follow multi-modal distributions,
916 suggesting varying driving behaviors across different traffic conditions. This variability of optimized
917 parameters calibrated shows both conservative and aggressive driving behaviors replicating real-
918 world driving patterns.

919 **IDM Phoenix Simulated Results**

920 The simulated results for the Intelligent Driver Model (IDM) on the Phoenix dataset are presented
921 in Figure 70. As shown in Figure 70(a) and Figure 70(d), the simulated follower closely aligns with
922 the calibrated position and speed of the target follower for vehicle 13 in Run 6 and vehicle 2 in Run
923 9NS. Noticeable speed deviations are observed for vehicle 31 in Run 8EW and vehicle 2 in Run 9ES,
924 as illustrated in Figure 70(b) and Figure 70(c). These deviations may reflect the IDM's sensitivity to
925 varying traffic conditions and highlight areas for potential model refinement in future work.

926 The optimized parameter ranges for the Intelligent Driver Model (IDM) in the Phoenix dataset are
927 presented in Figure 71, revealing notable variability across different parameters. The desired speed
928 (v_0) exhibits the largest variation, indicating that vehicles operate under diverse speed conditions,
929 due to differences in driver behavior or fluctuating traffic conditions.

930 In contrast, the maximum acceleration (a_{max}), time headway (T), and comfortable deceleration

931 (b) remain within a more confined range. These results indicate that vehicles experience fewer
932 abrupt acceleration and braking maneuvers, leading to more stable and safe car-following behavior.
933 The safe distance between vehicles (s_0) is relatively small, strongly suggesting that vehicles maintain
934 close following distances, due to high-density traffic scenarios in the dataset.

935 Additionally, some outliers are observed across multiple parameters during calibration, particu-
936 larly in (s_0) and (b), suggesting that some vehicles had more aggressive or conservative driving
937 behaviors. These outliers indicate that the vehicles had to adjust its control inputs in response
938 to exceptional cases of unusually short headways or higher deceleration rates, deviating from the
939 general traffic trend.

940 Figure 72 presents the distributions of the calibrated IDM parameters following multi-modal
941 distributions. The distribution of (v_0) suggests distinct driving groups with varying speed values,
942 while the acceleration and deceleration distributions indicate that most of the times, the vehicles
943 adhere to a common driving pattern with minimal deviations. Multiple peaks of the calibrated
944 parameters in the histograms shows the adaptability of IDM in replicating changing driving behaviors,
945 ensuring a realistic representation of vehicle interactions within the Phoenix dataset.

946 Model Comparison

947 The control spacing policies were evaluated across the major highway datasets from I-294L1,
948 I-90/94 and Phoenix. While the genetic algorithm calibrates the optimal parameters for each control
949 spacing policy, the fitness function calculates the critical error metrics including the Mean Squared
950 Error (MSE), Root Mean Squared Error (RMSE), Mean Absolute Error (MAE), Mean Absolute
951 Percentage Error (MAPE), Normalized Root Mean Squared Error (NMSE), Sum of Squared Errors
952 (SSE), and R^2 values to evaluate how well the model can align the simulated trajectories with
953 the target trajectories. Results for each model in different highway datasets are shown in Table
954 7. The overall performance of the models across all the highway datasets are presented in Table
955 8. These results implies that some control spacing policies may be suitable for varying traffic
956 environments where other control spacing policies may be more appropriate for less fluctuating
957 traffic environments.

958 The CSP model has demonstrated stable performance across all the highway datasets used for
959 this study, showing relatively low error values across all metrics calculated by the fitness function.
960 The CSP model had the lowest RMSE value of 0.243 and the highest R^2 value of 0.964 in the
961 I-90/94 dataset, indicating a strong alignment between the simulated and target trajectories during
962 calibration. However, the MAPE value of 8.949% in the Phoenix dataset suggests that the CSP
963 model struggles to encounter the external factors that affect the inter-vehicular spacing. Stability has
964 been maintained most of the time and the simulated trajectories generated by the CSP model closely
965 aligns then target trajectories.

966 The CTH model had slightly higher MSE and RMSE values compared to the CSP model,
967 suggesting a marginally weaker performance in tracking the trajectories. The high MAPE value of
968 13.556% in the I-90/94 dataset implies that the model is more sensitive to speed variations between
969 the leading and the surrounding vehicles. However, the R^2 values consistently remained above
970 0.940, suggesting that the simulated trajectories were mostly well-aligned with the target trajectories.
971 Overall, the CTH model performs comparably to CSP, although it appears more prone to speed
972 variations in dynamic traffic conditions.

973 The TFS policy had the highest error metrics across all the highway datasets, evidently showing
974 higher deviations between the simulated and target trajectories. The MAPE value of 15.661% in
975 the I-90/94 dataset is significantly higher than the MAPE values of other models, suggesting that
976 the TFS policy struggles to maintain stability in congested traffic conditions. While the R^2 values
977 remain above 0.91, the high error values indicate that the TFS policy is less robust compared to the
978 other models considered in this study. This suggests that TFS may not effectively handle variations
979 in acceleration and deceleration, leading to suboptimal trajectory predictions. Additionally, the
980 relatively higher RMSE and SSE values indicate that errors accumulate over time, further impacting
981 the ability to align itself with the target trajectory in dynamic highway conditions.

982 The CSF policy has demonstrated overall stable performance by effectively balancing vehicle
983 dynamics and trajectory alignment while prioritizing safety. The CSF model achieved the lowest
984 RMSE value of 0.566 in the I-294L1 dataset, indicating strong predictive accuracy. However, the

985 relatively high MAPE value of 14.533% suggests some difficulties in adapting to varying traffic
986 conditions, particularly in scenarios with abrupt speed changes. Despite this, with R^2 values
987 consistently above 0.94, the CSF model exhibits strong target trajectory tracking capabilities, making
988 it a reliable choice for maintaining smooth and stable traffic flow.

989 The IDM model has exhibited mixed performance across the highway datasets. The model
990 achieved the lowest RMSE value of 0.204 in the I-90/94 dataset, indicating strong trajectory
991 alignment under relatively stable highway conditions. However, the model struggled in the Phoenix
992 dataset, where it had the highest MAPE value of 22.665%, suggesting significant difficulty in
993 adapting to varying traffic conditions and external disturbances. The overall R^2 values remained
994 high, exceeding 0.92, showing that IDM can reasonably align itself with the target trajectories.
995 However, the MAPE in Phoenix indicates that IDM may be more sensitive to traffic flow variations
996 and abrupt decelerations compared to CSP and CSF.

997 Based on the overall dataset performance, it can be determined that the CSP and CSF policies
998 are the most reliable control spacing models, having the lowest RMSE values and consistently high
999 R^2 scores. The CTH model, while effective, appears less suitable for scenarios involving frequent
1000 speed variations. In contrast, the TFS policy displayed the highest errors, indicating challenges
1001 in maintaining stable traffic flow. The IDM model, while effective in stable conditions, exhibited
1002 higher errors in complex environments, suggesting a need for refined parameter tuning. Given the
1003 calibration results, CSP and CSF are the most appropriate models for simulating car-following
1004 behavior, while the TFS policy and IDM may require additional modifications to improve robustness
1005 in fluctuating traffic conditions.

1006 CONCLUSION

1007 Maintaining appropriate and safe following gap between vehicles is critical for autonomous
1008 vehicles. The five most commonly used policies which are Constant Spacing Policy (CSP), Constant
1009 Time Headway (CTH), Traffic Flow Stability (TFS), Constant Safety Factor (CSF), and the Intelligent
1010 Driver Model (IDM) were calibrated using the genetic algorithm to find the optimized parameters for
1011 each policy respectively using the highway datasets from I-294L1, I-90/94, and Phoenix self-driving

1012 vehicle trajectories for simulating the control spacing models.

1013 The simulated plots comparing trajectories generated by control spacing policies and observed
1014 trajectories illustrate how well the generated trajectories align with the observed trajectories. The
1015 trajectories simulated by CSP and CSF models closely aligned with the observed vehicle trajectories,
1016 demonstrating minimal perturbations in both position and speed of the vehicles across stable traffic
1017 conditions. These models effectively and safely maintained the inter-vehicular spacing, achieving
1018 smoother trajectory profiles with fewer oscillations. Conversely, the IDM model showed greater
1019 variability in certain conditions but the model was able to replicate realistic acceleration and
1020 deceleration patterns, making it suitable for dynamic traffic environments. The CTH model was
1021 effective in controlled conditions, despite the occasional perturbations under conditions where the
1022 surrounding vehicles rapidly change their speeds. The TFS model consistently demonstrated higher
1023 trajectory errors, particularly in congested scenarios, indicating its limited reliability in complex
1024 traffic conditions.

1025 The performance of the control spacing policies were contingent on the traffic conditions. The
1026 CSP and CSF policies were relatively more reliable by consistently achieving the lowest Root
1027 Mean Squared Error (RMSE) and highest R^2 values. The CSP model showed stable performance
1028 under low-density highway conditions by maintaining uniform spacing effectively with minimal
1029 perturbations. The CSF policy was determined to be performing optimally in high-density scenarios,
1030 effectively managing critical safety concerns, including abrupt acceleration and braking events, due
1031 to the dynamic safety-margin adjustments.

1032 While the CTH policy showed robust performance similar to CSP in stable conditions, it
1033 exhibited increased sensitivity and higher errors under scenarios with significant speed variations.
1034 This highlights the model's limitations in adapting swiftly to fluctuating speeds. The TFS policy
1035 consistently produced higher errors across datasets, reflecting challenges in handling congested,
1036 dynamically complex traffic scenarios, and thus was the least reliable for accurate trajectory
1037 prediction.

1038 The Intelligent Driver Model (IDM) demonstrated strong performance in accurately simulating

realistic driver behavior across diverse traffic conditions. The IDM model was also able to replicate smooth acceleration and deceleration patterns. However, achieving optimal performance required precise calibration, especially in high-density scenarios where dynamic adjustments to speed and spacing are frequent.

In conclusion, the CSP model is recommended for scenarios prioritizing stability and uniform traffic flow, typically in lower-density highway conditions. The CSF policy is effective when safety considerations need to be prioritized, such as dense traffic conditions requiring frequent adjustments to spacing between the surrounding vehicles. The IDM is suitable for accurately modeling realistic vehicle behavior but demands meticulous calibration. Future research should explore hybrid spacing policies integrating multiple strategies to integrate individual models for more adaptive and resilient implementations for self-driving technology.

ACKNOWLEDGMENTS

Special thanks to Assistant Professor Alireza Talebpour at the Department of Civil and Environmental Engineering at the University of Illinois at Urbana-Champaign, and to Post Doc Gihyeob An for the suggested control spacing models that were analyzed for this research. This research was supported by the U.S. National Science Foundation under the Centers of Research Excellence in Science and Technology (CREST) program, award number 2112650.

REFERENCES

- Ammourah, R., Beigi, P., Fan, B., Hamdar, S. H., Hourdos, J., Hsiao, C.-C., James, R., Khajeh-Hosseini, M., Mahmassani, H. S., Monzer, D., Radvand, T., Talebpour, A., Yousefi, M., and Zhang, Y. (2024). “Introduction to the third generation simulation dataset: Data collection and trajectory extraction.” *Transportation Research Record*, 1–17.
- An, G. and Talebpour, A. (2019). “Lane-changing trajectory optimization to minimize traffic flow disturbance in a connected automated driving environment.” *2019 IEEE Intelligent Transportation Systems Conference (ITSC)*, 1794–1799.
- An, G. and Talebpour, A. (2022). “Vehicle platooning control for merge coordination: A hybrid

- 1065 acc-dmpc approach.” *2022 IEEE 25th International Conference on Intelligent Transportation*
1066 *Systems (ITSC)*, 1611–1616.
- 1067 Barooah, P., Mehta, P. G., and Hespanha, J. P. (2009). “Mistuning-based control design to improve
1068 closed-loop stability margin of vehicular platoons.” *IEEE Transactions on Automatic Control*,
1069 54(9), 2100–2113.
- 1070 Cesari, G., Schildbach, G., Carvalho, A., and Borrelli, F. (2017). “Scenario model predictive control
1071 for lane change assistance and autonomous driving on highways.” *IEEE Intelligent Transportation*
1072 *Systems Magazine*, 9(3), 23–35.
- 1073 Chen, D., Ahn, S., Chitturi, M., and Noyce, D. (2018). “Truck platooning on uphill grades
1074 under cooperative adaptive cruise control (cacc).” *Transportation Research Part C: Emerging*
1075 *Technologies*, 94, 50–66 ISTTT22.
- 1076 Ciuffo, B., Mattas, K., Makridis, M., Albano, G., Anesiadou, A., He, Y., Josvai, S., Komnos, D.,
1077 Pataki, M., Vass, S., and Szalay, Z. (2021). “Requiem on the positive effects of commercial
1078 adaptive cruise control on motorway traffic and recommendations for future automated driving
1079 systems.” *Transportation Research Part C: Emerging Technologies*, 130, 103305.
- 1080 D. SWAROOP, J.K. HEDRICK, C. C. C. and IOANNOU, P. (1994). “A comparision of spacing and
1081 headway control laws for automatically controlled vehicles.” *Vehicle System Dynamics*, 23(1),
1082 597–625.
- 1083 Darbha, S. and Rajagopal, K. (1999). “Intelligent cruise control systems and traffic flow stability.”
1084 *Transportation Research Part C: Emerging Technologies*, 7(6), 329–352.
- 1085 Delis, A., Nikолос, I., and Papageorgiou, M. (2015). “Macroscopic traffic flow modeling with
1086 adaptive cruise control: Development and numerical solution.” *Computers and Mathematics with*
1087 *Applications*, 70(8), 1921–1947.
- 1088 Delpiano, R., Herrera, J. C., Laval, J., and Coeymans, J. E. (2020). “A two-dimensional car-following
1089 model for two-dimensional traffic flow problems.” *Transportation Research Part C: Emerging*
1090 *Technologies*, 114, 504–516.
- 1091 Donà, R., Mattas, K., He, Y., Albano, G., and Ciuffo, B. (2022). “Multianticipation for string

- 1092 stable adaptive cruise control and increased motorway capacity without vehicle-to-vehicle
1093 communication.” *Transportation Research Part C: Emerging Technologies*, 140, 103687.
- 1094 Federal Highway Administration (FHWA) (2024). “Third Generation Simulation (TGSIM) Data.
1095 Available: https://catalog.data.gov/dataset/?q=Third+Generation+Simulation+Data&sort=views_recent+desc&publisher=Federal+Highway+Administration&organization=dot-gov&ext_location=&ext_bbox=&ext_prev_extent=. Accessed: Nov.
1096
1097
1098 25, 2024.
- 1099 Ioannou, P. and Chien, C. (1993). “Autonomous intelligent cruise control.” *IEEE Transactions on*
1100 *Vehicular Technology*, 42(4), 657–672.
- 1101 Ioannou, P., Xu, Z., Eckert, S., Clemons, D., and Sieja, T. (1993). “Intelligent cruise control: theory
1102 and experiment.” *Proceedings of 32nd IEEE Conference on Decision and Control*, 1885–1890
1103 vol.2.
- 1104 Kesting, A., Treiber, M., Schönhof, M., and Helbing, D. (2008). “Adaptive cruise control design for
1105 active congestion avoidance.” *Transportation Research Part C: Emerging Technologies*, 16(6),
1106 668–683.
- 1107 Kilic, I., Yazici, A., Yildiz, O., Özçelikors, M., and Ondoan, A. (2015). “Intelligent adaptive cruise
1108 control system design and implementation.” *2015 10th System of Systems Engineering Conference,*
1109 *SoSE 2015*, 232–237.
- 1110 Li, P. Y. and Shrivastava, A. (2002). “Traffic flow stability induced by constant time headway policy
1111 for adaptive cruise control vehicles.” *Transportation Research Part C: Emerging Technologies*,
1112 10(4), 275–301.
- 1113 Li, S., Li, K., Rajamani, R., and Wang, J. (2011). “Model predictive multi-objective vehicular
1114 adaptive cruise control.” *IEEE Transactions on Control Systems Technology*, 19(3), 556–566.
- 1115 Luu, D. L., Lupu, C., Ismail, L. S., and Alshareefi, H. (2020). “Spacing control of cooperative
1116 adaptive cruise control vehicle platoon.” *2020 IEEE International Conference on Automation,*
1117 *Quality and Testing, Robotics (AQTR)*, 1–6.
- 1118 Maxim, A., Caruntu, C. F., and Lazar, C. (2017). “Cruise and headway control for vehicle platooning

- 1119 using a distributed model predictive control algorithm.” *2017 21st International Conference on*
1120 *System Theory, Control and Computing (ICSTCC)*, 146–151.
- 1121 Milanés, V., Shladover, S. E., Spring, J., Nowakowski, C., Kawazoe, H., and Nakamura, M. (2014).
1122 “Cooperative adaptive cruise control in real traffic situations.” *IEEE Transactions on Intelligent*
1123 *Transportation Systems*, 15(1), 296–305.
- 1124 Moon, S., Moon, I., and Yi, K. (2009). “Design, tuning, and evaluation of a full-range adaptive
1125 cruise control system with collision avoidance.” *Control Engineering Practice*, 17(4), 442–455.
- 1126 Naus, G. J. L., Vugts, R. P. A., Ploeg, J., van de Molengraft, M. J. G., and Steinbuch, M. (2010).
1127 “String-stable cacc design and experimental validation: A frequency-domain approach.” *IEEE*
1128 *Transactions on Vehicular Technology*, 59(9), 4268–4279.
- 1129 Nilsson, P., Hussien, O., Balkan, A., Chen, Y., Ames, A. D., Grizzle, J. W., Ozay, N., Peng, H., and
1130 Tabuada, P. (2016). “Correct-by-construction adaptive cruise control: Two approaches.” *IEEE*
1131 *Transactions on Control Systems Technology*, 24(4), 1294–1307.
- 1132 Rajamani, R., Tan, H.-S., Law, B. K., and Zhang, W.-B. (2000). “Demonstration of integrated
1133 longitudinal and lateral control for the operation of automated vehicles in platoons.” *IEEE*
1134 *Transactions on Control Systems Technology*, 8(4), 695–708.
- 1135 Rajamani, R. and Zhu, C. (2002). “Semi-autonomous adaptive cruise control systems.” *Vehicular*
1136 *Technology, IEEE Transactions on*, 51, 1186 – 1192.
- 1137 Santhanakrishnan, K. and Rajamani, R. (2003). “On spacing policies for highway vehicle automation.”
1138 *IEEE Transactions on Intelligent Transportation Systems*, 4(4), 198–204.
- 1139 Sipahi, R., Niculescu, S.-I., and Delice, I. I. (2009). “Asymptotic stability of constant time headway
1140 driving strategy with multiple driver reaction delays.” *2009 American Control Conference*,
1141 4898–4903.
- 1142 Swaroop, D. and Hedrick, J. K. (1999). “Constant spacing strategies for platooning in automated
1143 highway systems.” *Journal of Dynamic Systems, Measurement, and Control*, 121(3), 462–470.
- 1144 Talebpour, A. and Mahmassani, H. S. (2016). “Influence of connected and autonomous vehicles on
1145 traffic flow stability and throughput.” *Transportation Research Part C: Emerging Technologies*,

- 1146 71, 143–163.
- 1147 Talebpour, A., Mahmassani, H. S., and Hamdar, S. H. (2018). “Effect of information availability
1148 on stability of traffic flow: Percolation theory approach.” *Transportation Research Part B:
1149 Methodological*, 117, 624–638 TRB:ISTTT-22.
- 1150 Talebpour, A., Mahmassani, H. S., and Hamdar, S. H. (2024). “Third generation simulation data
1151 (tgSim): A closer look at the impacts of automated driving systems on human behavior.” *Report
1152 No. FHWA-JPO-24-133*, Federal Highway Administration, University of Illinois at Urbana-
1153 Champaign, Urbana, Illinois 61801 (5). The project CORs were Rachel James and John Hourdos.
1154 The JPO Program Manager was Hyungjun Park.
- 1155 Thede, S. (2004). “An introduction to genetic algorithms.” *Journal of Computing Sciences in
1156 Colleges*, 20.
- 1157 Treiber, M., Hennecke, A., and Helbing, D. (2000). “Congested traffic states in empirical observations
1158 and microscopic simulations.” *Physical Review E*, 62(2), 1805–1824.
- 1159 van Arem, B., van Driel, C. J. G., and Visser, R. (2006). “The impact of cooperative adaptive cruise
1160 control on traffic-flow characteristics.” *IEEE Transactions on Intelligent Transportation Systems*,
1161 7(4), 429–436.
- 1162 Wang, J. and Rajamani, R. (2004a). “The impact of adaptive cruise control systems on highway
1163 safety and traffic flow.” *Proceedings of the Institution of Mechanical Engineers, Part D: Journal
1164 of Automobile Engineering*, 218(2), 111–130.
- 1165 Wang, J. and Rajamani, R. (2004b). “Should adaptive cruise-control systems be designed to maintain
1166 a constant time gap between vehicles?” *IEEE Transactions on Vehicular Technology*, 53(5),
1167 1480–1490.
- 1168 Wang, M., Hoogendoorn, S. P., Daamen, W., van Arem, B., and Happee, R. (2015). “Game theoretic
1169 approach for predictive lane-changing and car-following control.” *Transportation Research Part
1170 C: Emerging Technologies*, 58, 73–92.
- 1171 Wu, C., Xu, Z., Liu, Y., Fu, C., Li, K., and Hu, M. (2020). “Spacing policies for adaptive cruise
1172 control: A survey.” *IEEE Access*, 8, 50149–50162.

- 1173 Yanakiev, D. and Kanellakopoulos, I. (1995). “Variable time headway for string stability of automated
1174 heavy-duty vehicles.” *Proceedings of 1995 34th IEEE Conference on Decision and Control*,
1175 Vol. 4, 4077–4081 vol.4.
- 1176 Zhang, Y., Kosmatopoulos, B., Ioannou, P., and Chien, C. (1999). “Using front and back information
1177 for tight vehicle following maneuvers.” *IEEE Transactions on Vehicular Technology*, 48(1),
1178 319–328.
- 1179 Zhang, Y., Monzer, D., Li, N., Okoth, V., Chen, Z., Hsiao, C.-C., Radvand, T., Mahmassani, H. S.,
1180 Hamdar, S. H., and Talebpour, A. (2025). “Coexistence in motion: Unveiling the behavioral
1181 dynamics of humans and highly automated vehicles in naturalistic mixed traffic (01). Presented at
1182 the Transportation Research Board (TRB) 103rd Annual Meeting, Paper No. TRBAM-25-05831,
1183 Washington, D.C.
- 1184 Zhao, J. and El Kamel, A. (2010). “Coordinated throttle and brake fuzzy controller design for vehicle
1185 following.” *13th International IEEE Conference on Intelligent Transportation Systems*, 659–664.
- 1186 Zhao, S. and Zhang, K. (2020). “A distributionally robust stochastic optimization-based model
1187 predictive control with distributionally robust chance constraints for cooperative adaptive cruise
1188 control under uncertain traffic conditions.” *Transportation Research Part B: Methodological*, 138,
1189 144–178.
- 1190 Zheng, Y., Li, S. E., Li, K., Borrelli, F., and Hedrick, J. K. (2017). “Distributed model predictive
1191 control for heterogeneous vehicle platoons under unidirectional topologies.” *IEEE Transactions
1192 on Control Systems Technology*, 25(3), 899–910.
- 1193 Zhou, Y., Ahn, S., Chitturi, M., and Noyce, D. A. (2017). “Rolling horizon stochastic optimal
1194 control strategy for acc and cacc under uncertainty.” *Transportation Research Part C: Emerging
1195 Technologies*, 83, 61–76.

1196	List of Tables		
1197	1	Constant parameters for simulating the genetic algorithm.	49
1198	2	Parameter ranges for Constant Spacing Policy.	50
1199	3	Parameter ranges for Constant Time Headway policy.	51
1200	4	Parameter ranges for Traffic Flow Stability policy.	52
1201	5	Parameter ranges for Constant Safety Factor policy.	53
1202	6	Parameter ranges for Intelligent Driver Model.	54
1203	7	Performance comparison of different models on various datasets.	55
1204	8	Overall performance of models across the highway datasets.	56

TABLE 1. Constant parameters for simulating the genetic algorithm.

Parameter	Value
Population Size	100
Number of Generations	100
Mutation Rate	0.1

TABLE 2. Parameter ranges for Constant Spacing Policy.

Parameter	Range
k_p	(0.01, 1.5)
k_v	(0.01, 0.9)
S_{desired}	(2.5, 10.0)

TABLE 3. Parameter ranges for Constant Time Headway policy.

Parameter	Range
t_h	(1.5, 2.0)
d_{min}	(2.5, 3.5)
λ	$(1.0 \times 10^{-5}, 1.0 \times 10^{-4})$

TABLE 4. Parameter ranges for Traffic Flow Stability policy.

Parameter	Range
ρ_m	(0.10, 0.15)
λ	(0.10, 0.40)
v_f	(25.00, 35.00)

TABLE 5. Parameter ranges for Constant Safety Factor policy.

Parameter	Range
d_{min}	(2.50, 3.00)
λ	(0.01, 0.40)
K	(0.50, 3.00)
γ	(0.10, 0.50)

TABLE 6. Parameter ranges for Intelligent Driver Model.

Parameter	Range
a_{max}	(0.1, 3.0)
v_0	(10.0, 30.0)
s_0	(3.0, 6.0)
T	(0.5, 3.0)
b	(0.5, 3.0)

TABLE 7. Performance comparison of different models on various datasets.

Model	Dataset	Error	MSE	RMSE	MAE	MAPE	NRMSE	SSE	R ²
CSP	I-294L1	494.344	0.473	0.604	0.435	3.359	0.066	49.174	0.902
CSP	I-90/94	125.986	0.063	0.243	0.188	11.443	0.052	44.904	0.964
CSP	Phoenix	177.835	0.252	0.443	0.337	8.949	0.047	136.000	0.968
CTH	I-294L1	514.590	0.527	0.639	0.457	3.805	0.069	48.538	0.894
CTH	I-90/94	129.926	0.067	0.245	0.198	13.556	0.054	45.883	0.956
CTH	Phoenix	166.755	0.227	0.421	0.311	8.501	0.044	125.144	0.971
TFS	I-294L1	526.597	0.493	0.619	0.428	3.845	0.063	55.824	0.911
TFS	I-90/94	162.373	0.094	0.305	0.246	15.661	0.068	63.905	0.939
TFS	Phoenix	175.720	0.290	0.458	0.336	11.781	0.048	153.492	0.966
CSF	I-294L1	495.446	0.417	0.566	0.400	3.897	0.058	42.474	0.929
CSF	I-90/94	137.392	0.074	0.266	0.208	15.025	0.059	50.214	0.952
CSF	Phoenix	182.762	0.270	0.473	0.363	14.353	0.051	143.946	0.964
IDM	I-294L1	414.087	0.368	0.538	0.384	2.993	0.064	389.799	0.893
IDM	I-90/94	106.421	0.046	0.204	0.161	8.302	0.045	31.795	0.971
IDM	Phoenix	176.835	0.370	0.577	0.448	22.665	0.072	152.224	0.916

TABLE 8. Overall performance of models across the highway datasets.

Model	Error	MSE	RMSE	MAE	MAPE	NRMSE	SSE	R^2
CSP	266.055	0.263	0.430	0.320	7.917	0.055	232.296	0.945
CTH	270.424	0.274	0.435	0.322	8.621	0.056	241.246	0.940
TFS	288.230	0.293	0.461	0.337	10.429	0.060	265.179	0.939
CSF	271.867	0.254	0.435	0.324	11.092	0.056	229.596	0.948
IDM	232.448	0.261	0.440	0.331	11.320	0.060	191.273	0.927

1205 **List of Figures**

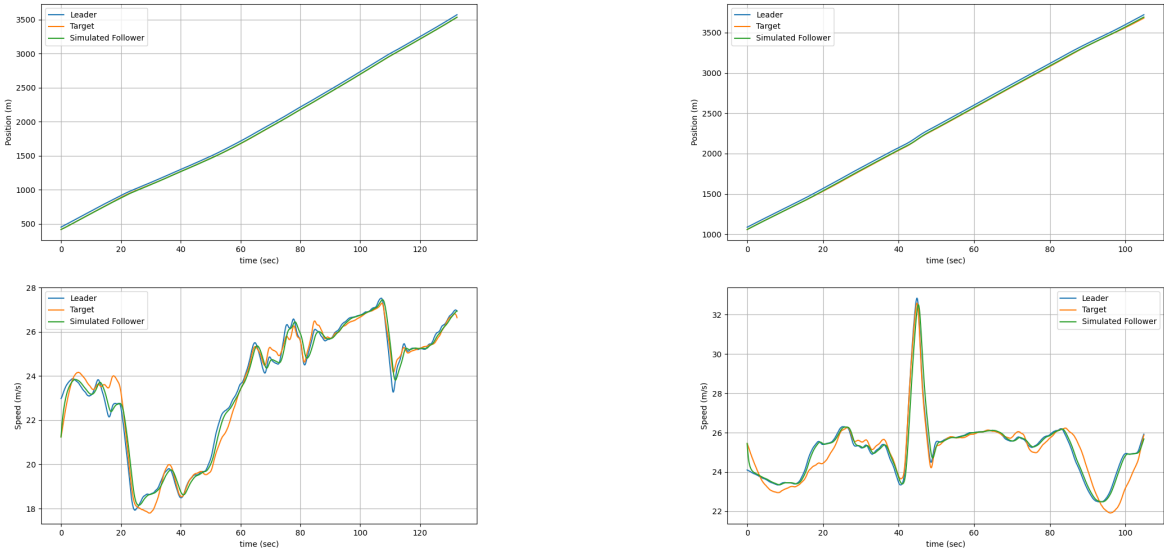
1206 1	Position and speed tracking results using the Constant Spacing Policy (CSP) model:	
1207 (a) Vehicle 11, Run 21; (b) Vehicle 11, Run 7.	62	
1208 2	Position and speed tracking results using the Constant Spacing Policy (CSP) model:	
1209 (a) Vehicle 12, Run 1; (b) Vehicle 19, Run 11; (c) Vehicle 19, Run 19.	63	
1210 3	Final position and speed tracking results using the Constant Spacing Policy (CSP)	
1211 model: (a) Vehicle 22, Run 11; (b) Vehicle 25, Run 19; (c) Vehicle 50, Run 20. . .	64	
1212 4	Position and speed tracking results using the Constant Spacing Policy (CSP) model	
1213 for the I-294L1 dataset: (a) Vehicle 51, Run 8; (b) Vehicle 54, Run 20; (c) Vehicle		
1214 56, Run 18.	65	
1215 5	Position and speed tracking results using the Constant Spacing Policy (CSP) model	
1216 for the I-294L1 dataset: (a) Vehicle 59, Run 18; (b) Vehicle 62, Run 8; (c) Vehicle		
1217 65, Run 8.	66	
1218 6	Position and speed tracking results using the Constant Spacing Policy (CSP) model	
1219 for the I-294L1 dataset: (a) Vehicle 8, Run 1; (b) Vehicle 9, Run 1.	67	
1220 7	Parameter ranges for Constant Spacing Policy (CSP) in the I-294L1 dataset.	68
1221 8	Parameter histogram for Constant Spacing Policy (CSP) in I-294L1 dataset.	69
1222 9	Simulated position and speed tracking using the Constant Spacing Policy (CSP)	
1223 model for the I-90/94 dataset: (a) Vehicle 5366, Run 1; (b) Vehicle 195, Run 2. . .	70	
1224 10	Parameter ranges for CSP in I-90/94.	71
1225 11	Parameter histogram for CSP in I-90/94.	72
1226 12	Simulated position and speed tracking using the Constant Spacing Policy (CSP)	
1227 model for the Phoenix dataset: (a) Vehicle 13, Run 6; (b) Vehicle 2, Run 9ES; (c)		
1228 Vehicle 2, Run 9NS.	73	
1229 13	Parameter ranges for CSP in Phoenix.	74
1230 14	Parameter histogram for CSP in Phoenix.	75

1231	15	Simulated position and speed tracking using the Constant Time Headway (CTH)	
1232		model For I-294L1 dataset: (a) Vehicle 11, Run 21; (b) Vehicle 11, Run 7.	76
1233	16	Performance of CTH model across different vehicles: (a) Vehicle 12, Run 1; (b)	
1234		Vehicle 19, Run 11; (c) Vehicle 19, Run 19.	77
1235	17	CTH model performance for vehicles 22, 25, and 35: (a) Vehicle 22, Run 11; (b)	
1236		Vehicle 25, Run 19; (c) Vehicle 35, Run 11.	78
1237	18	Simulated tracking results for CTH model: (a) Vehicle 50, Run 20; (b) Vehicle 51,	
1238		Run 8; (c) Vehicle 54, Run 20.	79
1239	19	CTH model results for vehicles 56, 59, and 62: (a) Vehicle 56, Run 18; (b) Vehicle	
1240		59, Run 18; (c) Vehicle 62, Run 8.	80
1241	20	Final comparison for CTH model: (a) Vehicle 65, Run 8; (b) Vehicle 9, Run 1. . .	81
1242	21	Parameter ranges for CTH in I-294L1 dataset.	82
1243	22	Parameter histogram for CTH in I-294L1 dataset.	83
1244	23	Simulated position and speed tracking using the Constant Time Headway (CTH)	
1245		model for the I-90/94 dataset: (a) Vehicle 5366, Run 1; (b) Vehicle 195, Run 2. .	84
1246	24	Parameter ranges for CTH in I-90/94.	85
1247	25	Parameter histogram for CTH in I-90/94.	86
1248	26	Simulated position and speed tracking using the Constant Time Headway (CTH)	
1249		model for the Phoenix dataset: (a) Vehicle 13, Run 6; (b) Vehicle 31, Run 8EW; (c)	
1250		Vehicle 2, Run 9ES; (d) Vehicle 2, Run 9NS.	87
1251	27	Parameter ranges for CTH in Phoenix.	88
1252	28	Parameter histogram for CTH in Phoenix.	89
1253	29	Simulated position and speed tracking using the Traffic Flow Stability (TFS) model:	
1254		(a) Vehicle 11, Run 21; (b) Vehicle 11, Run 7.	90
1255	30	TFS model tracking results: (a) Vehicle 17, Run 21; (b) Vehicle 19, Run 11; (c)	
1256		Vehicle 22, Run 11.	91
1257	31	Performance of TFS model for vehicles 25, 28, and 41.	92

1258	32	Tracking performance of the TFS model for vehicles 50, 51, and 54.	93
1259	33	TFS model tracking for vehicles 56, 59, and 62.	94
1260	34	Final comparison of the TFS model: (a) Vehicle 65, Run 8; (b) Vehicle 8, Run 1. .	95
1261	35	Position and speed for TFS for Vehicle 9 in Run 1 (I-294L1 dataset).	96
1262	36	Parameter ranges for TFS in I-294L1 dataset.	97
1263	37	Parameter histogram for TFS in I-294L1 dataset.	98
1264	38	Simulated position and speed tracking using the Traffic Flow Stability (TFS) model for the I-90/94 dataset: (a) Vehicle 5366, Run 1; (b) Vehicle 195, Run 2.	99
1265	39	Parameter ranges for TFS in I-90/94.	100
1266	40	Parameter histogram for TFS in I-90/94.	101
1267	41	Simulated position and speed tracking using the Traffic Flow Stability (TFS) model for the Phoenix dataset: (a) Vehicle 13, Run 6; (b) Vehicle 2, Run 9ES; (c) Vehicle	
1268		2, Run 9NS.	102
1269	42	Parameter ranges for TFS in Phoenix.	103
1270	43	Parameter histogram for TFS in Phoenix.	104
1271	44	Simulated position and speed tracking using the Constant Safety Factor (CSF) model: (a) Vehicle 11, Run 21; (b) Vehicle 11, Run 7.	105
1272	45	Performance of CSF model: (a) Vehicle 12, Run 1; (b) Vehicle 17, Run 7; (c)	
1273		Vehicle 19, Run 11.	106
1274	46	Tracking performance of the CSF model: (a) Vehicle 19, Run 19; (b) Vehicle 22,	
1275		Run 11; (c) Vehicle 24, Run 9.	107
1276	47	Simulated CSF results for vehicles 25, 28, and 50.	108
1277	48	CSF model tracking for vehicles 51, 54, and 56.	109
1278	49	Tracking results of the CSF model for vehicles 59, 62, and 65.	110
1279	50	Final comparison of CSF model tracking: (a) Vehicle 8, Run 1; (b) Vehicle 9, Run 1.111	
1280	51	Parameter ranges for CSF in I-294L1 dataset.	112
1281	52	Parameter histogram for CSF in I-294L1 dataset.	113

1285	53	Simulated position and speed tracking using the Constant Safety Factor (CSF) model for the I-90/94 dataset: (a) Vehicle 5366, Run 1; (b) Vehicle 195, Run 2.	114
1286	54	Parameter ranges for CSF in I-90/94.	115
1287	55	Parameter histogram for CSF in I-90/94.	116
1288	56	Simulated position and speed tracking using the Constant Safety Factor (CSF) model for the Phoenix dataset: (a) Vehicle 13, Run 6; (b) Vehicle 2, Run 9ES; (c) Vehicle 2, Run 9NS.	117
1289	57	Parameter ranges for CSF in Phoenix.	118
1290	58	Parameter histogram for CSF in Phoenix.	119
1291	59	Simulated position and speed tracking using the Intelligent Driver Model (IDM): (a) Vehicle 11, Run 21; (b) Vehicle 12, Run 1.	120
1292	60	Performance of IDM: (a) Vehicle 17, Run 21; (b) Vehicle 19, Run 11; (c) Vehicle 22, Run 11.	121
1293	61	IDM tracking results: (a) Vehicle 25, Run 19; (b) Vehicle 28, Run 9; (c) Vehicle 35, Run 11.	122
1294	62	Simulated IDM performance for vehicles 41, 50, and 51.	123
1295	63	Tracking results of IDM model: (a) Vehicle 54, Run 20; (b) Vehicle 56, Run 18; (c) Vehicle 59, Run 18.	124
1296	64	Final IDM model tracking comparison: (a) Vehicle 62, Run 8; (b) Vehicle 65, Run 8; (c) Vehicle 9, Run 1.	125
1297	65	Parameter ranges for IDM in I-294L1 dataset.	126
1298	66	Parameter histogram for IDM in I-294L1 dataset.	127
1299	67	Simulated position and speed tracking using the Intelligent Driver Model (IDM) for the I-90/94 dataset: (a) Vehicle 5366, Run 1; (b) Vehicle 195, Run 2.	128
1300	68	Parameter ranges for IDM in I-90/94.	129
1301	69	Parameter histogram for IDM in I-90/94.	130

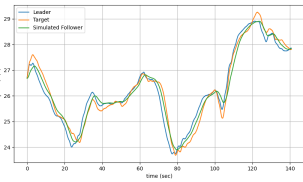
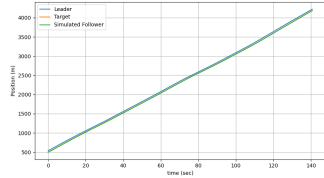
1311	70	Simulated position and speed tracking using the Intelligent Driver Model (IDM) for	
1312		the Phoenix dataset: (a) Vehicle 13, Run 6; (b) Vehicle 31, Run 8EW; (c) Vehicle 2,	
1313		Run 9ES; (d) Vehicle 2, Run 9NS.	131
1314	71	Parameter ranges for IDM in Phoenix.	132
1315	72	Parameter histogram for IDM in Phoenix.	133



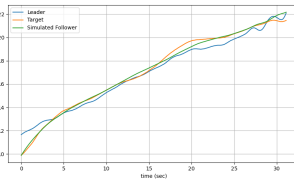
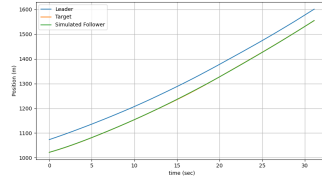
(a) Vehicle 11, Run 21

(b) Vehicle 11, Run 7

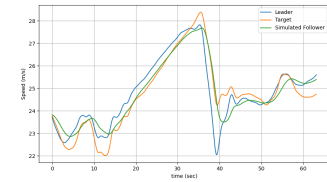
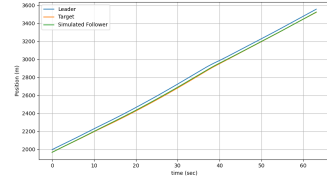
Fig. 1. Position and speed tracking results using the Constant Spacing Policy (CSP) model: (a) Vehicle 11, Run 21; (b) Vehicle 11, Run 7.



(a) Vehicle 12, Run 1

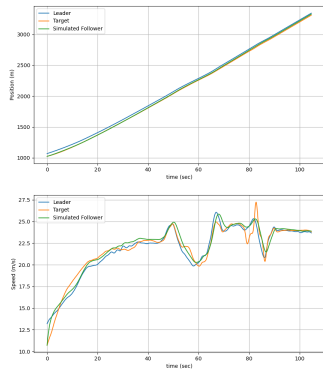


(b) Vehicle 19, Run 11

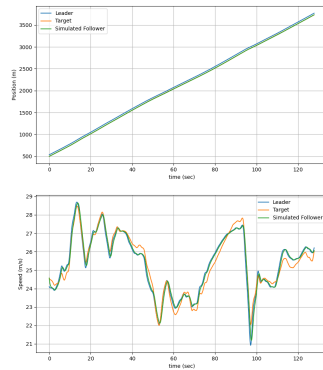


(c) Vehicle 19, Run 19

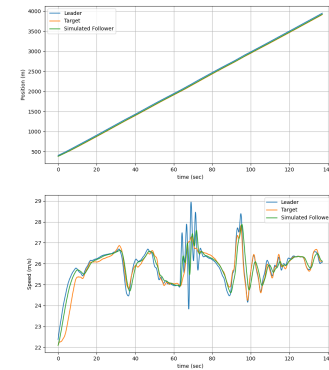
Fig. 2. Position and speed tracking results using the Constant Spacing Policy (CSP) model: (a) Vehicle 12, Run 1; (b) Vehicle 19, Run 11; (c) Vehicle 19, Run 19.



(a) Vehicle 22, Run 11

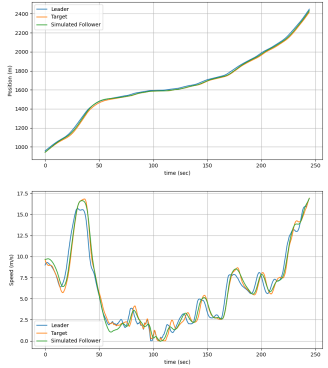


(b) Vehicle 25, Run 19

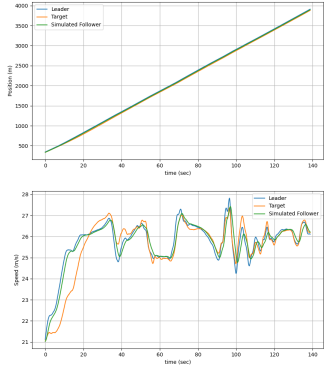


(c) Vehicle 50, Run 20

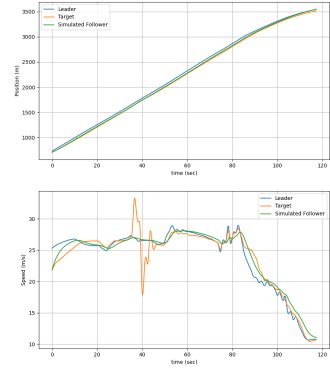
Fig. 3. Final position and speed tracking results using the Constant Spacing Policy (CSP) model:
 (a) Vehicle 22, Run 11; (b) Vehicle 25, Run 19; (c) Vehicle 50, Run 20.



(a) Vehicle 51, Run 8

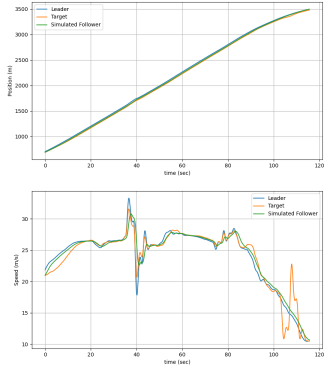


(b) Vehicle 54, Run 20

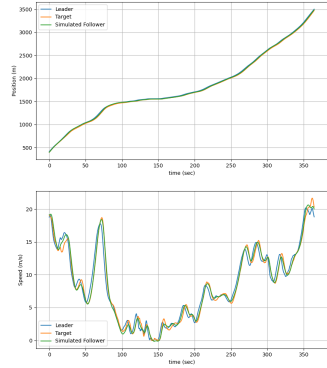


(c) Vehicle 56, Run 18

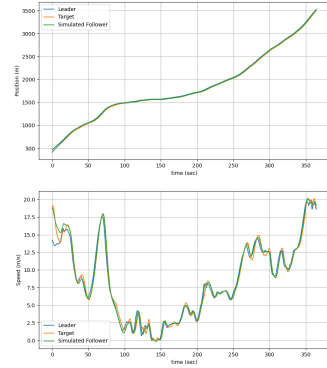
Fig. 4. Position and speed tracking results using the Constant Spacing Policy (CSP) model for the I-294L1 dataset: (a) Vehicle 51, Run 8; (b) Vehicle 54, Run 20; (c) Vehicle 56, Run 18.



(a) Vehicle 59, Run 18

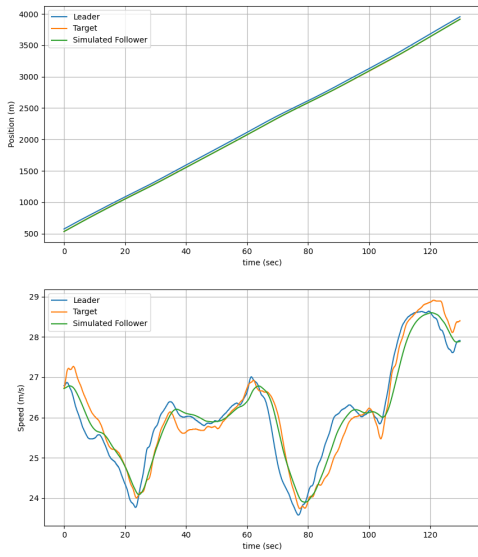


(b) Vehicle 62, Run 8

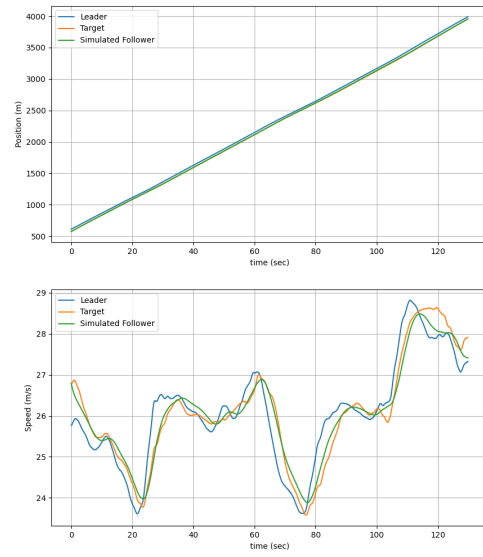


(c) Vehicle 65, Run 8

Fig. 5. Position and speed tracking results using the Constant Spacing Policy (CSP) model for the I-294L1 dataset: (a) Vehicle 59, Run 18; (b) Vehicle 62, Run 8; (c) Vehicle 65, Run 8.



(a) Vehicle 8, Run 1



(b) Vehicle 9, Run 1

Fig. 6. Position and speed tracking results using the Constant Spacing Policy (CSP) model for the I-294L1 dataset: (a) Vehicle 8, Run 1; (b) Vehicle 9, Run 1.

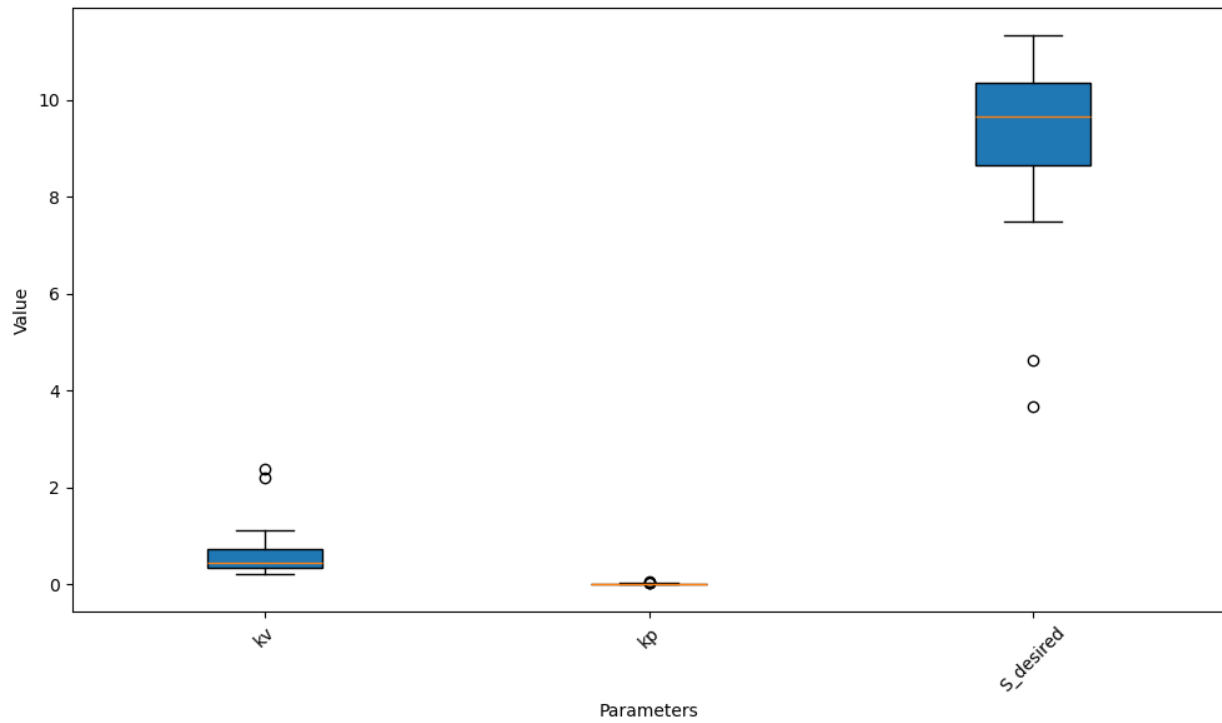


Fig. 7. Parameter ranges for Constant Spacing Policy (CSP) in the I-294L1 dataset.

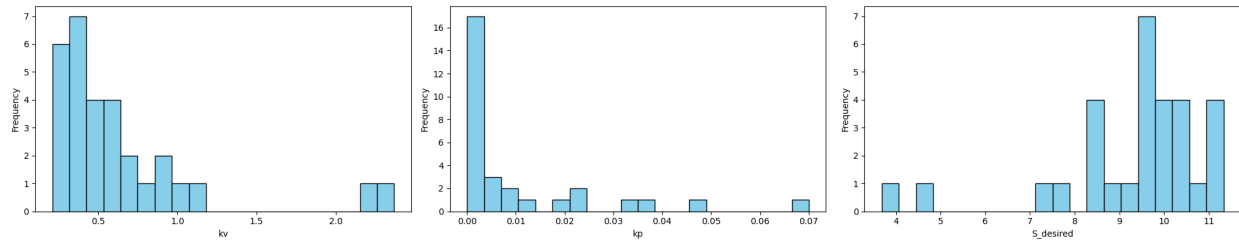
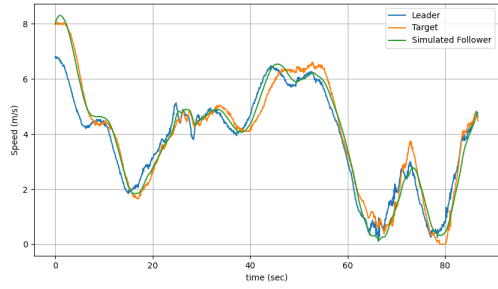
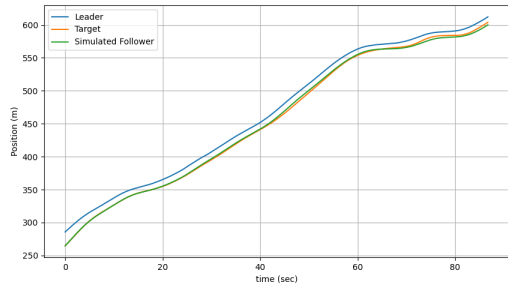
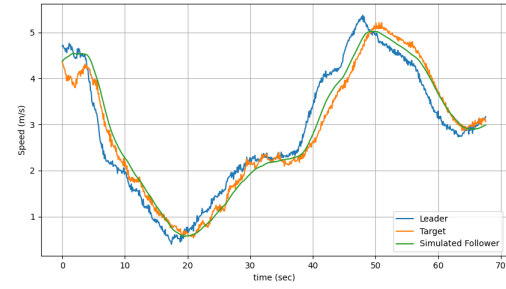
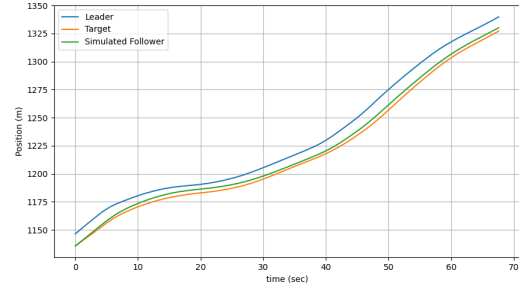


Fig. 8. Parameter histogram for Constant Spacing Policy (CSP) in I-294L1 dataset.



(a) Vehicle 5366, Run 1



(b) Vehicle 195, Run 2

Fig. 9. Simulated position and speed tracking using the Constant Spacing Policy (CSP) model for the I-90/94 dataset: (a) Vehicle 5366, Run 1; (b) Vehicle 195, Run 2.

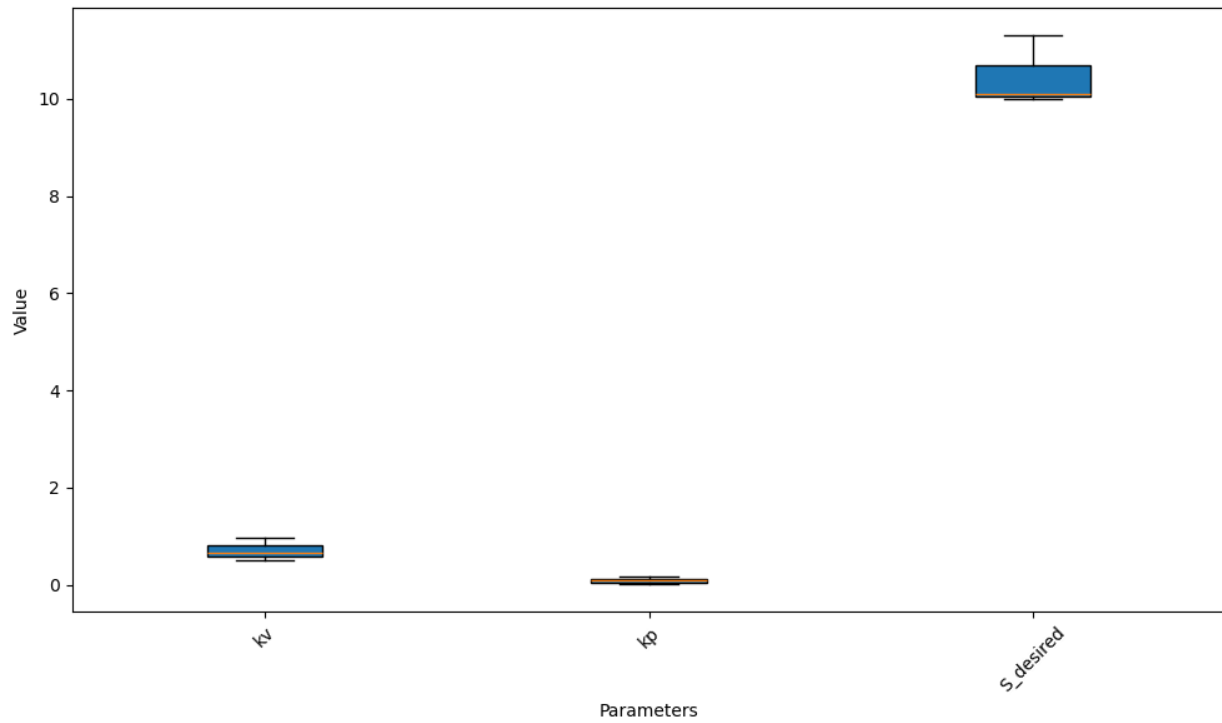


Fig. 10. Parameter ranges for CSP in I-90/94.

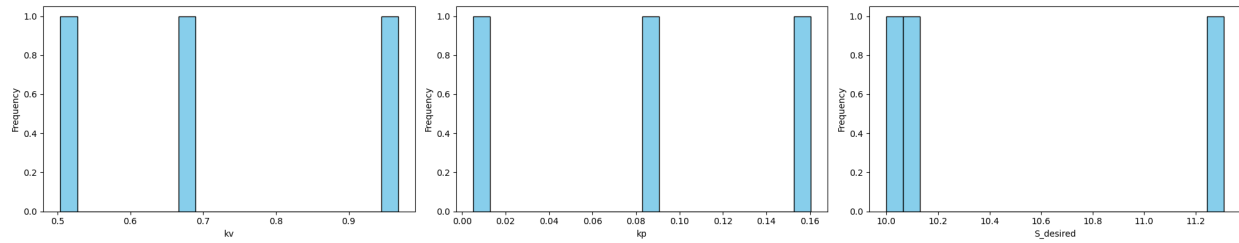
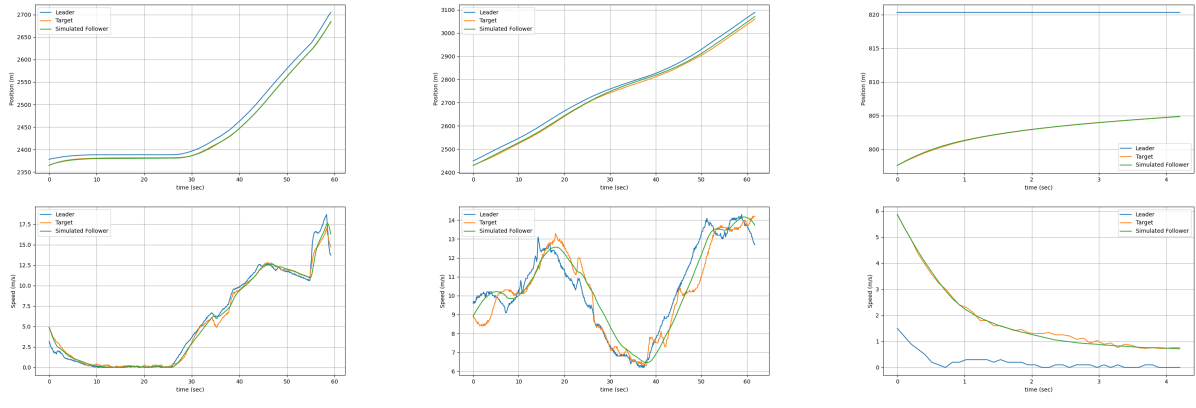


Fig. 11. Parameter histogram for CSP in I-90/94.



(a) Vehicle 13, Run 6 (H1A3)

(b) Vehicle 2, Run 9ES (H1A3)

(c) Vehicle 2, Run 9NS (H1A3)

Fig. 12. Simulated position and speed tracking using the Constant Spacing Policy (CSP) model for the Phoenix dataset: (a) Vehicle 13, Run 6; (b) Vehicle 2, Run 9ES; (c) Vehicle 2, Run 9NS.

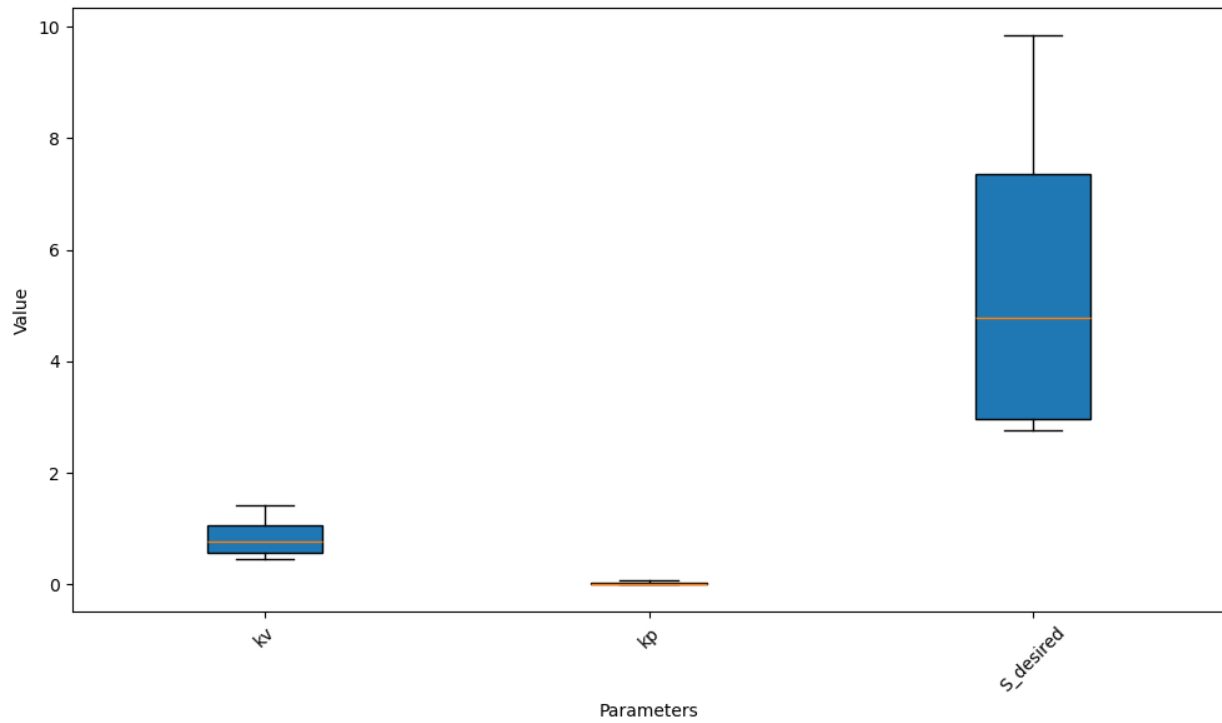


Fig. 13. Parameter ranges for CSP in Phoenix.

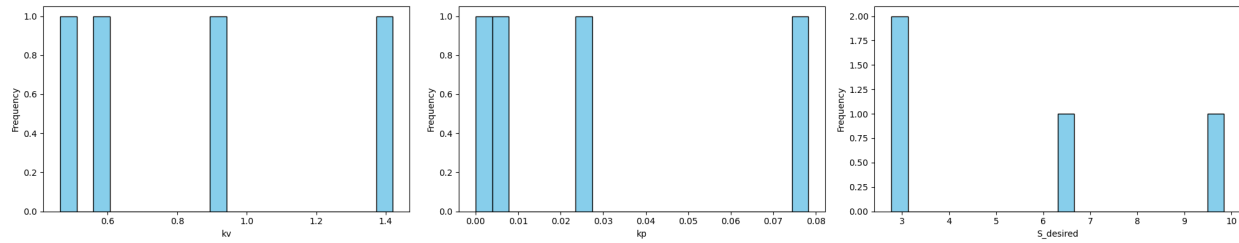
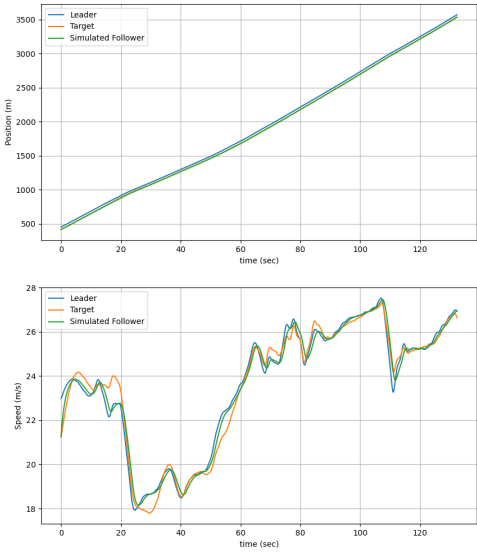
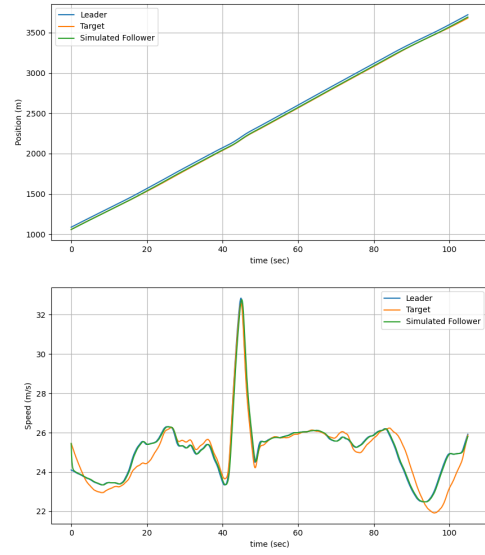


Fig. 14. Parameter histogram for CSP in Phoenix.

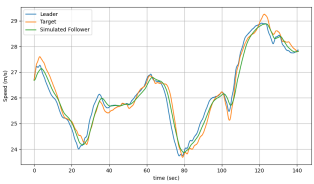
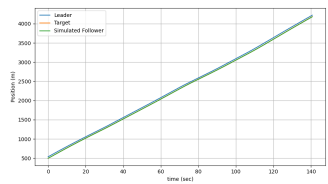


(a) Vehicle 11, Run 21

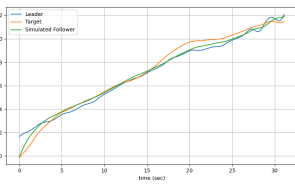
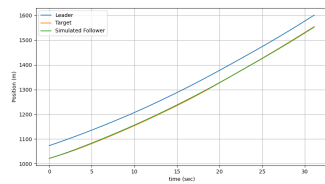


(b) Vehicle 11, Run 7

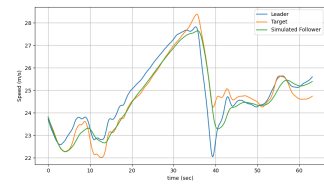
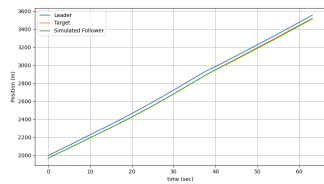
Fig. 15. Simulated position and speed tracking using the Constant Time Headway (CTH) model For I-294L1 dataset: (a) Vehicle 11, Run 21; (b) Vehicle 11, Run 7.



(a) Vehicle 12, Run 1

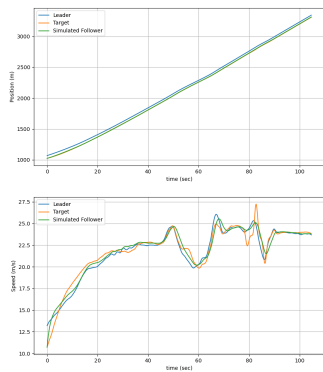


(b) Vehicle 19, Run 11

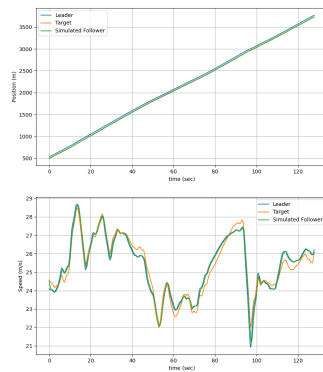


(c) Vehicle 19, Run 19

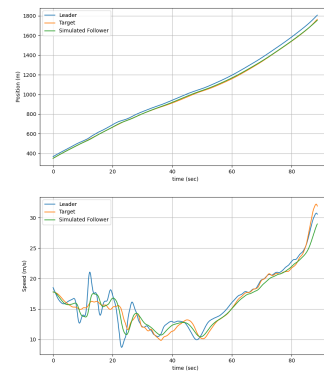
Fig. 16. Performance of CTH model across different vehicles: (a) Vehicle 12, Run 1; (b) Vehicle 19, Run 11; (c) Vehicle 19, Run 19.



(a) Vehicle 22, Run 11

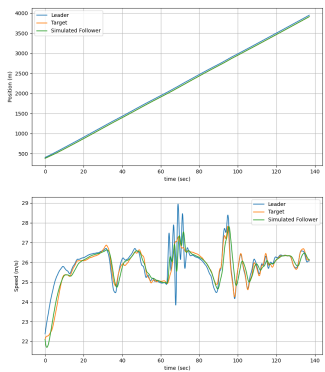


(b) Vehicle 25, Run 19

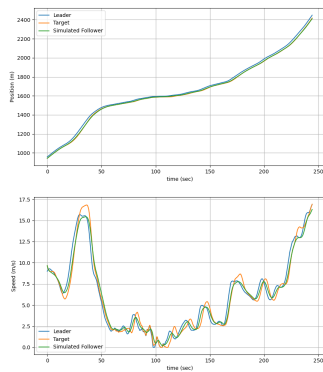


(c) Vehicle 35, Run 11

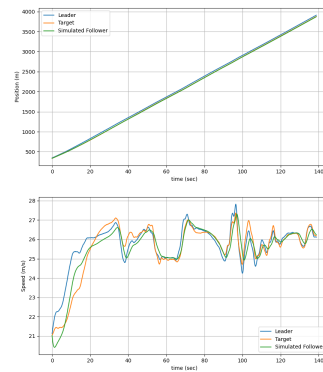
Fig. 17. CTH model performance for vehicles 22, 25, and 35: (a) Vehicle 22, Run 11; (b) Vehicle 25, Run 19; (c) Vehicle 35, Run 11.



(a) Vehicle 50, Run 20

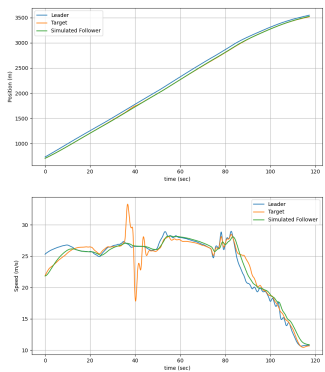


(b) Vehicle 51, Run 8

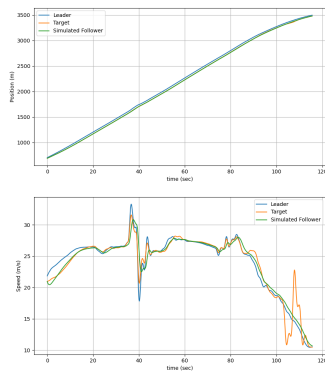


(c) Vehicle 54, Run 20

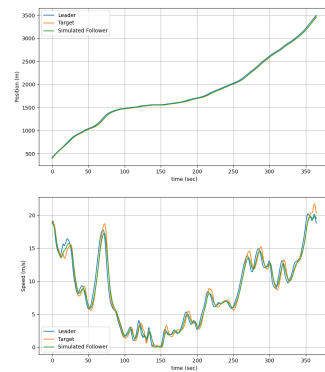
Fig. 18. Simulated tracking results for CTH model: (a) Vehicle 50, Run 20; (b) Vehicle 51, Run 8; (c) Vehicle 54, Run 20.



(a) Vehicle 56, Run 18

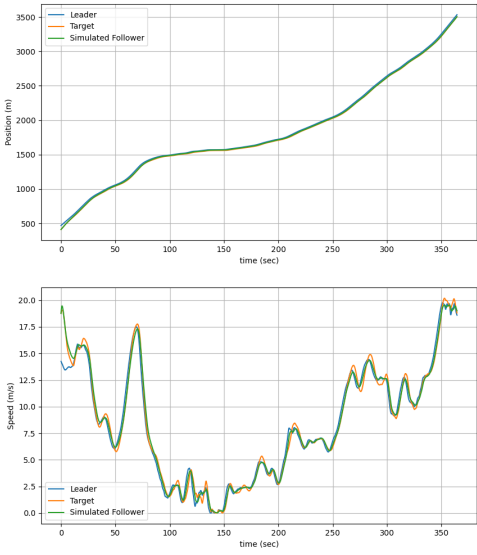


(b) Vehicle 59, Run 18

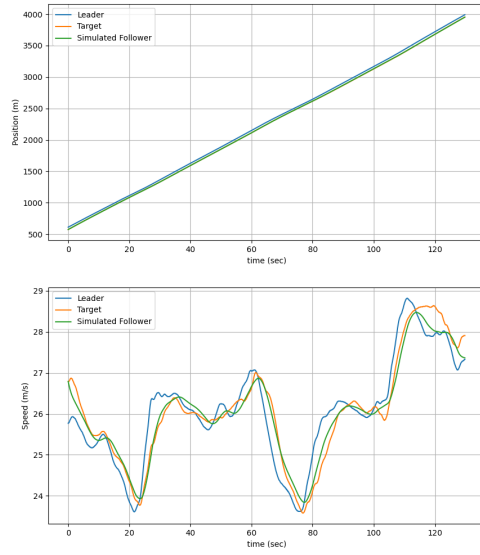


(c) Vehicle 62, Run 8

Fig. 19. CTH model results for vehicles 56, 59, and 62: (a) Vehicle 56, Run 18; (b) Vehicle 59, Run 18; (c) Vehicle 62, Run 8.



(a) Vehicle 65, Run 8



(b) Vehicle 9, Run 1

Fig. 20. Final comparison for CTH model: (a) Vehicle 65, Run 8; (b) Vehicle 9, Run 1.

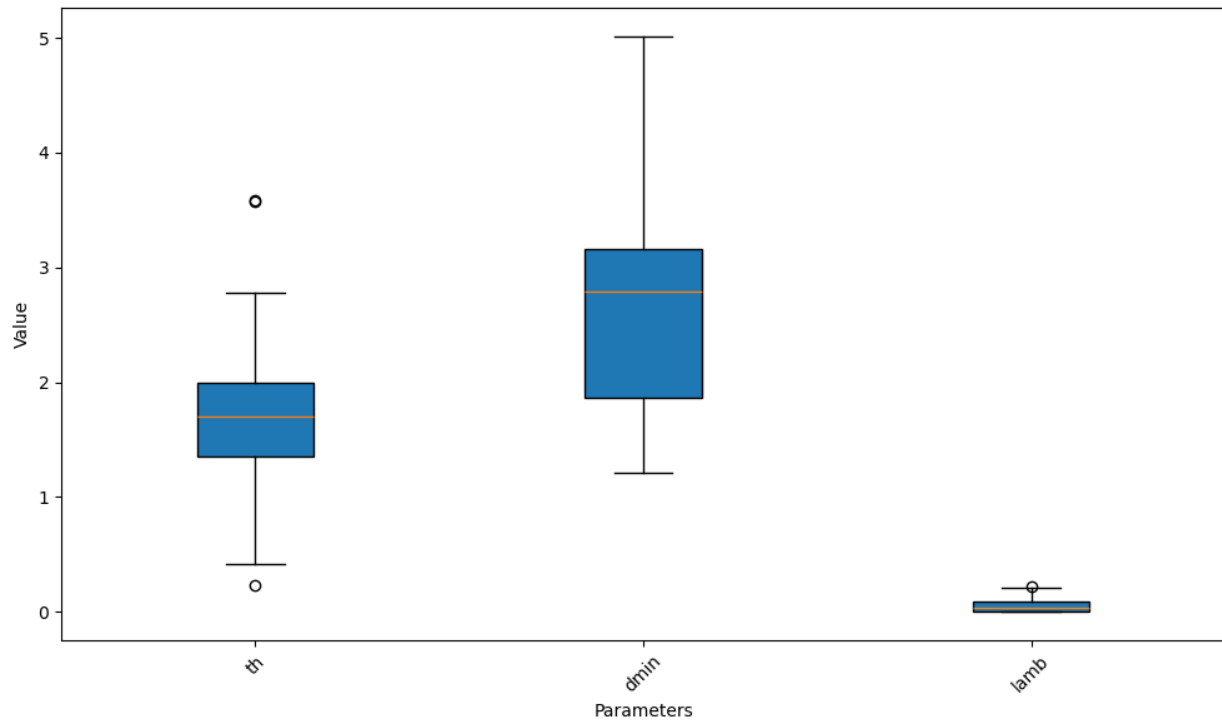


Fig. 21. Parameter ranges for CTH in I-294L1 dataset.

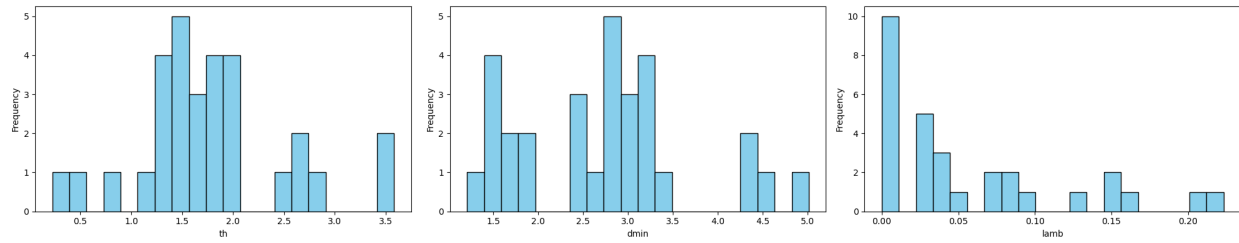
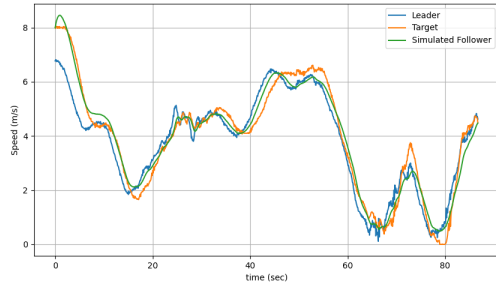
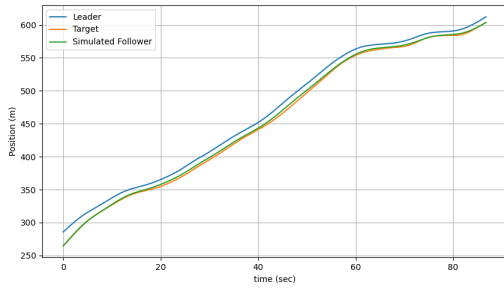
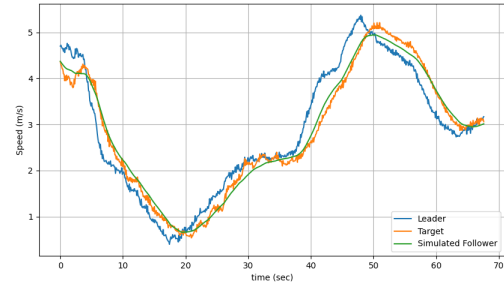
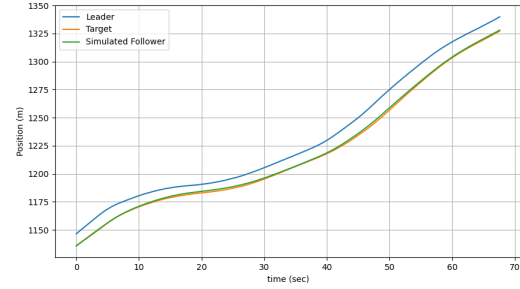


Fig. 22. Parameter histogram for CTH in I-294L1 dataset.



(a) Vehicle 5366, Run 1



(b) Vehicle 195, Run 2

Fig. 23. Simulated position and speed tracking using the Constant Time Headway (CTH) model for the I-90/94 dataset: (a) Vehicle 5366, Run 1; (b) Vehicle 195, Run 2.

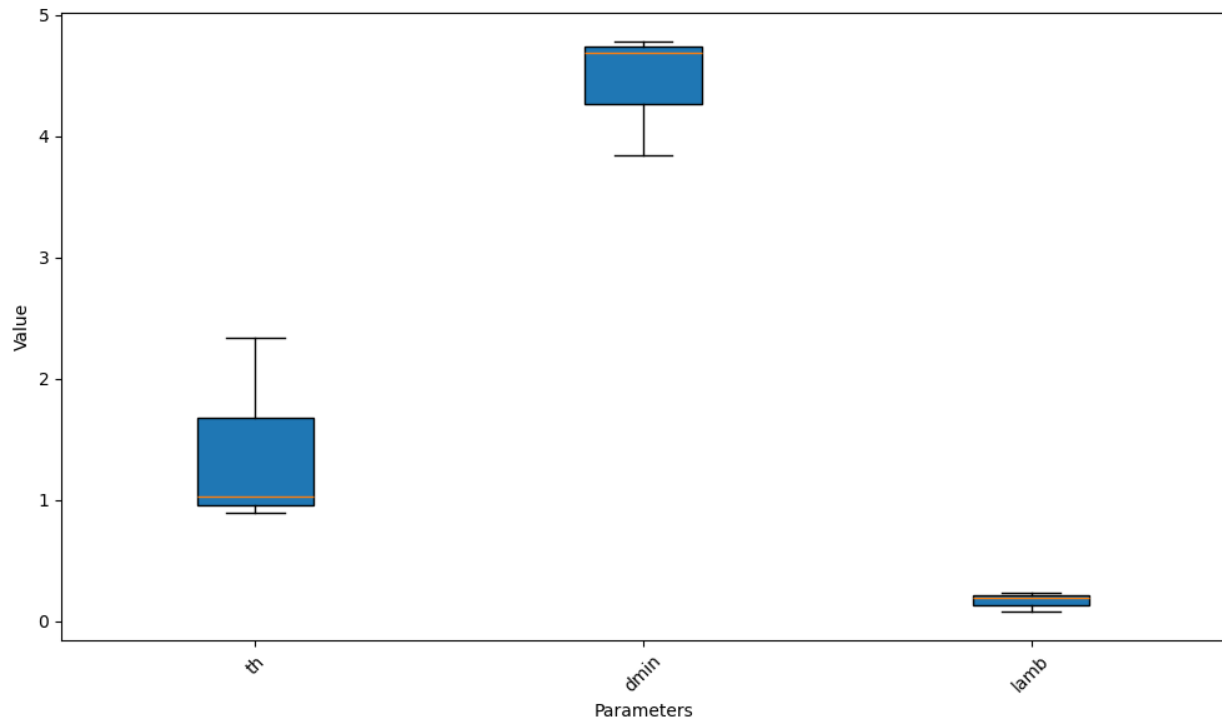


Fig. 24. Parameter ranges for CTH in I-90/94.

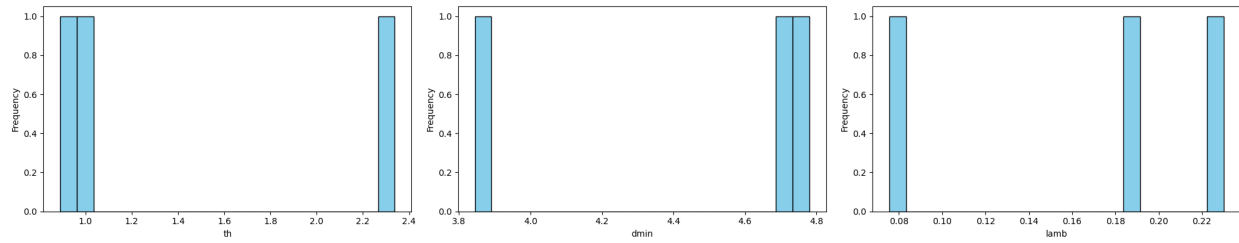
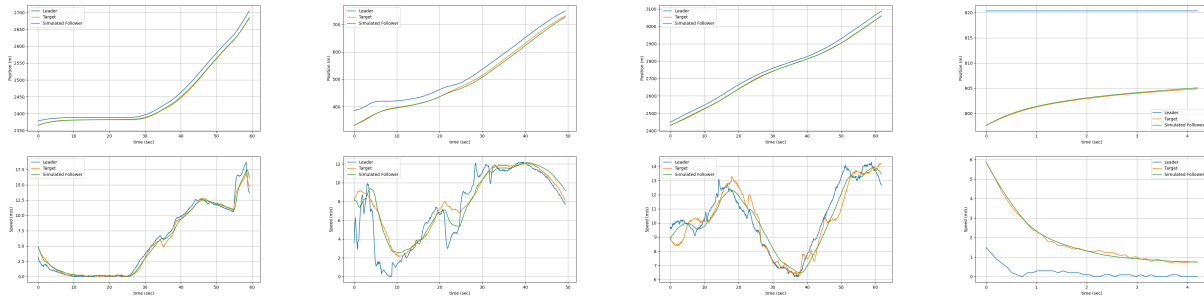


Fig. 25. Parameter histogram for CTH in I-90/94.



(a) Vehicle 13, Run 6 **(b)** Vehicle 31, Run 8EW **(c)** Vehicle 2, Run 9ES **(d)** Vehicle 2, Run 9NS
(H1A3) (H1A3) (H1A3) (H1A3)

Fig. 26. Simulated position and speed tracking using the Constant Time Headway (CTH) model for the Phoenix dataset: (a) Vehicle 13, Run 6; (b) Vehicle 31, Run 8EW; (c) Vehicle 2, Run 9ES; (d) Vehicle 2, Run 9NS.

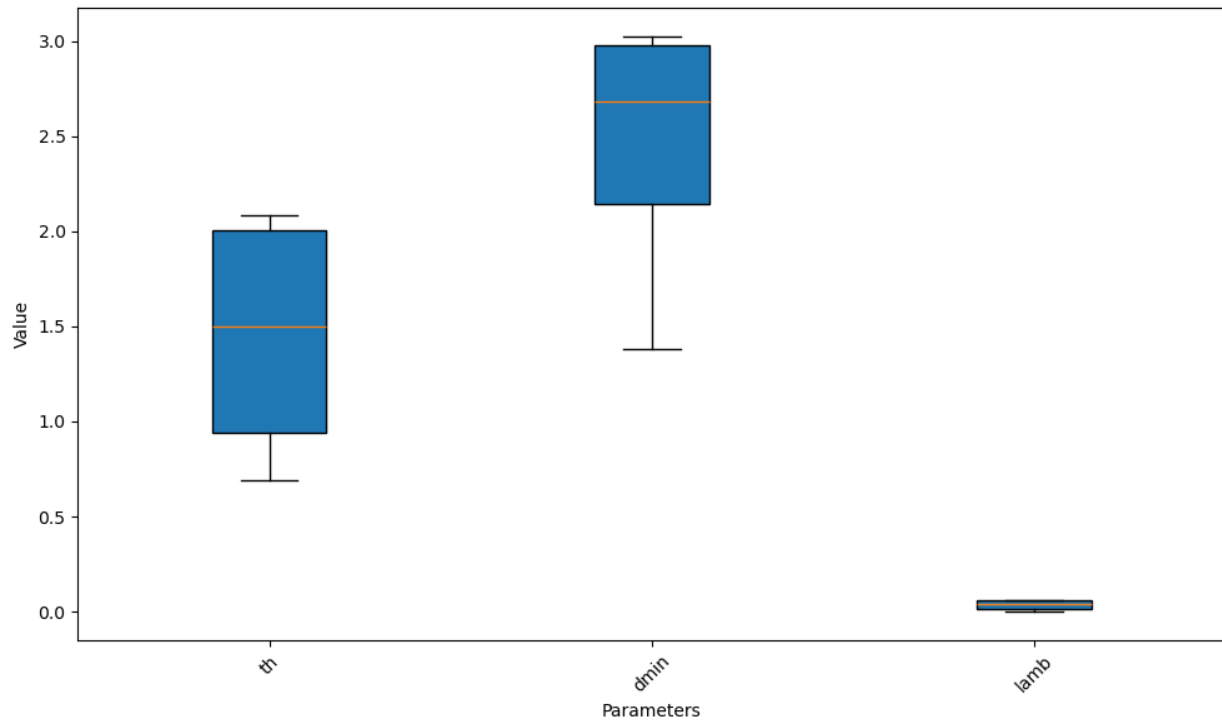


Fig. 27. Parameter ranges for CTH in Phoenix.

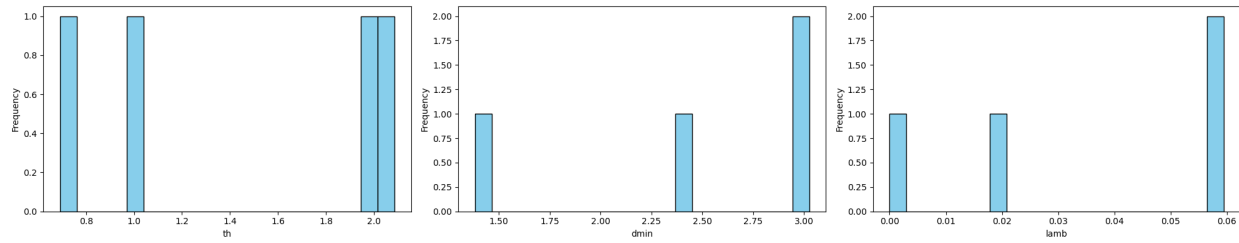
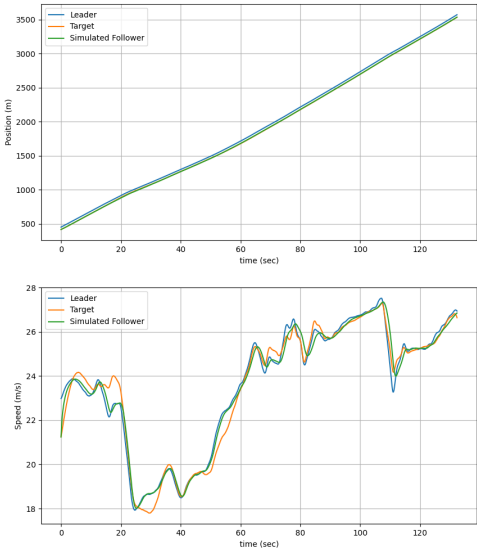
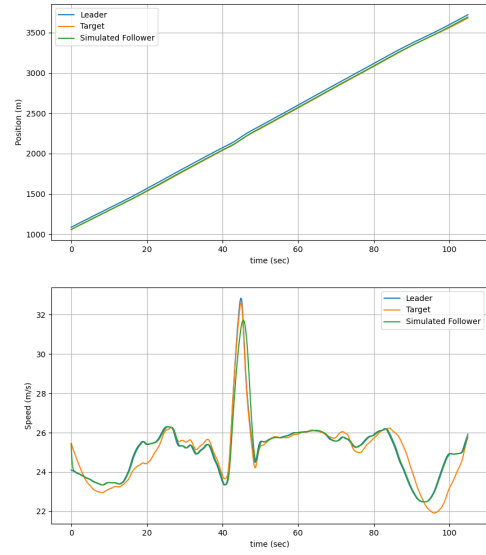


Fig. 28. Parameter histogram for CTH in Phoenix.

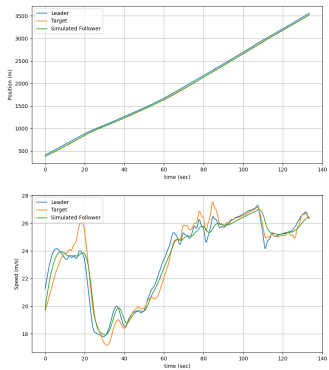


(a) Vehicle 11, Run 21

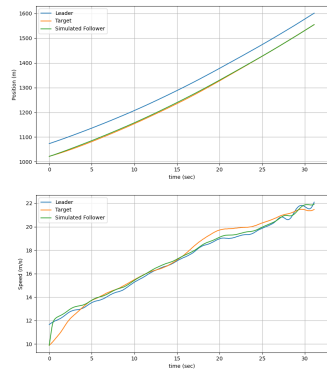


(b) Vehicle 11, Run 7

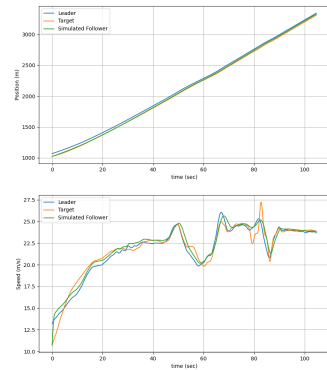
Fig. 29. Simulated position and speed tracking using the Traffic Flow Stability (TFS) model: (a) Vehicle 11, Run 21; (b) Vehicle 11, Run 7.



(a) Vehicle 17, Run 21

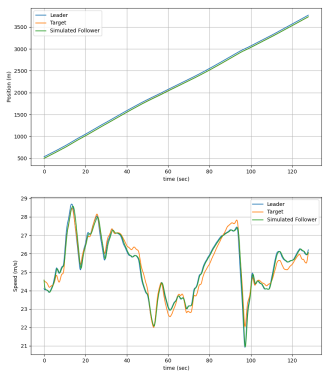


(b) Vehicle 19, Run 11

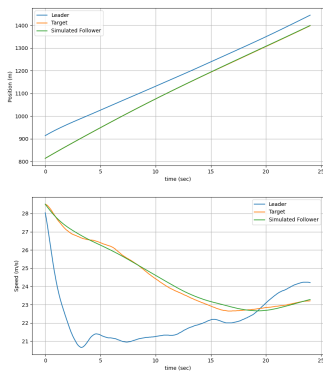


(c) Vehicle 22, Run 11

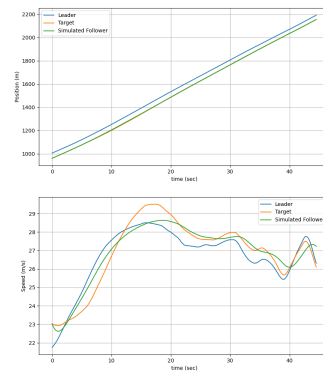
Fig. 30. TFS model tracking results: (a) Vehicle 17, Run 21; (b) Vehicle 19, Run 11; (c) Vehicle 22, Run 11.



(a) Vehicle 25, Run 19

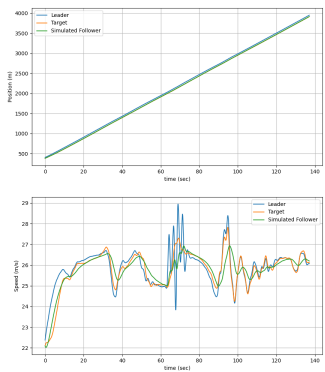


(b) Vehicle 28, Run 9

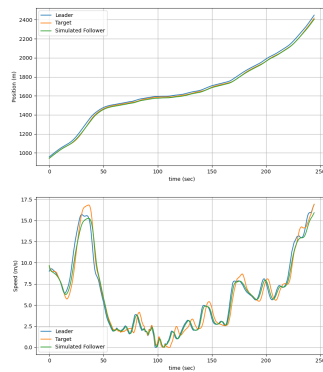


(c) Vehicle 41, Run 3

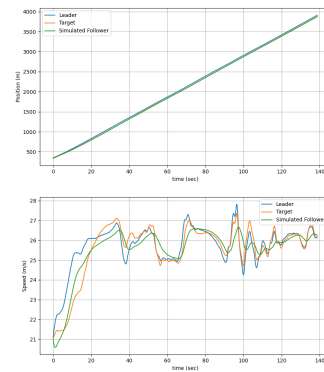
Fig. 31. Performance of TFS model for vehicles 25, 28, and 41.



(a) Vehicle 50, Run 20

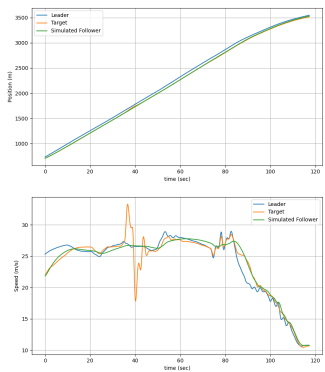


(b) Vehicle 51, Run 8

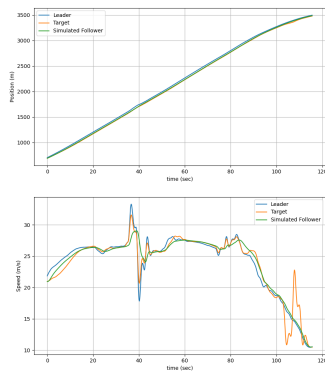


(c) Vehicle 54, Run 20

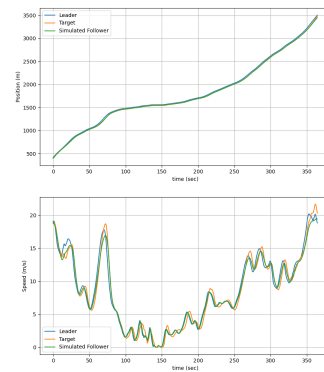
Fig. 32. Tracking performance of the TFS model for vehicles 50, 51, and 54.



(a) Vehicle 56, Run 18

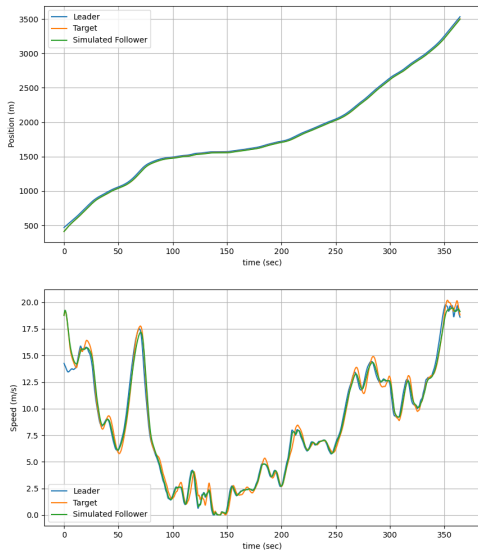


(b) Vehicle 59, Run 18

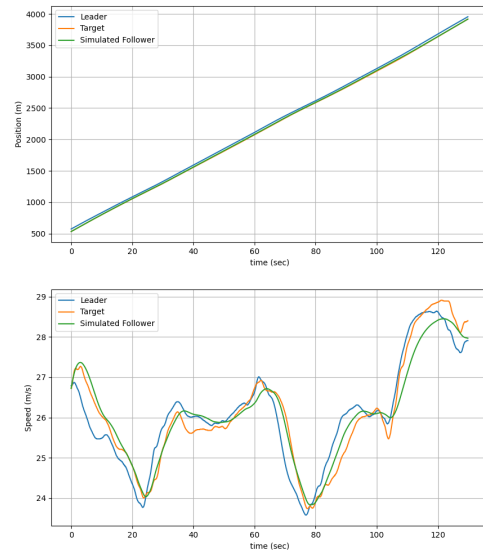


(c) Vehicle 62, Run 8

Fig. 33. TFS model tracking for vehicles 56, 59, and 62.



(a) Vehicle 65, Run 8



(b) Vehicle 8, Run 1

Fig. 34. Final comparison of the TFS model: (a) Vehicle 65, Run 8; (b) Vehicle 8, Run 1.

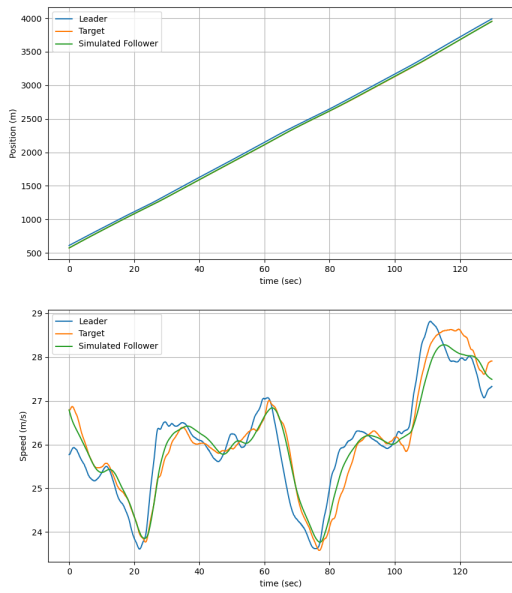


Fig. 35. Position and speed for TFS for Vehicle 9 in Run 1 (I-294L1 dataset).

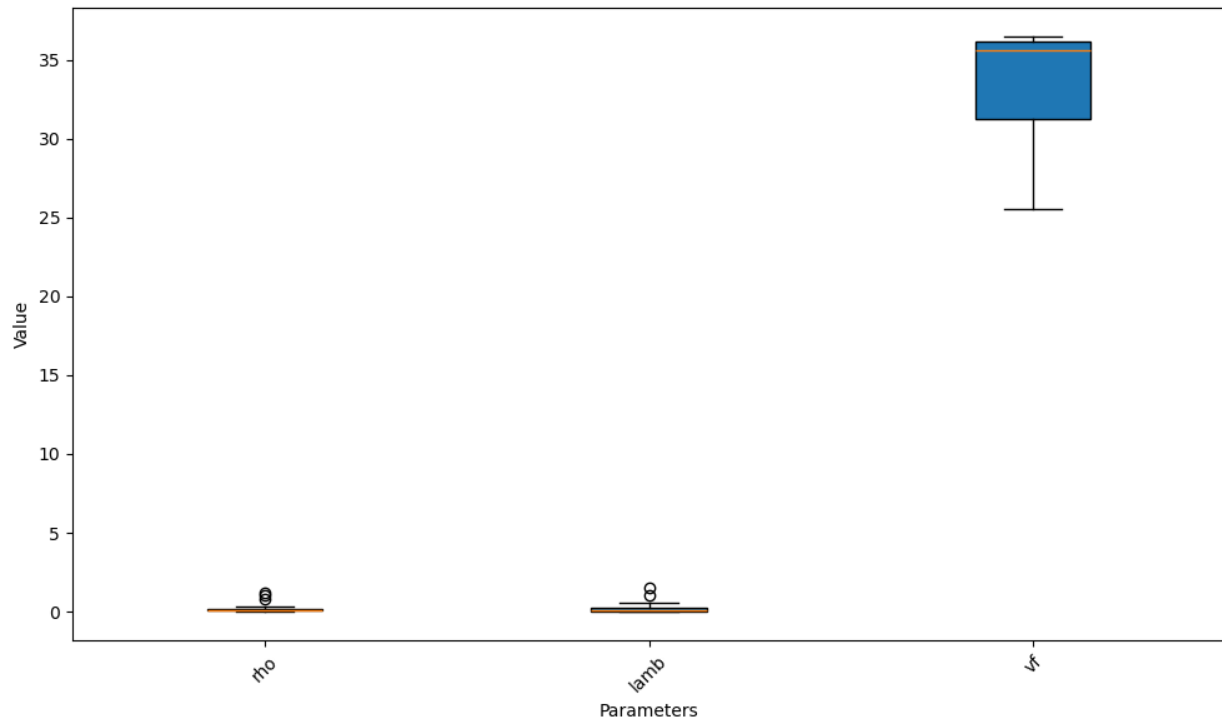


Fig. 36. Parameter ranges for TFS in I-294L1 dataset.

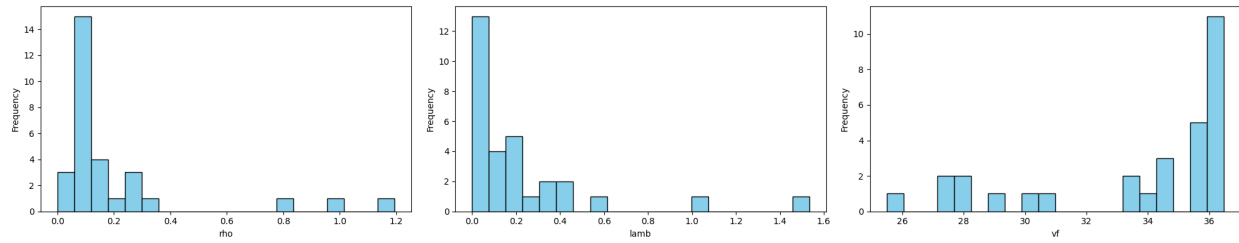
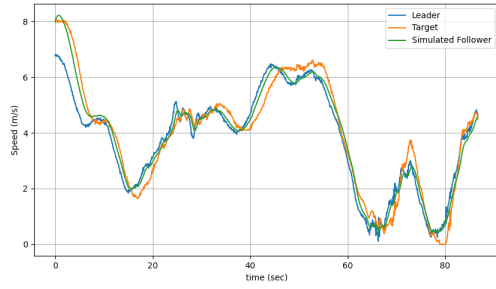
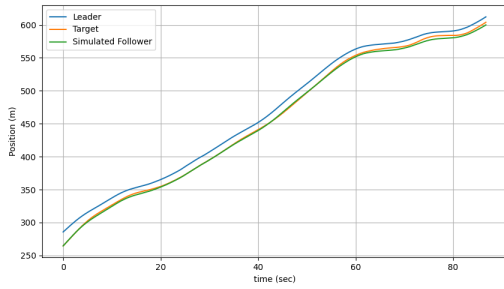
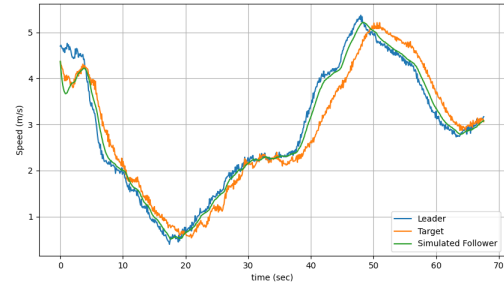
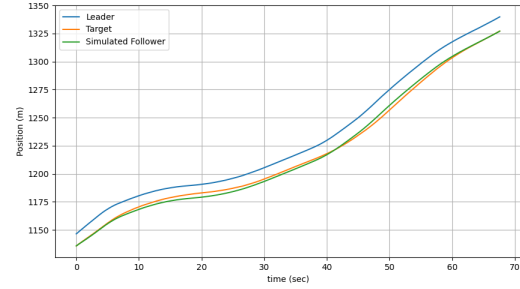


Fig. 37. Parameter histogram for TFS in I-294L1 dataset.



(a) Vehicle 5366, Run 1



(b) Vehicle 195, Run 2

Fig. 38. Simulated position and speed tracking using the Traffic Flow Stability (TFS) model for the I-90/94 dataset: (a) Vehicle 5366, Run 1; (b) Vehicle 195, Run 2.

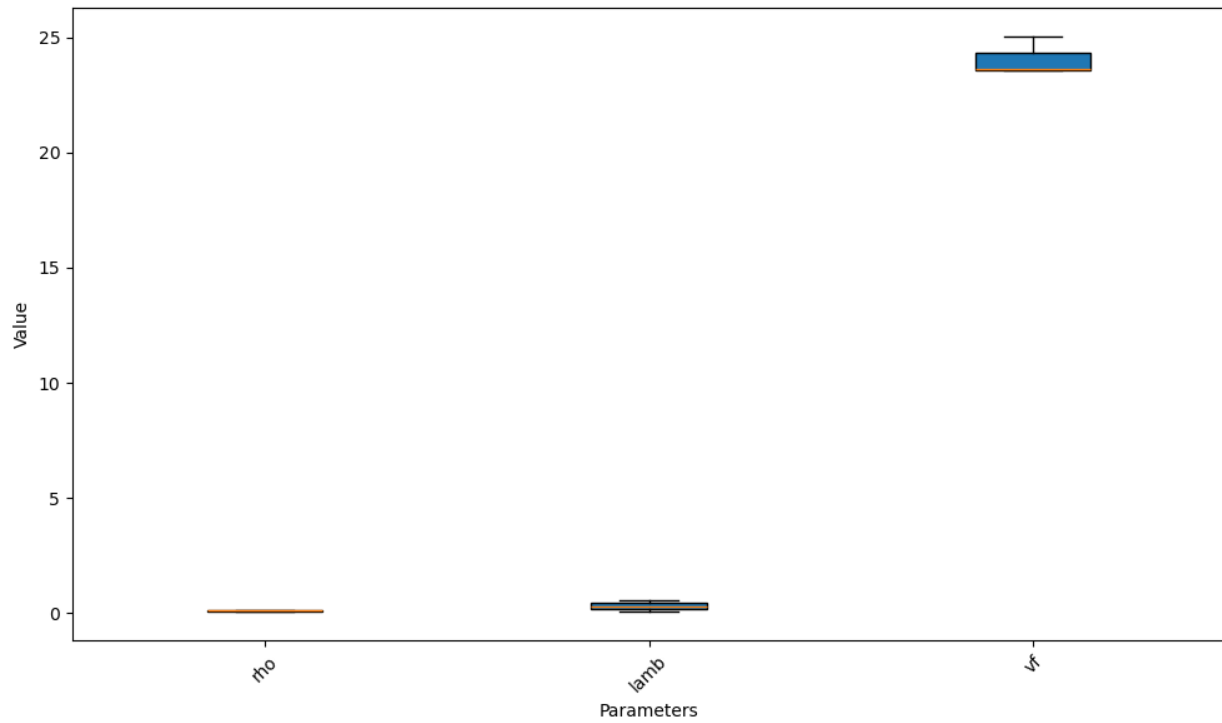


Fig. 39. Parameter ranges for TFS in I-90/94.

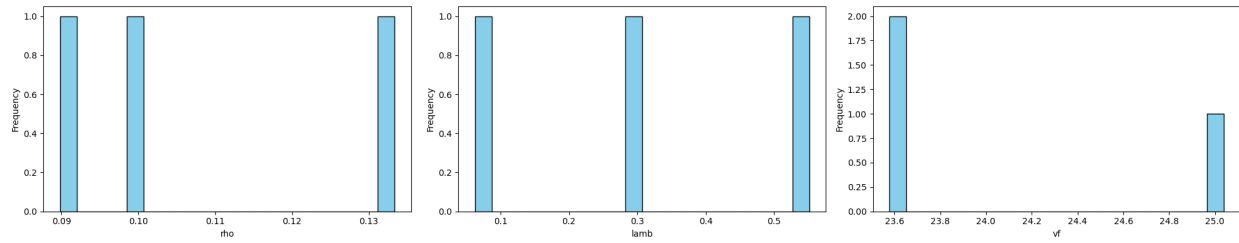
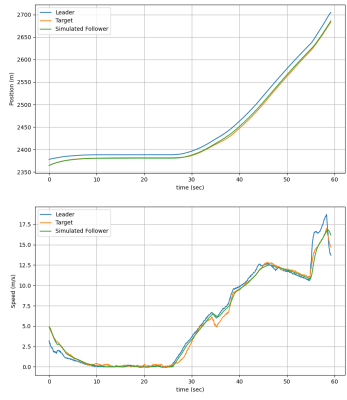
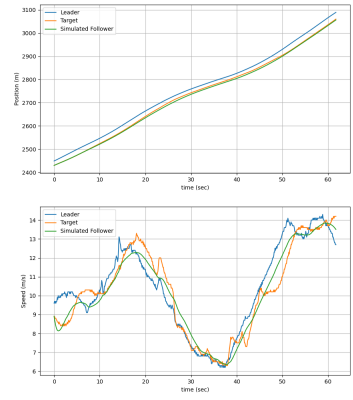


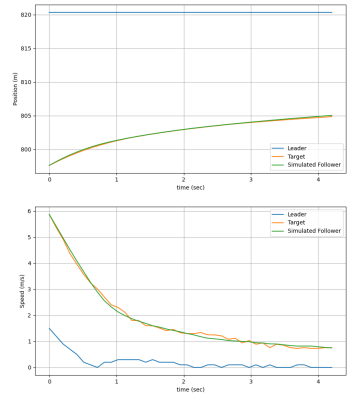
Fig. 40. Parameter histogram for TFS in I-90/94.



(a) Vehicle 13, Run 6 (H1A3)



(b) Vehicle 2, Run 9ES (H1A3)



(c) Vehicle 2, Run 9NS (H1A3)

Fig. 41. Simulated position and speed tracking using the Traffic Flow Stability (TFS) model for the Phoenix dataset: (a) Vehicle 13, Run 6; (b) Vehicle 2, Run 9ES; (c) Vehicle 2, Run 9NS.

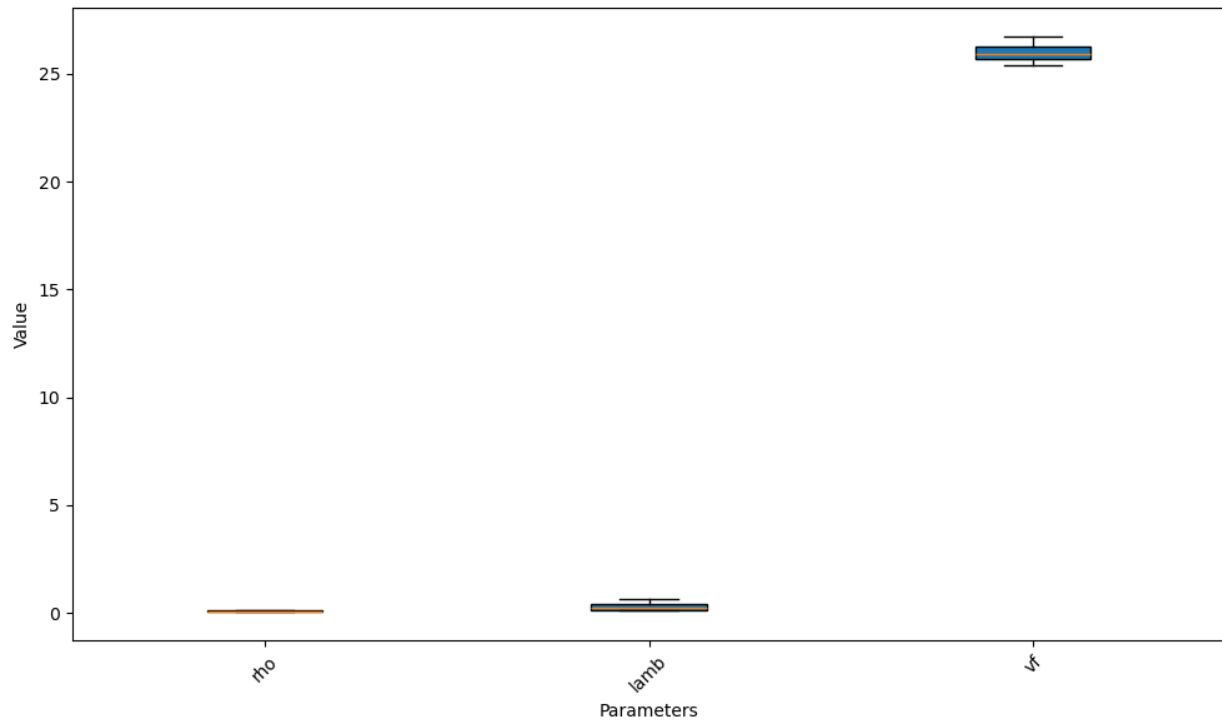


Fig. 42. Parameter ranges for TFS in Phoenix.

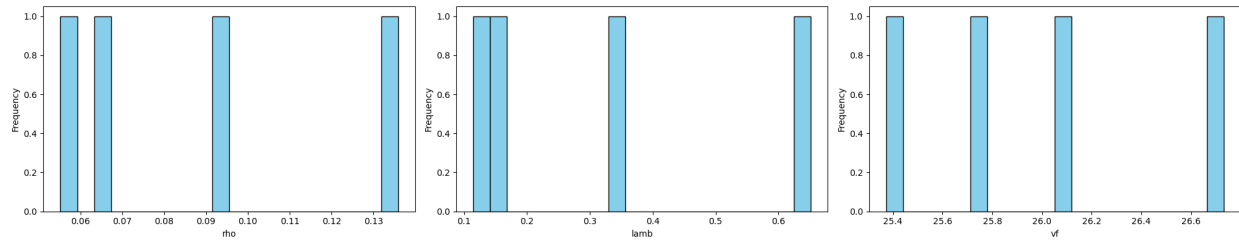
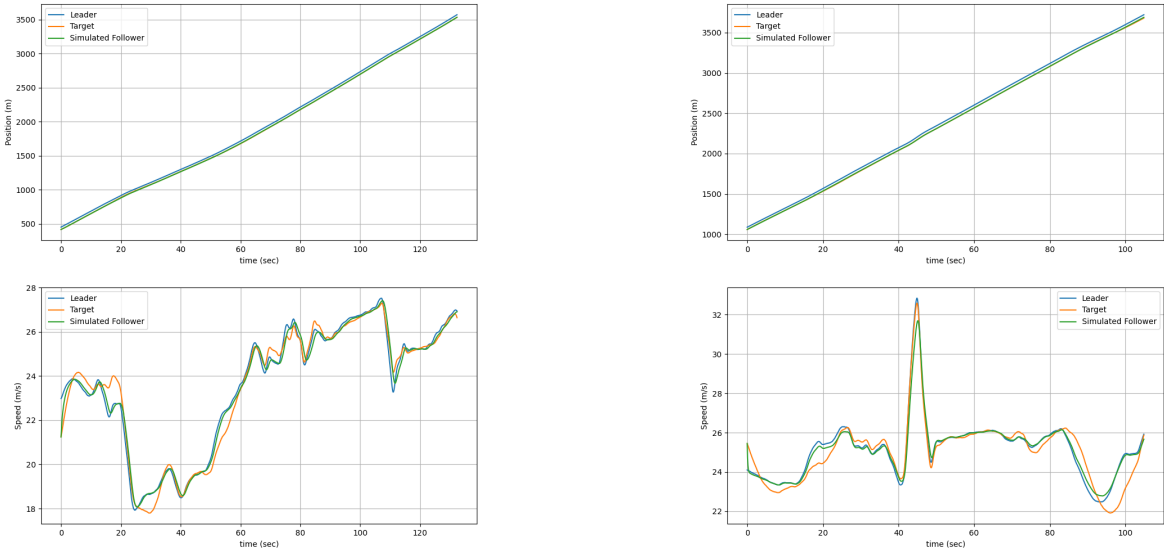


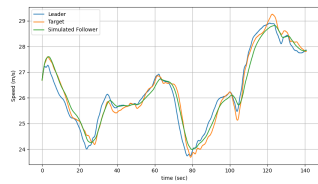
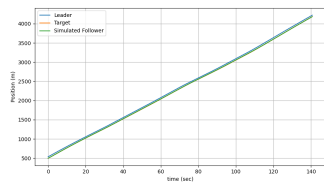
Fig. 43. Parameter histogram for TFS in Phoenix.



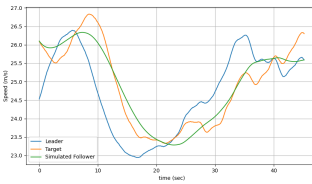
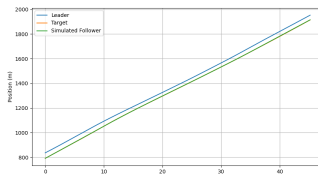
(a) Vehicle 11, Run 21

(b) Vehicle 11, Run 7

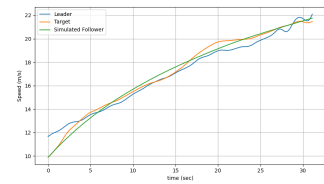
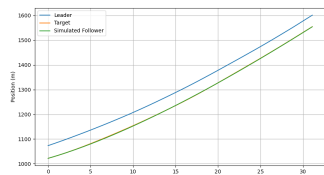
Fig. 44. Simulated position and speed tracking using the Constant Safety Factor (CSF) model: (a) Vehicle 11, Run 21; (b) Vehicle 11, Run 7.



(a) Vehicle 12, Run 1

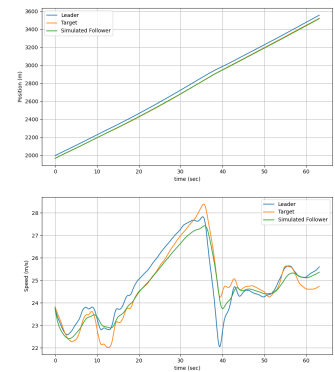


(b) Vehicle 17, Run 7

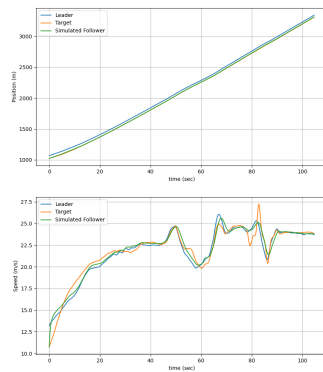


(c) Vehicle 19, Run 11

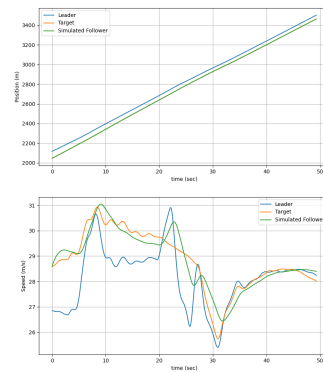
Fig. 45. Performance of CSF model: (a) Vehicle 12, Run 1; (b) Vehicle 17, Run 7; (c) Vehicle 19, Run 11.



(a) Vehicle 19, Run 19

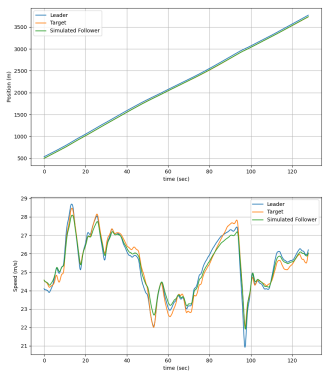


(b) Vehicle 22, Run 11

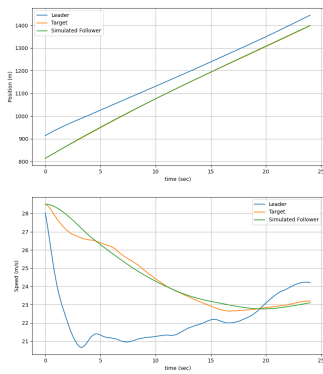


(c) Vehicle 24, Run 9

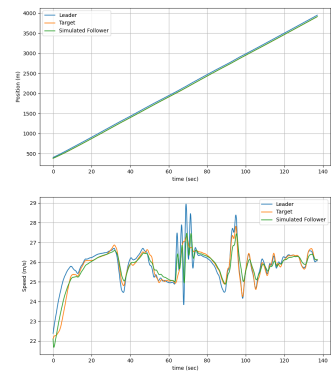
Fig. 46. Tracking performance of the CSF model: (a) Vehicle 19, Run 19; (b) Vehicle 22, Run 11; (c) Vehicle 24, Run 9.



(a) Vehicle 25, Run 19

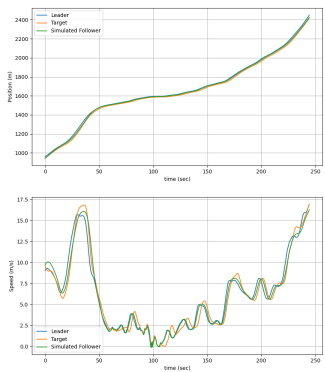


(b) Vehicle 28, Run 9

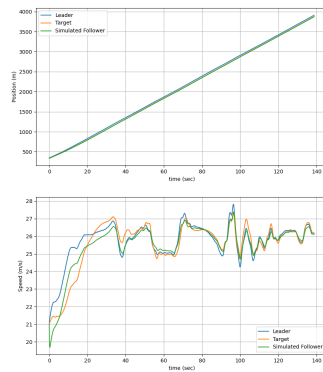


(c) Vehicle 50, Run 20

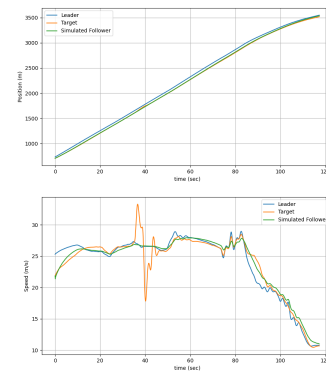
Fig. 47. Simulated CSF results for vehicles 25, 28, and 50.



(a) Vehicle 51, Run 8

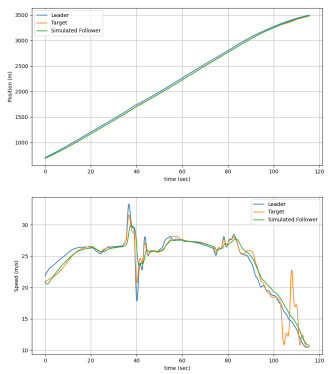


(b) Vehicle 54, Run 20

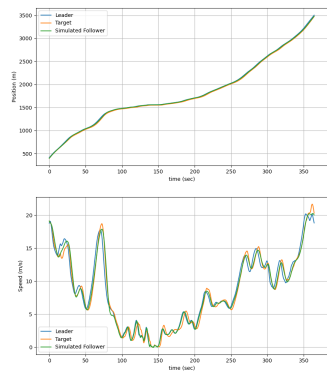


(c) Vehicle 56, Run 18

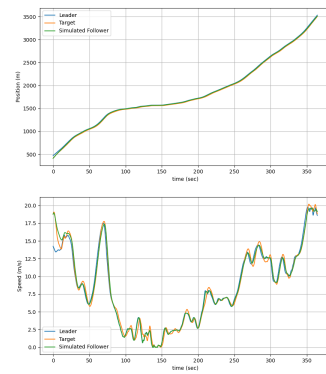
Fig. 48. CSF model tracking for vehicles 51, 54, and 56.



(a) Vehicle 59, Run 18

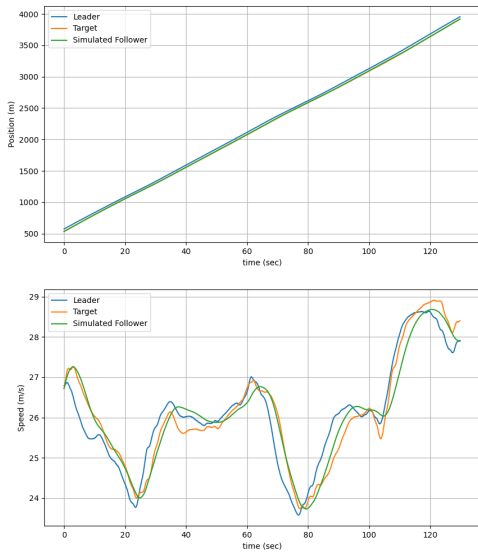


(b) Vehicle 62, Run 8

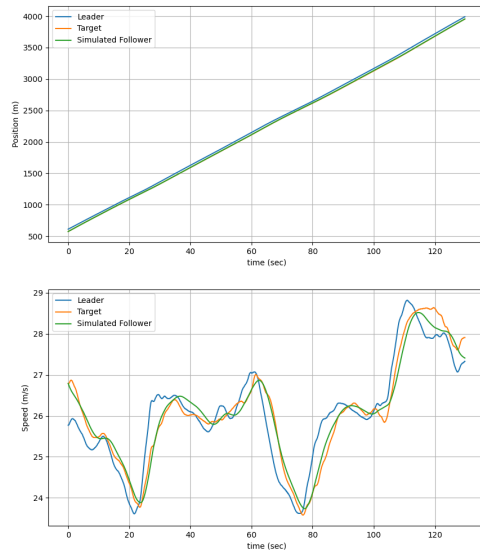


(c) Vehicle 65, Run 8

Fig. 49. Tracking results of the CSF model for vehicles 59, 62, and 65.



(a) Vehicle 8, Run 1



(b) Vehicle 9, Run 1

Fig. 50. Final comparison of CSF model tracking: (a) Vehicle 8, Run 1; (b) Vehicle 9, Run 1.

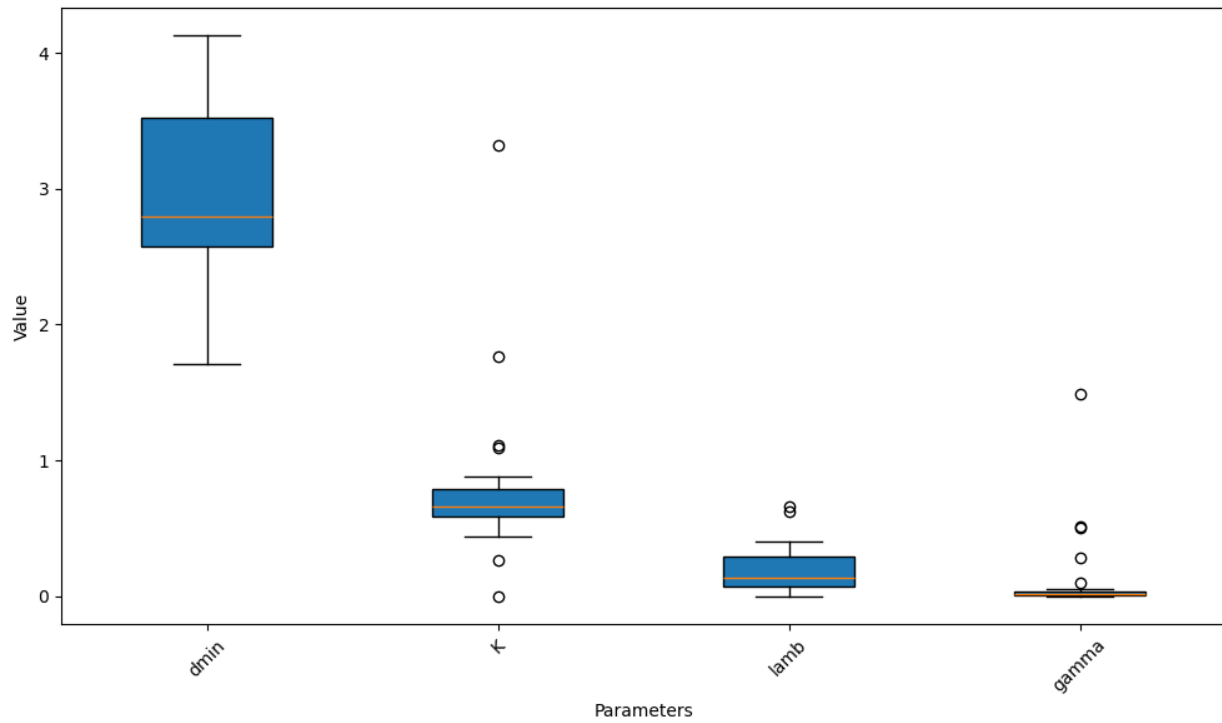


Fig. 51. Parameter ranges for CSF in I-294L1 dataset.

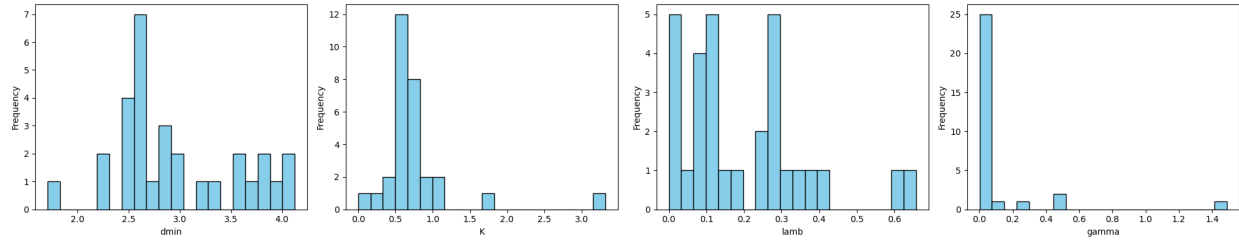
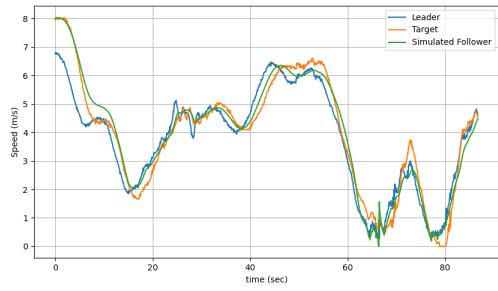
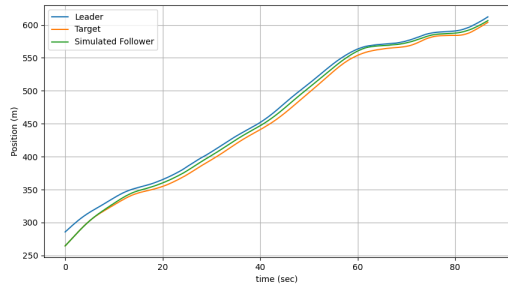
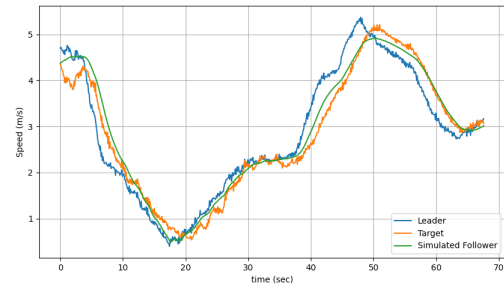
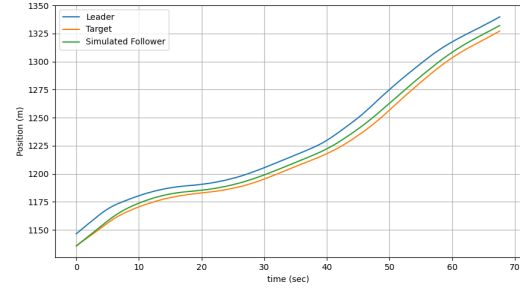


Fig. 52. Parameter histogram for CSF in I-294L1 dataset.



(a) Vehicle 5366, Run 1



(b) Vehicle 195, Run 2

Fig. 53. Simulated position and speed tracking using the Constant Safety Factor (CSF) model for the I-90/94 dataset: (a) Vehicle 5366, Run 1; (b) Vehicle 195, Run 2.

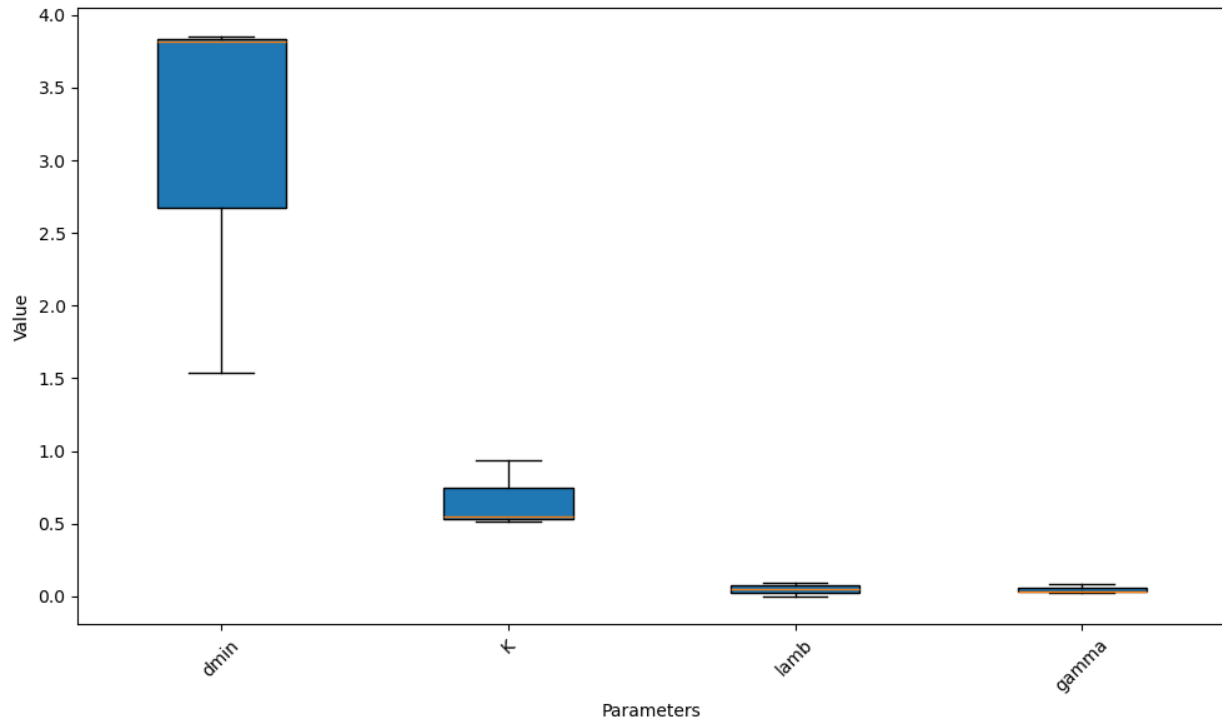


Fig. 54. Parameter ranges for CSF in I-90/94.

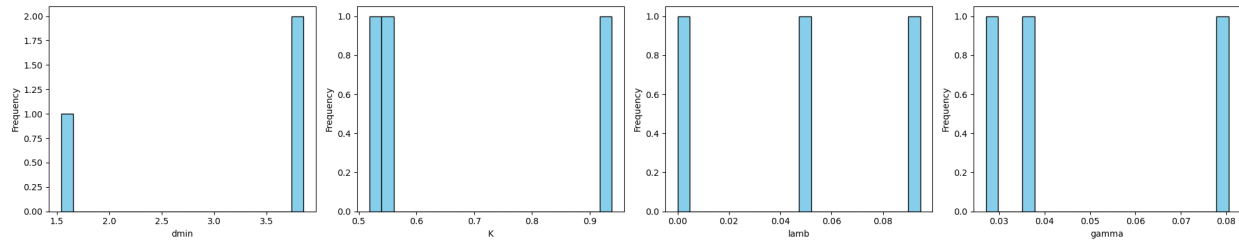
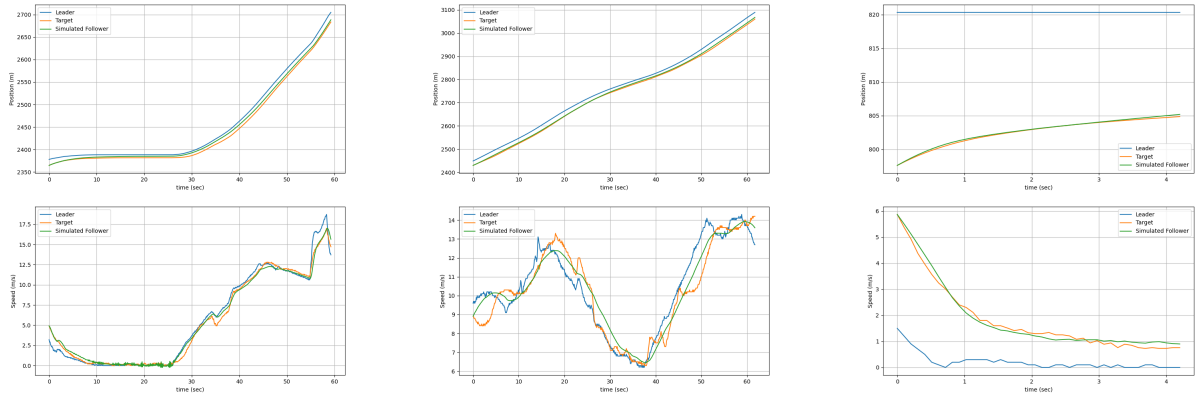


Fig. 55. Parameter histogram for CSF in I-90/94.



(a) Vehicle 13, Run 6 (H1A3)

(b) Vehicle 2, Run 9ES (H1A3)

(c) Vehicle 2, Run 9NS (H1A3)

Fig. 56. Simulated position and speed tracking using the Constant Safety Factor (CSF) model for the Phoenix dataset: (a) Vehicle 13, Run 6; (b) Vehicle 2, Run 9ES; (c) Vehicle 2, Run 9NS.

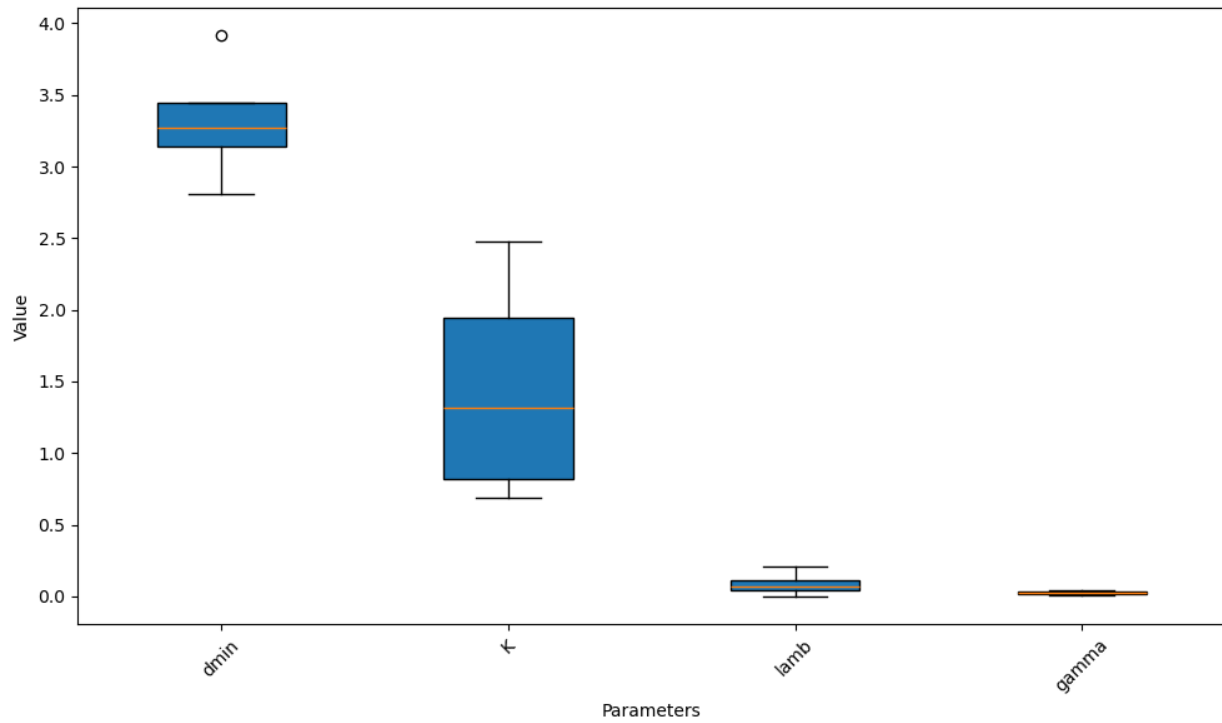


Fig. 57. Parameter ranges for CSF in Phoenix.

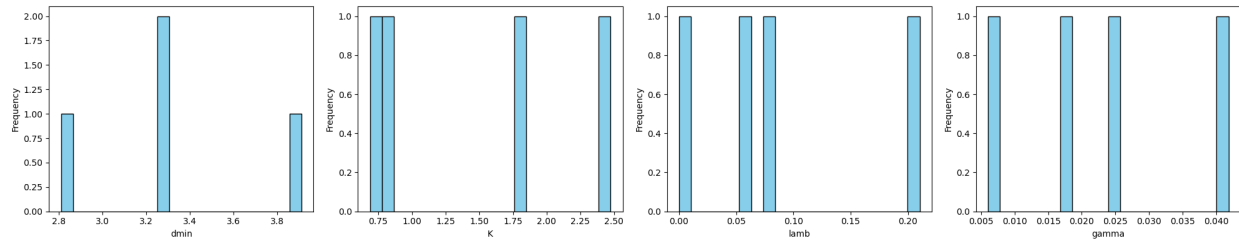
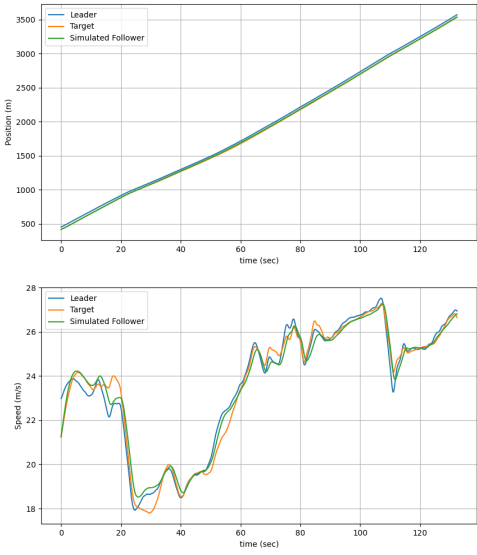
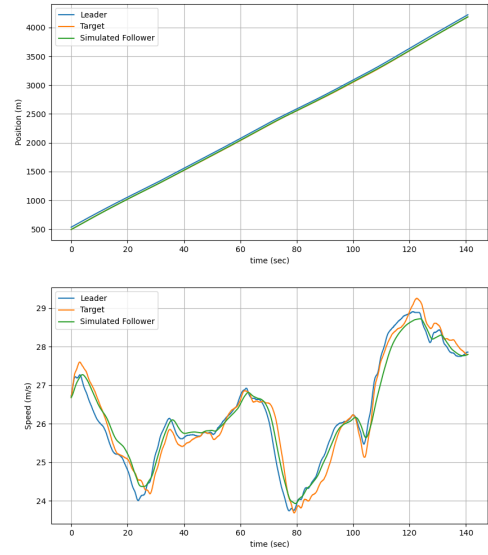


Fig. 58. Parameter histogram for CSF in Phoenix.

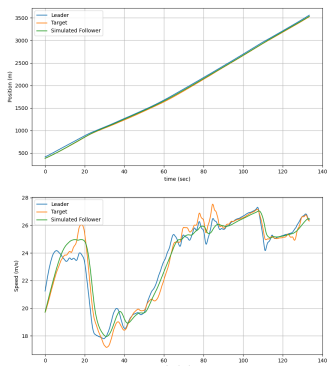


(a) Vehicle 11, Run 21

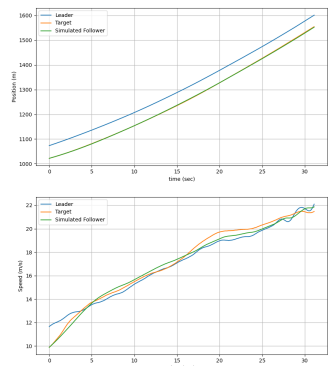


(b) Vehicle 12, Run 1

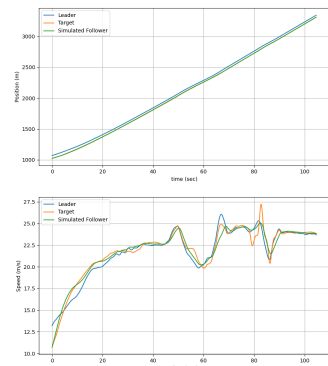
Fig. 59. Simulated position and speed tracking using the Intelligent Driver Model (IDM): (a) Vehicle 11, Run 21; (b) Vehicle 12, Run 1.



(a) Vehicle 17, Run 21

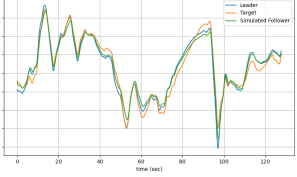
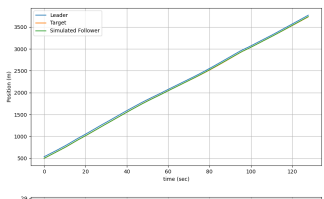


(b) Vehicle 19, Run 11

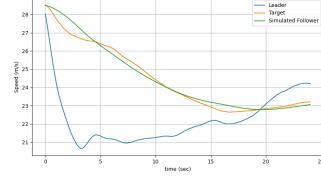
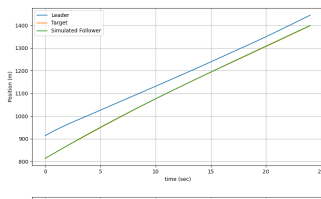


(c) Vehicle 22, Run 11

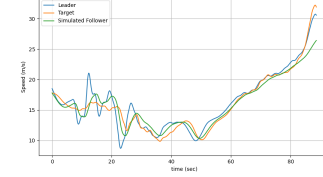
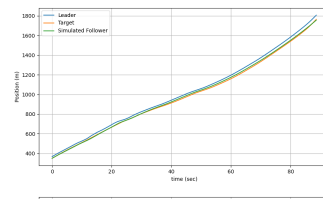
Fig. 60. Performance of IDM: (a) Vehicle 17, Run 21; (b) Vehicle 19, Run 11; (c) Vehicle 22, Run 11.



(a) Vehicle 25, Run 19

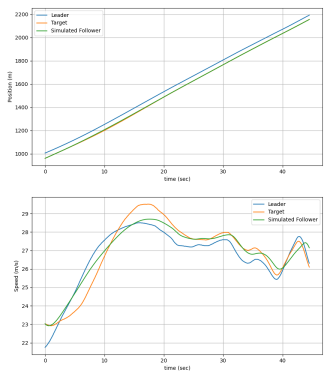


(b) Vehicle 28, Run 9

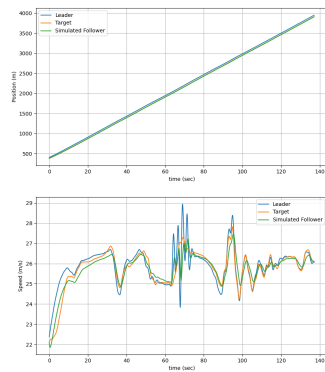


(c) Vehicle 35, Run 11

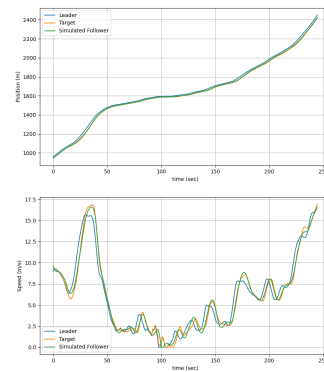
Fig. 61. IDM tracking results: (a) Vehicle 25, Run 19; (b) Vehicle 28, Run 9; (c) Vehicle 35, Run 11.



(a) Vehicle 41, Run 3

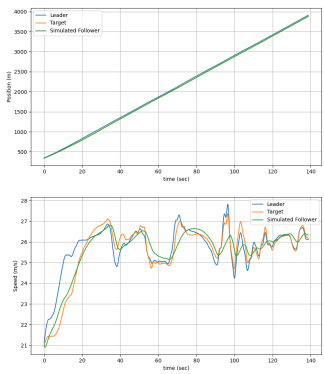


(b) Vehicle 50, Run 20

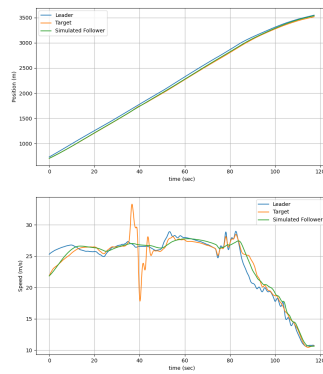


(c) Vehicle 51, Run 8

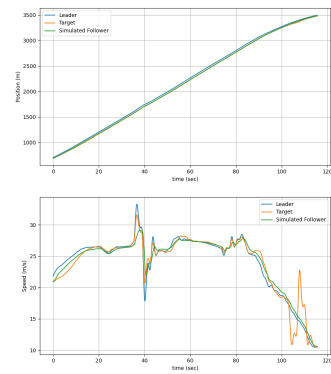
Fig. 62. Simulated IDM performance for vehicles 41, 50, and 51.



(a) Vehicle 54, Run 20

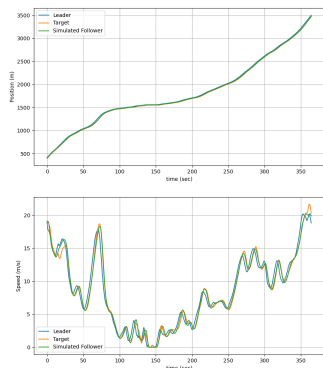


(b) Vehicle 56, Run 18

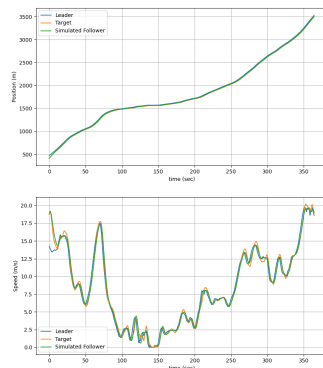


(c) Vehicle 59, Run 18

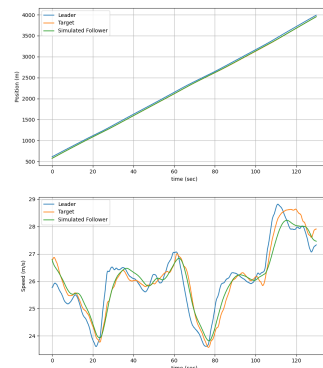
Fig. 63. Tracking results of IDM model: (a) Vehicle 54, Run 20; (b) Vehicle 56, Run 18; (c) Vehicle 59, Run 18.



(a) Vehicle 62, Run 8



(b) Vehicle 65, Run 8



(c) Vehicle 9, Run 1

Fig. 64. Final IDM model tracking comparison: (a) Vehicle 62, Run 8; (b) Vehicle 65, Run 8; (c) Vehicle 9, Run 1.

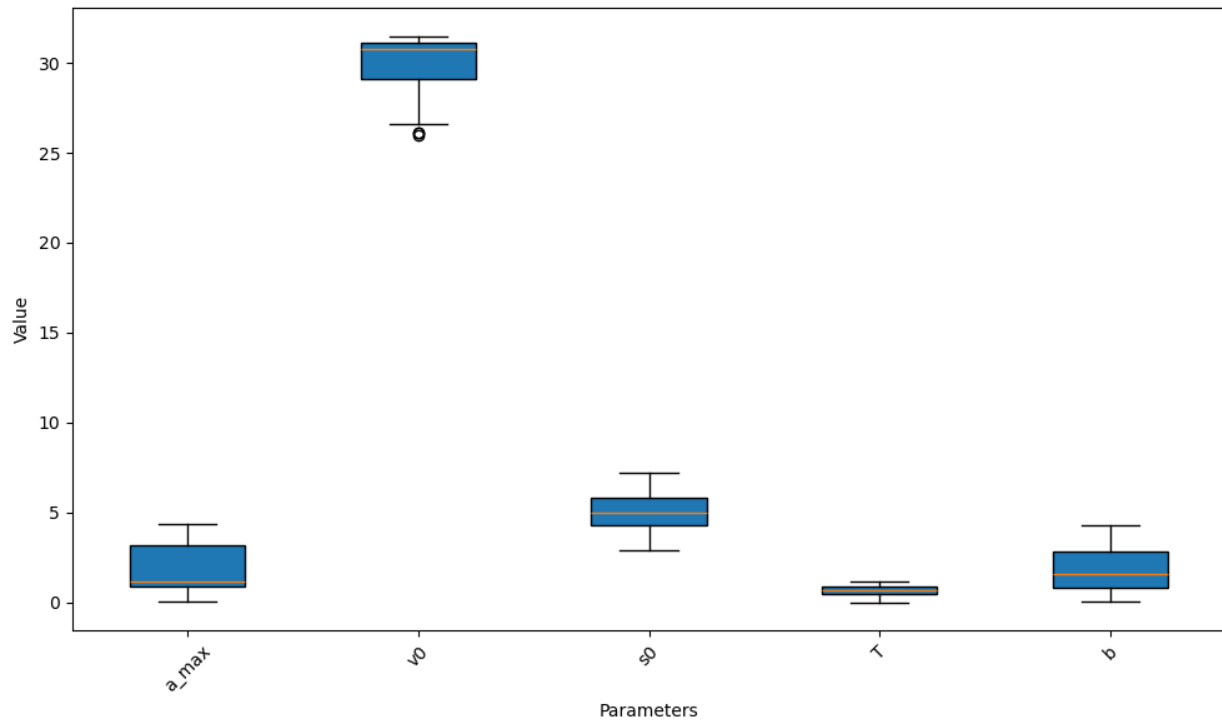


Fig. 65. Parameter ranges for IDM in I-294L1 dataset.

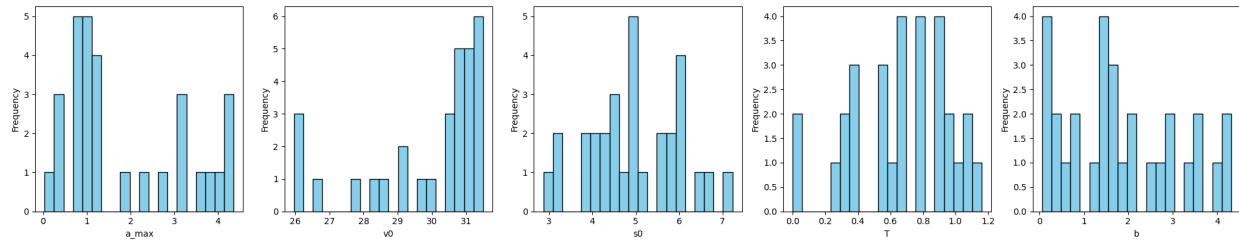
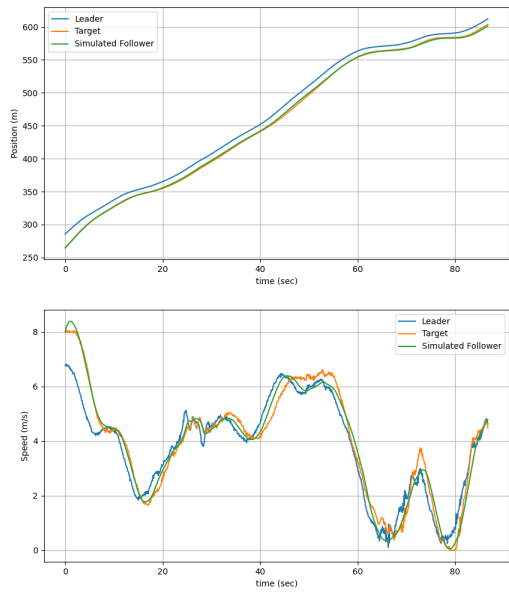
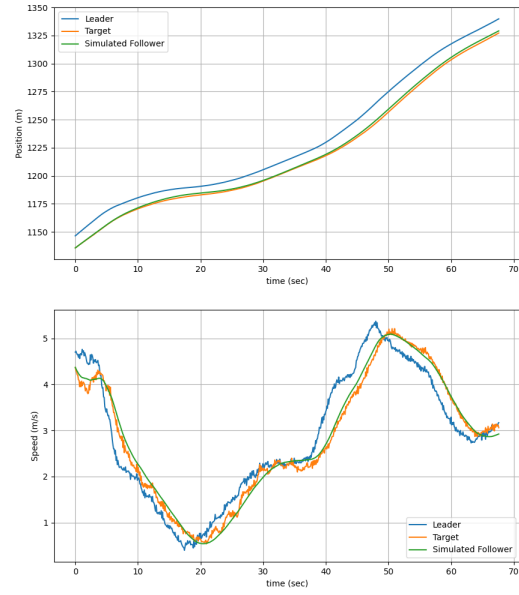


Fig. 66. Parameter histogram for IDM in I-294L1 dataset.



(a) Vehicle 5366, Run 1



(b) Vehicle 195, Run 2

Fig. 67. Simulated position and speed tracking using the Intelligent Driver Model (IDM) for the I-90/94 dataset: (a) Vehicle 5366, Run 1; (b) Vehicle 195, Run 2.

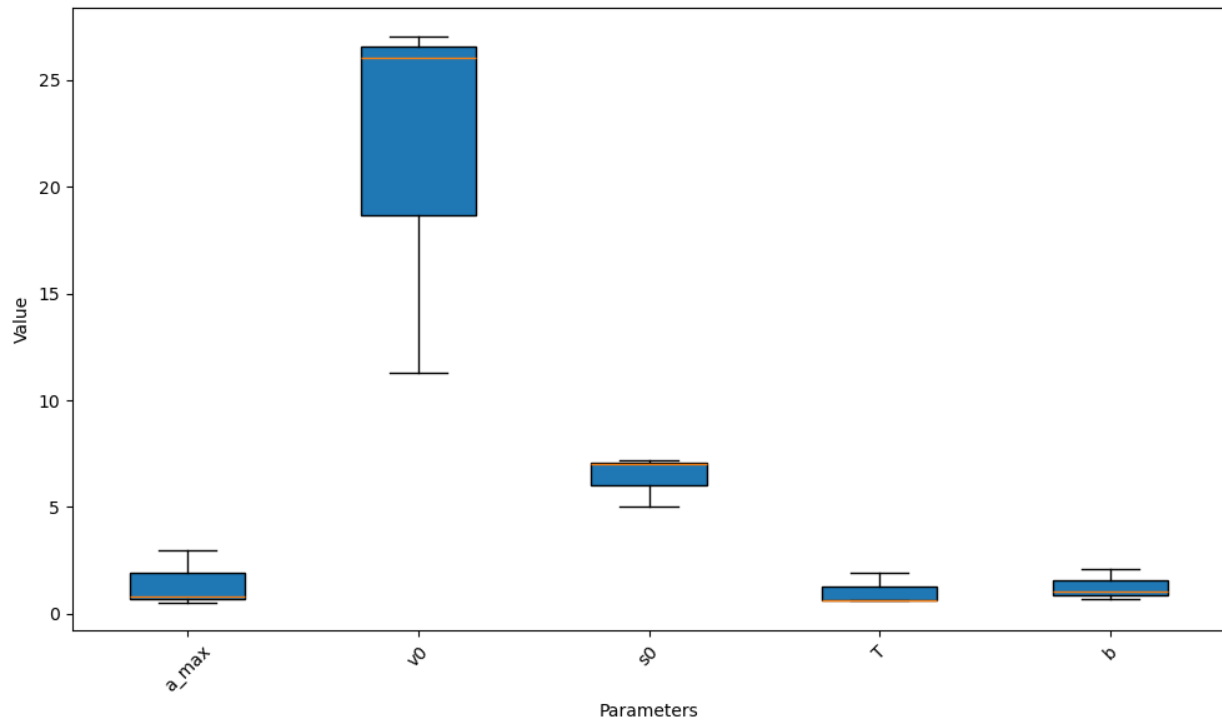


Fig. 68. Parameter ranges for IDM in I-90/94.

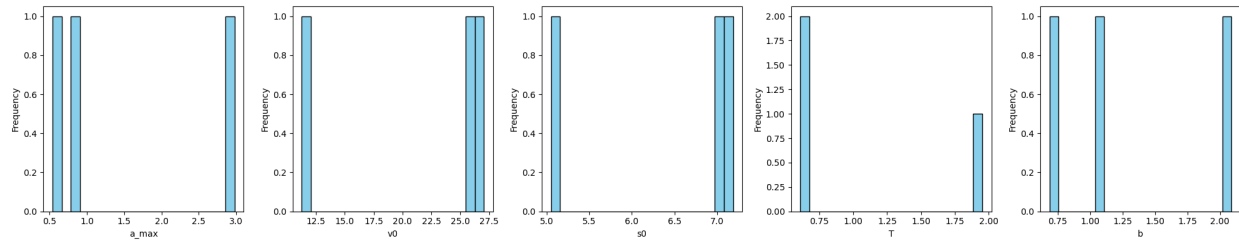
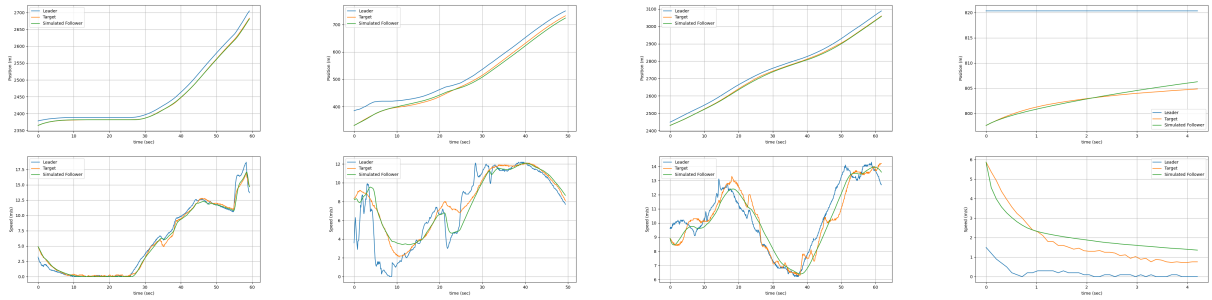


Fig. 69. Parameter histogram for IDM in I-90/94.



(a) Vehicle 13, Run 6 **(b)** Vehicle 31, Run 8EW **(c)** Vehicle 2, Run 9ES **(d)** Vehicle 2, Run 9NS
(H1A3) (H1A3) (H1A3) (H1A3)

Fig. 70. Simulated position and speed tracking using the Intelligent Driver Model (IDM) for the Phoenix dataset: (a) Vehicle 13, Run 6; (b) Vehicle 31, Run 8EW; (c) Vehicle 2, Run 9ES; (d) Vehicle 2, Run 9NS.

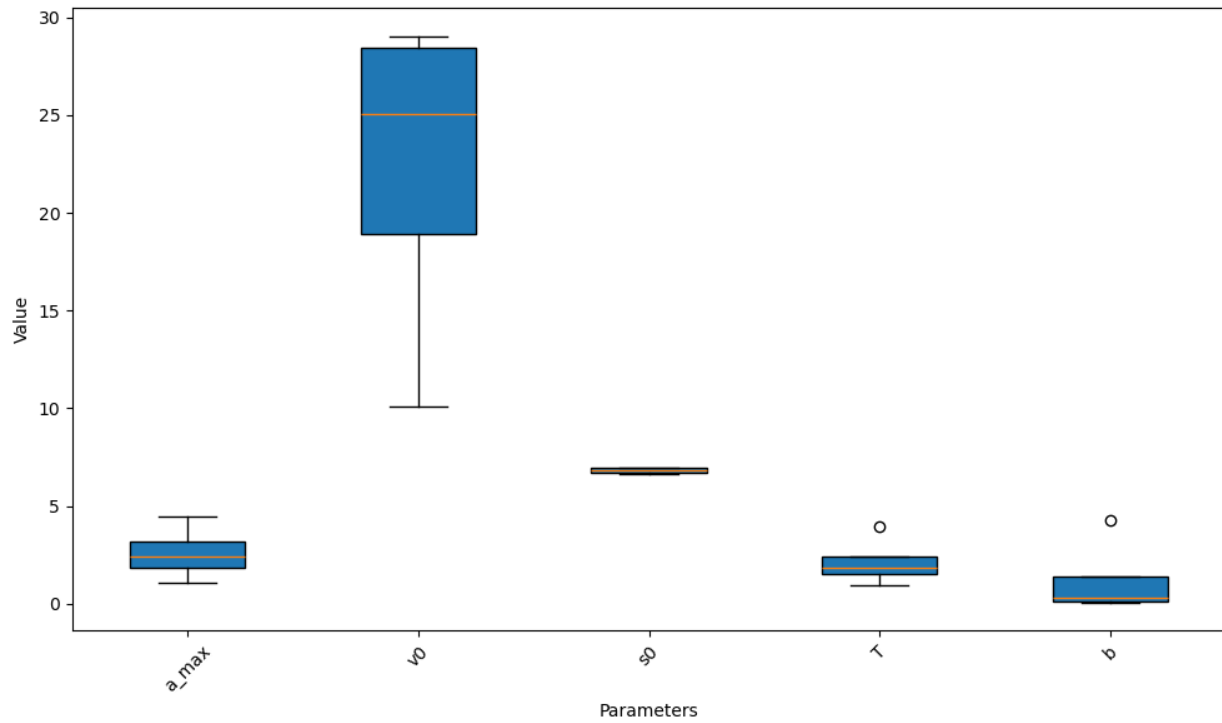


Fig. 71. Parameter ranges for IDM in Phoenix.

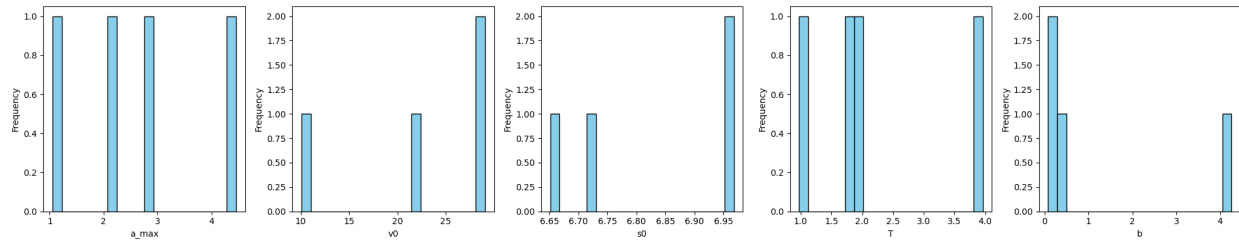


Fig. 72. Parameter histogram for IDM in Phoenix.